

UC Davis

UC Davis Electronic Theses and Dissertations

Title

Modeling and Simulation of Carbon Dioxide Removal for Environmental Control and Life Support Systems for Deep Space Habitats

Permalink

<https://escholarship.org/uc/item/0x45s832>

Author

Torralba, Monica

Publication Date

2022

Peer reviewed|Thesis/dissertation

Modeling and Simulation of Carbon Dioxide Removal for Environmental Control and Life Support
Systems for Deep Space Habitats

By

MONICA GODINEZ TORRALBA
THESIS

Submitted in partial satisfaction of the requirements for the degree of

MASTER OF SCIENCE

in

Mechanical and Aerospace Engineering

in the

OFFICE OF GRADUATE STUDIES

of the

UNIVERSITY OF CALIFORNIA

DAVIS

Approved:

Stephen K. Robinson, Chair

Zhaodan Kong

Xinfan Lin

Committee in Charge

2022

Table of Contents

List of Figures.....	iv
List of Tables	viii
Acknowledgements	ix
Abstract	x
Chapter 1 Introduction	1
1.1 HOME & Self-Awareness	1
1.2 ECLSS Overview	1
1.3 CO2 Removal Life Support Subsystem.....	2
1.4 Modeling and Simulation of Life Support Systems	4
1.5 Model Selection to Simulate CO ₂ Removal	7
Chapter 2 Background	10
2.1 Open to Closed Loop ECLSS	10
2.2 ECLSS Roadmaps	12
2.3 Consideration for Future ECLSS Design	15
2.4 Defining Degradation in ECLSS.....	18
2.5 Degradation & Packed Beds (Air & Water).....	19
2.6 Packed Bed Service Life	21
2.7 Degradation & Spares Logistics.....	24
2.8 ECLSS Maintenance and Resupply.....	25
2.9 ECLSS Anomaly Resolution	26
2.10 Current ISS Anomaly Resolution Process.....	27
2.11 Considerations for Future Life Support Anomaly Resolution	28
Chapter 3 Carbon Dioxide Removal Model Using Aspen Adsorption.....	29
3.1 ECLSS Simulations and Modeling Purpose & Objectives.....	29
3.2 STEVE Testbed.....	30
3.3 STEVE Aspen Model	31
3.4 Aspen Adsorption Model	34
3.5 Aspen Adsorption Model Set Up	37
3.6 Aspen Adsorption Model Block Descriptions	38
3.7 Simulation Experiment Design	55
3.8 Simulation Results.....	56
3.9 Simulating Nominal Operations.....	57
3.10 Simulating Off-Nominal (Faulty) Operation	64

3.11 Model Validation & Limitations	75
3.12 Discussion.....	81
Chapter 4 Carbon Dioxide Removal Model Using MATLAB	86
4.1 STEVE MATLAB Model & Estimation.....	86
4.2 MATLAB Model Development.....	86
4.3 Estimation of System States	90
4.4 Estimation of 1-Phase Operation.....	93
4.5 Estimation for Cyclic Operation	96
4.6 Discussion	97
Chapter 5 Zeolite Degradation Testbed for Deep Space Habitat Research.....	99
5.1 ZeoDe Testbed.....	99
5.2 Sorbent Degradation.....	100
5.3 ZeoDe Testbed.....	102
5.4 ZeoDe Results.....	105
5.5 Discussion	109
Chapter 6 Conclusions and Future Work	110
6.1 Conclusions	110
6.2 Suggestions for Future Work.....	112
References	115

List of Figures

Figure 1. NASA ISS ECLSS Diagram [9]	2
Figure 2. Metabolic Inputs and Outputs for a Crew Member [12], [13].....	3
Figure 3. Data Flow Example from Shuttle Missions [21].....	6
Figure 4. Open to Closed Loop ECLSS Progression	11
Figure 5. ISS Demonstrations Fly-Off Plan	15
Figure 6. Air String Schematic with Packed Beds colored in yellow [49].....	20
Figure 7. Water String Schematic with Packed Beds colored in yellow [49].....	21
Figure 8. STEVE Testbed.....	30
Figure 9. Diagram of a Sorbent Packed Bed with a Close-Up of a Spherical Porous Adsorbent Particle [60]	33
Figure 10. STEVE Schematic [23].....	34
Figure 11. Aspen Adsorption Model of the STEVE Testbed	35
Figure 12. Aspen Adsorption Model of the STEVE Testbed where the blue dotted line is the Adsorption flow and the red dotted line is the Desorption flow.....	36
Figure 13. Images of the a) GasFeed block, b) GasFeed configure screen and c) the GasFeed Specification table.....	39
Figure 14. Images of the a) reactor block labeled “Zeolite13XBed” and b) the main configure screen where orientation and heater options are selected.....	41
Figure 15. Image of the reactor block General tab where the discretization method and number of nodes are selected. This screen appears when clicking on the diagram of the reactor in the previous figure.	42
Figure 16. Image of the Material/Momentum Balance tab where the material and momentum balance assumption options are selected.	42
Figure 17. Image of the Kinetic Model tab where the kinetic model and mass transfer options are selected.	42
Figure 18. Image of the Isotherm tab where the isotherm model and dependency options are selected. ...	43
Figure 19. Image of the Material/Momentum Balance tab where the material and momentum balance assumption options are selected.	43
Figure 20. Image of the Specifications Table where all appropriate parameter values are populated such as physical, mass transfer, and heat transfer properties.	44
Figure 21. Image of the Presets/Initials where the initial conditions for gas and solid phase compositions as well as velocity and temperatures are populated.....	46
Figure 22. Images of the a) void blocks labeled “B4” and “B5” and b) the main configure screen.	47
Figure 23. Image of the void block specification for volume.	47
Figure 24. Image of the Presets/Initials for the downstream void block “B5” where the initial conditions for gas phase compositions as well as pressure and temperatures are populated.....	47

Figure 25. Image of the Presets/Initials for the downstream void block “B4” where the initial conditions for gas phase compositions as well as pressure and temperatures are populated.....	47
Figure 26. Image of the valve blocks labeled “VI”, “VL”, “VA”, “VO”, and “VD”.....	48
Figure 27. Image of the Specifications table for the inlet valve block “VI” which acts as a mass flow controller.	49
Figure 28. Image of the leak blocks which include another GasFeed block labeled “Leak” and a valve to command the leak labeled “VL” which is located at the outlet downstream portion of the sorbent bed at “B5”.	50
Figure 29. Image of the Specification table for the GasFeed block labeled “Leak” where gas composition, pressure, and temperature are populated.	50
Figure 30. Image of the Specification table for the valve block labeled “VL” where the valve operation, Cv, and flow rate can be set.....	50
Figure 31. Images of the a) junction void block labeled “B1” and b) the main configure screen.....	51
Figure 32. Image of the void block specification for volume.	51
Figure 33. Image of the Presets/Initials for the junction void block “B1” where the initial conditions for gas phase compositions as well as pressure and temperature are populated.	52
Figure 34. Images of the a) GasProduct block and b) the main configure screen.....	52
Figure 35. Image of the Specification table for the GasProduct block where the reverse gas composition, pressure, and temperature can be set.....	52
Figure 36. Images of the a) Cycle Organizer and b) the main Cycle configure screen.	53
Figure 37. Images of the Cycle Control screens for a) step 1 - adsorption and b) step 2 – desorption with time-driven setpoints.....	54
Figure 38. Images of the initial values for the manipulated variables for a) step 1 - adsorption and b) step 2 – desorption.....	54
Figure 39. Images of the values for the manipulated variables for subsequent a) adsorption and b) desorption steps. The main difference is that the jacket heater temperature and exhaust pressure are set to linearly decrease or increase from its hot to cold or ambient to vacuum (and vice versa) states at a specified rate.	55
Figure 40. Fault Injection Schematic.....	57
Figure 41. Breakthrough Curves with Varying Crew Size.....	58
Figure 42. a) Outlet CO ₂ Concentration and b) Sorbent Loading with varying Crew Size.....	59
Figure 43. Gas Temperature in the Sorbent Bed with varying Crew Size	60
Figure 44. Breakthrough Curve and Temperatures for 4 Crew.....	60
Figure 45. Breakthrough Curve with Varying Bed Length	61
Figure 46. a) Outlet CO ₂ Concentration and b) Sorbent Loading with varying Bed Length.....	62
Figure 47. Diagram of Aspen Adsorption Model with Blower Flow Rate Control	63
Figure 48. Breakthrough Curves with Varying Flow Rates	63
Figure 49. a) Outlet CO ₂ Concentration and b) Sorbent Loading with varying Flow Rate.....	63

Figure 50. Diagram of Aspen Adsorption Model with Valve Stiction Fault Injection.....	64
Figure 51. a) Outlet CO ₂ Concentration and b) Sorbent Loading with Valve Stiction.....	64
Figure 52. Diagram of Aspen Adsorption Model with Heater Fault Injection	65
Figure 53. a) Outlet CO ₂ Concentration and b) Sorbent Loading with Sustained Heater Fault	66
Figure 54. a) Outlet CO ₂ Concentration and b) Sorbent Loading with Temporary Heater Fault	67
Figure 55. Diagram of Aspen Adsorption Model with Vacuum Pump Fault Injection	68
Figure 56. a) Outlet CO ₂ Concentration and b) Sorbent Loading with varying Vacuum Faults	68
Figure 57. Aspen Adsorption Model with Leak Fault Injection	69
Figure 58. a) Outlet CO ₂ Concentration with Leak and b) Close-Up.....	70
Figure 59. Sorbent Loading with Leak	70
Figure 60. Aspen Adsorption Model with Filter Clog Fault Injection.....	71
Figure 61. a) Outlet CO ₂ Concentration and b) Sorbent Loading with Filter Clog.....	71
Figure 62. Aspen Adsorption Model with Dormancy Water Loading Fault Injection	72
Figure 63. a) Outlet CO ₂ Concentration and b) Sorbent Loading Post-Dormancy Water Loading	72
Figure 64. Aspen Adsorption Model with Multiple Fault Injections with (1) temporary low heat followed by (2) temporary valve stiction in VD and ending (3) with a sustained leak at the outlet of the bed.....	74
Figure 65. a) Outlet CO ₂ Concentration and b) Sorbent Loading with Multiple Faults	74
Figure 66. Model Validation with Breakthrough Curve Sensitivity Analysis by Varying Bed Length where the arrow indicates reduction of bed length to achieve correlation with STEVE experimental data.	76
Figure 67. Model Validation with Breakthrough Curve Sensitivity Analysis by Varying Flow Rate where the arrow indicates increase of flow rate to achieve correlation with STEVE experimental data.	77
Figure 68. Outlet CO ₂ Concentration with Leak Fault Injection Experimental and Simulation Correlation	78
Figure 69. Sorbent Bed Temperature Experimental and Simulation Correlation	79
Figure 70. Outlet Concentration and Sorbent Loading Difference Factors for Nominal versus Off-Nominal Operation	83
Figure 71. Spatial discretization along the length of the sorbent bed where N is the total number of nodes chosen for the calculation.	90
Figure 72. Concentration profile of CO ₂ in the gas phase along the length of the bed and over time.....	94
Figure 373. Theoretical measurement data for mole fraction of CO ₂ in the exhaust stream of the bed.	94
Figure 74. Experimental Measurement Data of CO ₂ Mole Percent from the STEVE test bed.....	95
Figure 75. Comparison of Actual Data and Kalman Filter Estimation of CO ₂ Mole Percent	95
Figure 76. Error of CO ₂ Mole Percent	95
Figure 77. Covariance of CO ₂ Mole Percent	95
Figure 78. a) Outlet CO ₂ Concentration and b) Estimation Error for Cyclic Operation	96

Figure 79. a) Outlet CO ₂ Concentration and b) Estimation Error for Cyclic Operation	97
Figure 80. Results of working capacity for candidate materials for the development of the 4-BMS where Grade 544 (zeolite 13X) displayed short-term degradation (restoration) to nearly full capacity through normal operating cycles even after water loading [73].....	101
Figure 81. Differential Pressure across the testbed with different sorbent materials displaying pressure drop increase for materials that accumulated dust due to long term degradation. [74]	102
Figure 82. Zeolite Degradation Testbed a) Schematic and b) Image	103
Figure 83. ZeoDe Schematic for Adsorption.....	104
Figure 84. ZeoDe Schematic for Desorption	105
Figure 85. Breakthrough Curve Comparison for Varying Bed Lengths	106
Figure 86. Breakthrough Curve Comparison for 5 inch Bed.....	106
Figure 87. Outlet CO ₂ Concentration and Temperature Profile for Baseline Cyclic Test 1.....	107
Figure 88. Outlet CO ₂ Concentration and Temperature Profile for Baseline Cyclic Test 2.....	108

List of Tables

Table 1.1 Types of Key Performance Parameters (KPPs) for NASA ECLSS	11
Table 1.2 Key Performance Parameters (KPPs) in NASA ECLSS 2020-2021 Overview	11
Table 2. Moon to Mars Habitation Considerations for ECLSS [35]	13
Table 3. Failure Modes that can be simulated in Aspen Adsorption [23]	36
Table 4. Conversion of Dual-Site Langmuir Parameters from Literature to Aspen Adsorption	45
Table 5. Valve Settings	49
Table 6. Aspen Adsorption Simulation Test Plan	56
Table 7. STEVE Control (Nominal) Test Conditions	57
Table 8. Crew Size Effect on Breakthrough Time	58
Table 9. Aspen Adsorption Test Results	81
Table 10. Faults, Key Indicators based on Simulation Results, and Corrective Actions	84

Acknowledgements

Thank you to my family, friends, colleagues, and mentors over the years.
I would not have gone as far and wide as I did without all your love and support.

Abstract

The Environmental Control and Life Support System (ECLSS) of a spacecraft is an integral part of human exploration. Current efforts to advance state of the art ECLSS subsystems in the International Space Station (ISS) are geared towards modeling and simulating various conditions and mission types. NASA and private partners are looking to enable life on the Moon and Mars, and a key factor to enabling that is carbon dioxide (CO₂) removal. Astronauts depend on the removal of metabolic CO₂ to keep cabin atmosphere at breathable levels which typically utilize adsorbent-based systems. Thus, modeling and simulating carbon dioxide removal aligns with the effort to advance future ECLSS technology while saving cost and time as compared to the traditional design-build-test approach. In addition, modeling and simulation can generate copious amounts of data and benefits research and development into ECLSS diagnostics and prognostics that require masses of data. This thesis aims to provide models of a carbon dioxide removal system that mimic the physical system, test what-if scenarios, simulate faulty and degraded conditions, implement state estimation and describes the development and results of an adsorbent degradation-focused testbed with relevance to deep space habitat settings.

Chapter 1 is an introduction to the thesis with focus on the NASA HOME Institute which has funded this work, an overview of ECLSS, a description of CO₂ Removal technology, modeling and simulation objectives, and model options and selection for CO₂ removal. Chapter 2 provides an extensive literature review of the current status of ECLSS roadmaps, lessons learned, maintenance and spares logistics as well as ECLSS data analysis processes relevant to diagnostics and prognostics applications for deep space habitats. Chapter 3 details the development of a one-bed carbon dioxide removal system using Aspen Adsorption, a ready-made platform with built-in mathematical computations and capabilities for fault injection, to

generate a multitude of data signatures, nominal and off-nominal, and validate against experimental data. Next, Chapter 4 describes model development using MATLAB, a mathematical program with full customization and algorithm integration capabilities but challenging development of numerical computations and fault injections, to generate nominal data signatures with the off shoot of applying state estimation to increase the model's overall ability to combine measurement data with theoretical models to estimate sensor data, whether available or not. Finally, Chapter 5 details the assembly and test of a supplementary carbon dioxide removal testbed focused on sorbent degradation which achieved proof of concept operation and ultimately generated test protocols and documentation for hardware and software improvements for the next generation testbed.

Chapter 1 Introduction

1.1 HOME & Self-Awareness

This thesis supports the Habitats Optimized for Missions of Exploration (HOME) Space Technology Research Institute (STRI) which is funded through NASA [1]. The scope of the HOME STRIS's research is driven by two primary objectives: (1) Keep humans alive while they are resident, and (2) Keep the vehicle alive while they are not. The institute's charter is to develop a highly autonomous deep-space habitat, i.e. a SmartHab, for human crew using three primary classes of control: (1) autonomy, (2) robotics, and (3) humans. Under the four research thrusts (RT) in HOME which are (1) Vehicle Functional Design, (2) Spacecraft Self-Awareness, (3) Human-Autonomy Teaming, and (4) Self-Sufficiency, this project falls under RT2, working with integrated predictive and prescriptive analytical methodology, specifically for Environmental Control and Life Support Systems (ECLSS).

Under the research objectives of HOME, this thesis work addresses two for deep space ECLSS research: (1) design evolvable data-driven analytics to assess, model, and predict system and infrastructure state, performance, and maintenance needs, and (2) develop and test methods to autonomously maintain spacecraft, utilizing subsystem redundancy, engineered graceful degradation, and robotic repair, with intermittent human assistance/supervision. This study builds on past work by members of the HOME community that include, but is not limited to, maintenance reliability, remaining useful life predictions, space habitat subsystem sizing, and ECLSS robustness [2]–[4].

1.2 ECLSS Overview

Environmental Control and Life Support System (ECLSS) units are composed of microgravity-compatible parts that range from hardware like valves, pumps, filters, tanks,

separators, mixers, and reactors which handle various streams of solids, gasses, and liquids. Two primary parts of the ECLSS in the International Space Station (ISS) are the air string and the water string which you can see pictured in Figure 1. The Air String controls the cabin atmosphere at safe and comfortable levels, recycling generated oxygen back into the cabin, maintaining habitable and comfortable pressure, temperature, and humidity, and scrubbing excess carbon dioxide and any contaminants from the air. The Water String processes and recycles water from waste streams, coming from cabin condensate, human hygiene, and other water sources, to provide potable water for drinking, food rehydration, and other uses on station [5]–[8].

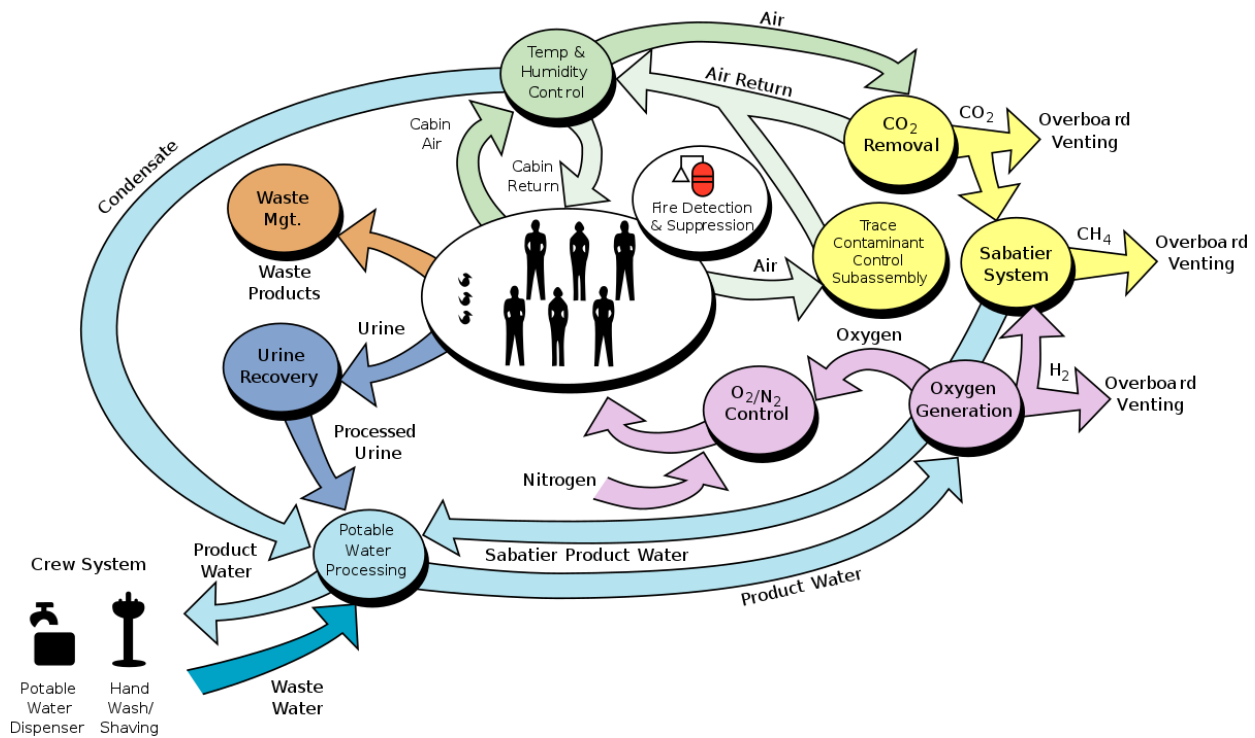


Figure 1. NASA ISS ECLSS Diagram [9]

1.3 CO₂ Removal Life Support Subsystem

A key element of the Air Revitalization system is Carbon Dioxide Removal. In the ISS cabin atmosphere, oxygen and nitrogen is supplied to the crew at ambient pressure, temperature,

and composition for breathable air. Over time, crew inhale about 5% of the oxygen and exhale carbon dioxide. Through baseline cabin atmosphere evaluations, NASA found that one crew member will produce approximately 1.04 kg of CO₂ per day [10]. The carbon dioxide produced must be removed due to the detrimental health effects associated with high levels of carbon dioxide, approximately above 2000 ppm. For reference, Earth atmosphere and outdoor air is typically around 400 ppm. High levels of carbon dioxide starting at 2% CO₂ in air can lead to a range of effects like headaches, dizziness, rapid breathing, and loss of consciousness. At the worst case, for levels at or above 17% CO₂, there can be severe consequences like convulsions, coma, or loss of crew [11]. Carbon dioxide removal has and will continue to be an extremely critical part of spacecraft ECLSS.

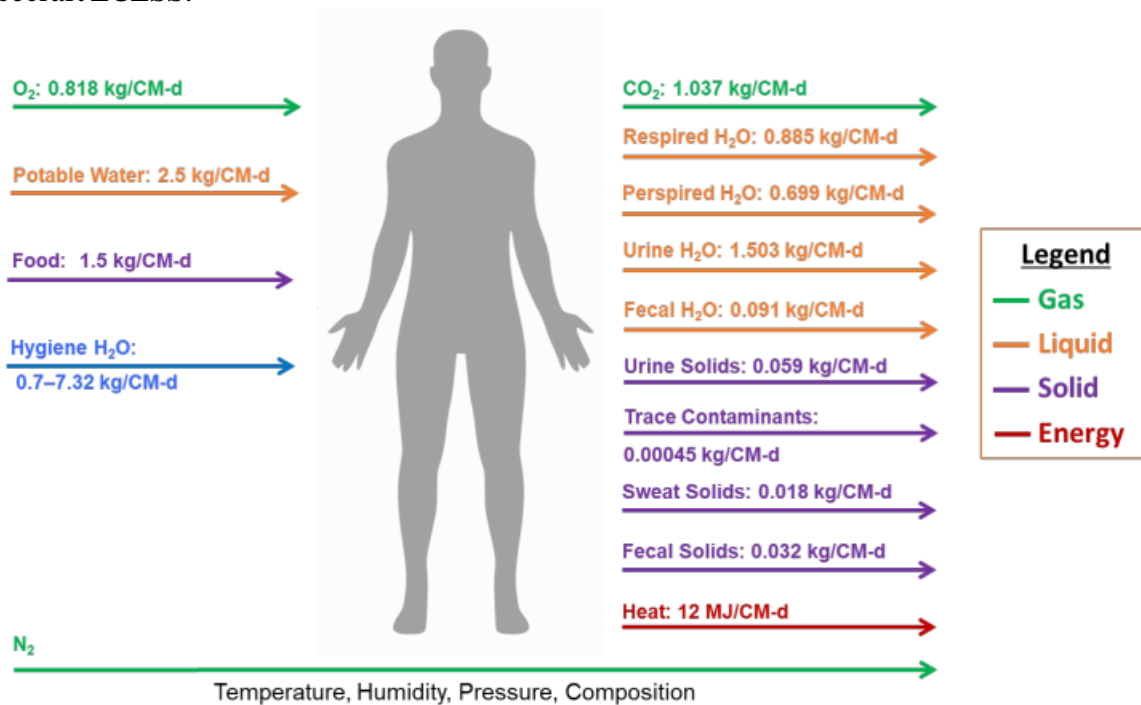


Figure 2. Metabolic Inputs and Outputs for a Crew Member [12], [13]

There are multiple carbon dioxide removal technologies at varying Technology Readiness Levels (TRL) for spacecraft ECLSS over the years. CO₂ removal technologies fall into different

categories of removal and separation through physisorption or chemisorption: 1) solid adsorbents/catalysts, 2) liquid sorbent/solvent, and 3) non-sorbent processes like thermal and pressure swing as well as biological reactions [14]. On the ISS, LiOH canisters are consumable one-time use units that remove carbon dioxide from localized areas such as sleeping quarters. The primary carbon dioxide removal system is the Carbon Dioxide Removal Assembly (CDRA) which uses regenerable zeolite 5A sorbent material [15]. The 4BCO₂ is an advanced version of CDRA that uses regenerable zeolite 13X material and is currently under test in the ISS as of 2022 [16]. In addition to those technologies, the Thermal Amine Scrubber (TAS) is also under test in the ISS and uses a regenerable amine-based material [17]. The current status is to process and remove carbon dioxide produced by 4-crew in the ISS with a target inlet composition of 2 mmHg CO₂ [16]. For deep space habitats, these performance factors are dependent on dormancy periods, crew size, and other long-term cabin requirements.

1.4 Modeling and Simulation of Life Support Systems

There is a myriad of tools analysts can use to monitor and analyze ECLSS subsystems aboard the ISS. The purpose and objective are to keep systems healthy and, when they are not, investigate faults and bring them back to a healthy status. The primary analysis tools for ECLSS are data and models. Data can come in the form of direct telemetry from systems in the ISS to sensor data from ground units. Data can also come from historical archives from past operations. Models can come in the form of (1) subsystem models that can mimic the physical system, (2) models that generate metrics like resupply and maintenance logistics or (3) models that optimize subsystem design and configuration for varying scenarios and mission types.

Understanding system behavior is not possible without data. There are multiple databases that NASA and its contractors use to archive and extract data from to forecast trends and

understand subsystem behavior. The ISS Logistics and Maintenance (L&M) Office, supported by a Boeing L&M team, maintains the Modeling Analysis Data Set (MADS), a database of ISS ORU characteristics to support maintenance analyses, including failure rate estimates. These failure rate estimates are updated on a regular basis using a Bayesian technique that accounts for observed failures [18]. Boeing, the primary ISS contractor, manages direct telemetry from the ISS in their database called JMEWS. The Maintenance and Reliability Spreadsheet (MaRS) database is derived from data from the Problem Report and Corrective Action (PRACA) system for ISS [19]. MaRS is also built from information from another database called SPIDER which contains the entire ISS configuration complete with individual component schematics and data sheets [20].

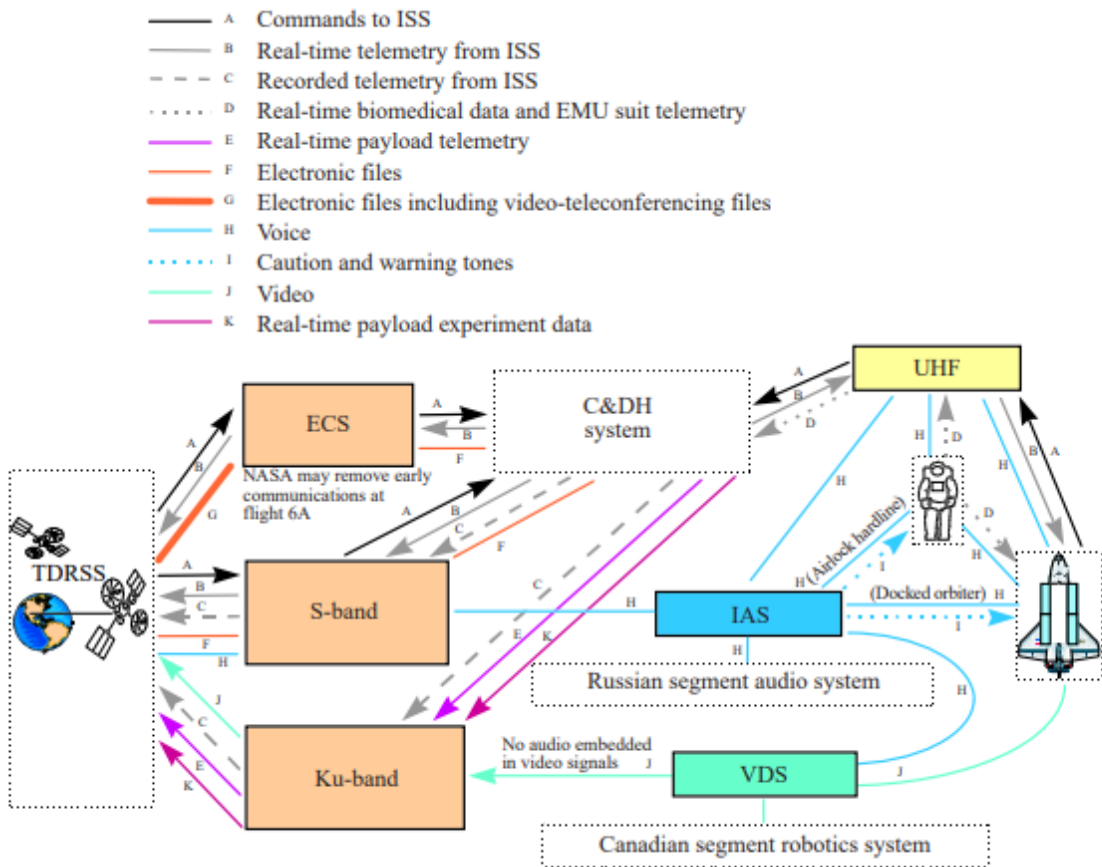


Figure 3. Data Flow Example from Shuttle Missions [21]

The role of modeling and simulation for spacecraft life support design and operation continues to grow as NASA and the space community set their sights on deep space habitats and vehicles beyond Low Earth Orbit (LEO). The farther these spacecrafts are from Earth and Mission Control, the more critical autonomy and awareness are. To maintain high operational performance for the duration of their missions, spacecraft would need embedded cause and effect databases and a means of understanding system states to execute maintenance and repairs. Models generate simulation data to answer complex and dynamic problems which are especially useful for interconnected system like the ISS ECLSS [22].

For space habitation and life support, some models aim to mimic the physical system, taking on the role of a digital twin, to simulate what-if scenarios that point to design flaws, weaknesses, and edge cases that may cause failures [23]–[25]. Other models aim to design completely new systems and determine operational performance metrics for systems that have not yet been built [26]. Other modeling efforts aim to optimize the design of a system by generating sensitivity analyses to size hardware components, materials flows, and buffers to maximize performance while minimizing mass and cost. Adjacent to simulating ECLSS components are models that specifically determine failure rate estimates and remaining useful life (RUL) of components [27]. All the model types mentioned here may also generate reliability metrics, provide recommendations for resupply and maintenance logistics, and facilitate the development of system controllers. A list of life support system specific models that have been published can be found in [22]; however, more models should likely be in that list since the time of publishing.

Within the scope of this study, the modeling and simulation work presented here focuses on packed beds, specifically for carbon dioxide removal but with applications in water processing, oxygen generation and crop production. Packed beds play an integral role in ISS ECLSS and may be used for exploration class vehicles as this technology has been heavily studied and qualified for space applications for decades. In concert with the modeling types mentioned prior, the carbon dioxide removal assembly model aims to mimic the physical system, test what-if scenarios, and simulate faulty conditions and degradation with relevance to deep space habitat settings like long life cycles and dormancy to enable diagnostics and prognostics of similar systems and conditions [12], [28], [29].

1.5 Model Selection to Simulate CO₂ Removal

Carbon Dioxide Removal can be challenging to model and simulate, but there are multiple modeling platforms to choose from. To start, carbon dioxide removal is a gas separation process where carbon dioxide is separated from air. This process can be done using physisorption, chemisorption, phase change, or through a biological process. Some examples are physisorption of carbon dioxide gas onto the surface of pores of a rock material, chemisorption of carbon dioxide in ionic liquid, phase change of gaseous carbon dioxide into solid frozen carbon dioxide, or consumption of carbon dioxide through photosynthesis in plant material [14]. Modeling these processes requires mass balance equations that represent the process of carbon dioxide adsorption or absorption. Physisorption of carbon dioxide with zeolite pellets is used in the International Space Station (ISS). In this case, physics-based and first principles-based equations are utilized in conjunction with equations that represent the adsorption behavior for the zeolite 13X material.

Models can be developed through programming or through ready-made platforms. Through programming, a physics-based model or data-based model can be written in languages like C++, python, and MATLAB, to name a few. Programming increases customization capabilities. Physics-based models are beneficial when the physical system has not yet been built and/or has not generated measurement data, whereas data-based models are beneficial for older systems and utilize measurement data to determine and essentially reverse engineer system mechanics and states. Aspen Adsorption, Aspen Plus, COMSOL, GProms, and other ready-made programs can be used to model carbon dioxide removal. Based on literature, C++ and COMSOL models of the carbon dioxide removal system on the ISS have been developed [30], [31]. Before advanced computation, models for carbon dioxide removal were developed and operated using spreadsheets. Advanced computation allows current models of the subsystem to experiment with many more test conditions and optimize for sizing and other trade or cost analyses. To increase the knowledge base of the space life support system community in modeling carbon dioxide removal in space habitats, this thesis provides the setup, demonstration, and results from two physics-based models: Aspen Adsorption and MATLAB.

There are advantages and disadvantages to using Aspen Adsorption and MATLAB for carbon dioxide removal modeling [23]. Aspen Adsorption is a program specifically made for adsorption processes like that of physisorption of carbon dioxide in solid pellets. All mass, momentum, and energy balances are incorporated into the model and a model designer only needs to populate parameters with empirical or theoretical values. The beauty of using a ready-made platform is that heavy computation like partial differentiation is already enabled and built into the model. The disadvantage is that the model designer does not have easy access to customize or visualize the programming beneath the user interface of the model – it is a black

box with some options for customization using FORTRAN. The other model uses MATLAB and enables full customization. However, handling partial differentiation and determining boundary conditions are difficult and not easily described in literature, especially in the case of desorption which switches operation from ambient temperature and pressure to high temperature and vacuum pressure with opposite flow direction. Model development and operation using Aspen Adsorption can be achieved faster than with MATLAB. Modeling cyclic operation with desorption as well as fault injection can be achieved with Aspen Adsorption. However, unlike the Aspen Adsorption model, a MATLAB model can be easily incorporated into a Simulink model or interfaced with models developed with other programming languages. Isolated models, however capable they may be, would not be useful if they cannot integrate and communicate with other models, especially in an interconnected system such as spacecraft life support. Both the Aspen Adsorption and MATLAB models were developed in parallel to demonstrate model development, generate data signatures for the HOME community, and highlight technology gaps for SmartHab diagnostics and prognostics for life support subsystems like CO₂ removal.

Chapter 2 Background

ECLSS design for future spacecraft is dependent on understanding current life support system architectures and processes. The International Conference for Environmental Systems (ICES) is one of the main resources for ECLSS knowledge capture and it holds information for past, present, and future states of various ECLSS technologies. However, information can be disparate and difficult to synthesize. It can be challenging to see the big picture since the process is akin to assembling an expansive and multi-level jigsaw puzzle. Thus, an attempt to unify and gather relevant information for modeling ECLSS can be seen in this chapter which includes background on ECLSS roadmaps, lessons learned, maintenance, and data analysis.

2.1 Open to Closed Loop ECLSS

ECLSS research and development is moving towards regenerable technologies that close the loop on survival elements like air and water. There are multiple ECLSS projects across all technology readiness levels (TRL) that aim to potentially fill gaps in the loop. The concept of open loop and closed loop systems is integral to the design, build, test, operation, and maintenance of all subsystems.

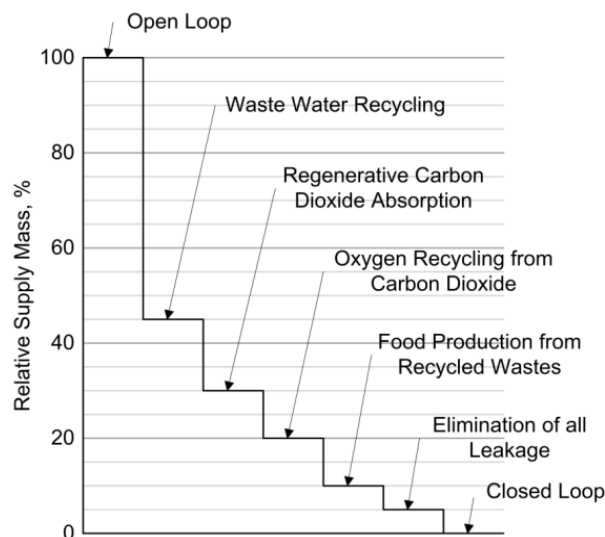


Figure 4. Open to Closed Loop ECLSS Progression

There is a spectrum of open to closed loop subsystems that are evaluated against key performance parameters (KPPs) which are used by NASA to meet requirements for manned exploration-class vehicles, spanning traditional performance metrics, storage and resupply logistics, and reliability and maintenance metrics. These KPPs help NASA and commercial partners quantify the level of technology development and inform down-selection of competing technologies. Since the goal of closed loop ECLSS, a requirement for all space habitats outside of the radius of economical or even possible frequent resupply from Earth, is to enable fully regenerable life support, understanding gaps and KPPs relevant to major units in past and current ECLSS systems onboard the ISS is critical for future ECLSS design and integration [32], [33].

Table 1.1 Types of Key Performance Parameters (KPPs) for NASA ECLSS

#	Type	Description
1	Performance	e.g. Mass flow rate (kg/hr) averaged over one hour and concentration (ppm) averaged over one hour, etc.
2	Storage & Supply	e.g. kg consumables + limited life components/kg processed, etc.
3	Reliability	e.g. kg of spares to achieve 99% probability of sufficiency

Table 1.2 Key Performance Parameters (KPPs) in NASA ECLSS 2020-2021 Overview

KPP	Value
ppCO ₂	Maintain at 2600 ppm for crew of 4
O ₂ recovery %	Greater than 75% O ₂ recovered from CO ₂ for long-duration transit missions
O ₂ recovery %	Greater than 90% O ₂ recovered from CO ₂ for planetary surface missions

EVA suit O2 source	At least 3600 psi O2 source
Atmospheric Particulate allowable amount	Less than 0.05 mg/m ³ for lunar and cabin dust
Atmospheric Particulate allowable size	Between 0.1 - 10 um

2.2 ECLSS Roadmaps

At the time of writing, spaceflight development is booming with the onset of commercial space habitat development and the growing focus on exploration-class ECLSS as more humans work to live in and beyond low earth orbit. Diving deeper into requirements for exploration-class systems, there are key factors and differences in life support for Lunar versus Martian habitats and even further granularity between surface versus transit habitats. ECLSS requirements for surface habitats aim to provide crew, likely a group of four on approximately 30-day missions, with a nominal operating pressure of 10.2 psia and 26.5% oxygen concentration and the capability to operate at a lower pressure (8.2 psia) and higher oxygen concentration (34%). A surface habitat may need to ramp up and down to crewed and uncrewed (dormant) settings and share life support with a pressurized rover as well as spacesuits. The surface habitat ECLSS will need to also process and remove dust that may enter the cabin atmosphere and water lines. For transit habitats, the ECLSS may or may not be closed loop, recycling waste products to maintain a specified balance in available water and oxygen or using readily available consumables throughout the mission. The transit habitat ECLSS will provide crew with 10.2 psia and 14.7 psia, changing depending on crewed and uncrewed (dormant) settings. On long-duration missions like those to Mars, tested first at Gateway, the pressure will be maintained at 14.7 psia.

Unique to the transit habitat, ECLSS will need to support 1,200-day missions without resupply and it is planned to use regenerative, or closed-loop, ECLSS to minimize spares logistics. [34]

Table 2. Moon to Mars Habitation Considerations for ECLSS [35]

	Surface Habitat (SH)	Transit Habitat (TH)
ECLSS Ground Truth	<p>The SH will include an Environmental Control and Life Support System (ECLSS) that provides for crew health and safety over the duration of the crewed mission with a nominal operating pressure of 10.2 psia (70.3 kPa) and 26.5% Oxygen concentration and the capability to operate at 8.2 psi (56.5 kPa) and 34% Oxygen.</p> <p>Rationale: The SH will provide ECLSS equipment and sparing provisions to enable safe operation of the SH for crewed periods. ECLSS closure assessments are ongoing and more closed systems may be considered in habitat concepts if deemed beneficial. NASA is currently assessing ECLSS options for water processing during uncrewed illuminated periods in order to preserve power during crewed periods.</p>	<p>Description: The TH will include an Environmental Control and Life Support System (ECLSS) that provides for crew health and safety and which recycles waste products to a degree that the balance of available water and oxygen is maintained, assuming water is only added to the balance through metabolism and food ingestion. The TH will support operational pressures at 10.2 psia and 14.7 psia while at Gateway. The TH will support long duration transits at 14.7 psia. Hardware and consumables for pressure transitions will be provided by the TH. The number of repressurization/transition events is TBD.</p> <p>Rationale: The TH will require an ECLSS capable of supporting 1,200-day missions without resupply. Regenerative ECLSS technologies should be used to minimize the logistics that must be manifested.</p>
ECLSS Assumption	<p>Description: The SH should accommodate processing wastewater collected in the Pressurized Rover and provide the Pressurized Rover with potable water and oxygen needed for Rover activities. Commodity exchanges between the SH and the Pressurized Rover should be assumed to correspond with crew rotations between the SH and Pressurized Rover.</p> <p>Rationale: It is assumed that the Pressurized Rover will have the capability to collect humidity condensate and urine for processing in the SH.</p>	N/A
Functional Allocation	<p>The SH ECLSS must establish and maintain a habitable volume for a crew of four and internal payloads on missions of approximately 30 days. When the SH is uncrewed, the ECLSS will maintain a threshold atmosphere to protect itself and other SH systems. This includes maintaining a minimum pressure and temperature to protect against freezing and removing cabin air humidity to protect against condensation. The ECLSS will provide a habitable atmosphere prior to crew return by re-establishing an acceptable total pressure, oxygen partial pressure, trace gaseous contaminant levels, and temperature. During ramp-up for crew arrival, full recovery and verification of ECLSS functionality should be achieved to support the next crewed mission phase. Applicable functions: control cabin pressure, remove air</p>	<p>The TH should utilize a closed-loop ECLSS that establishes and maintains a habitable volume for a crew of four and internal payloads on missions up to 1,100 days without resupply. When the TH is uncrewed, the ECLSS will maintain a threshold atmosphere to protect itself and other TH systems. This includes maintaining a minimum pressure and temperature to protect against freezing and removing cabin air humidity to protect against condensation. The ECLSS will provide a habitable atmosphere prior to crew return by reestablishing an acceptable total pressure, oxygen partial pressure, trace gaseous contaminant levels, and temperature. During ramp-up for crew arrival, full recovery and verification of ECLSS functionality should be achieved to support the next crewed mission phase. While docked at Gateway, the TH ECLSS will continue to maintain its own habitable volume and should be capable of exchanging pressurized gases between modules in the stack. Applicable</p>

	contaminants, conditioning cabin air, provide water, protect crew and vehicle from hazardous conditions, manage crew metabolic waste, and remove lunar dust.	functions: control cabin pressure, remove air contaminants, conditioning cabin air, provide water, and protect crew and vehicle from hazardous conditions.
--	--	---

The International Space Station (ISS) has and will continue to serve as the state-of-the-art testbed for ECLSS. As of the 2022 ISS Transition Report, NASA is targeting long-duration ECLSS project completions for 2030 before the projected ISS de-orbit event. Based on the ISS Fly-Off plan for ECLSS development, specifically related to the air and water strings, 9 projects are in progress for exploration-class atmosphere subsystems and 12 projects are in progress for exploration-class water usage and recovery subsystems. The Integrated ECLSS testing needed for the Commercial LEO Destination (CLD) habitat are the Exploration Potable Water Dispenser for Sparing/Dormancy Periods, Recover >90% Water from Urine Brine, Robust Advanced Water Recovery System, Compact Low Logistics Commode, Recover/Recycle O₂ from CO₂, Improve Reliability/Decrease Complexity of the Oxygen Generation System, Robust Condensing Heat Exchanger, and the Atmosphere CO₂ Removal System. Among the list of ECLSS projects, key ECLSS units like reactors and separators will be put to the test for long-duration missions. [36]

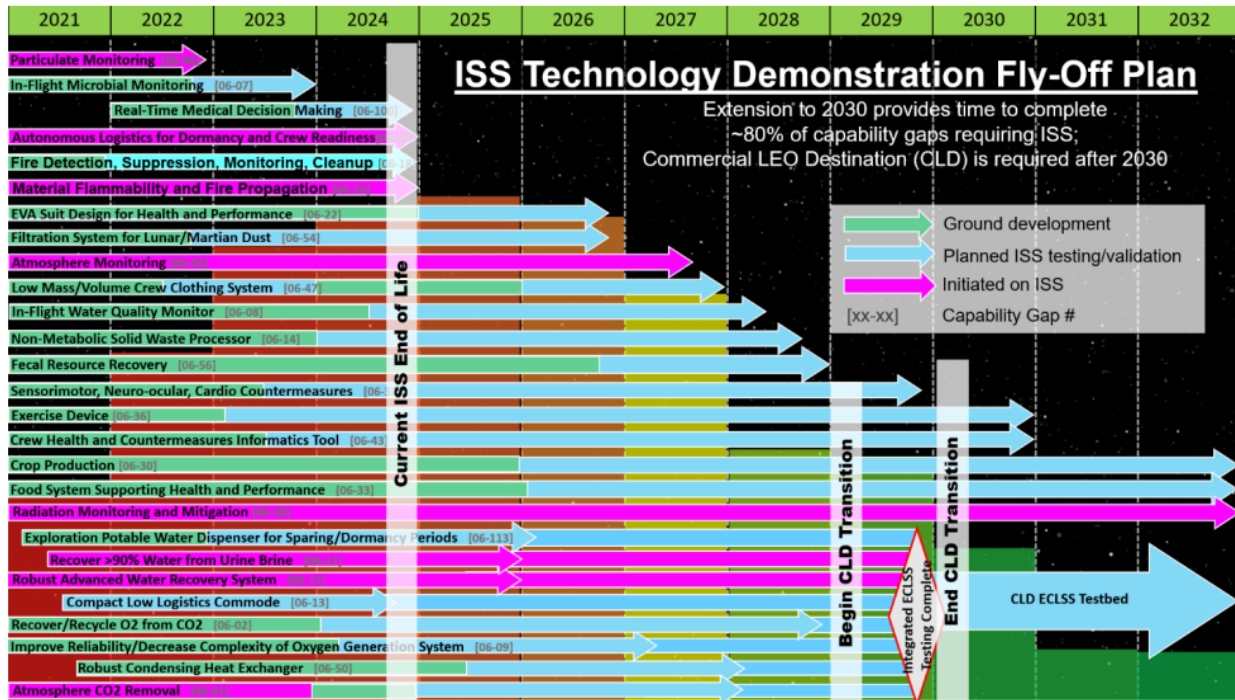


Figure 5. ISS Demonstrations Fly-Off Plan

2.3 Consideration for Future ECLSS Design

Designing closed loop life support systems is a challenging feat, especially as these technologies become more interconnected and complex. Work has been done to employ computational networks and frameworks to understand the impact of complexity on cost and performance like the System Complexity Metric (SCM) and various other reliability tools for determining spares and maintenance logistics. As the ECLSS loop closes, complexity and interconnectivity increases, making it more challenging to understand the resilience, sufficiency, and robustness of the overall system [37]. The work done by Yang et. al. investigated the difference in complexity between an ECLSS design scheme that improved system closure and another that reduced system power consumption and concluded that different schemes had little effect on system complexity at the information level - this is a key finding for data management of ECLSS sensors and what it means for changing ECLSS subsystem configurations [38].

According to Detrell et. al., a comparison in ECLSS design between an ISS-like system and one that uses reduced mass options has similar reliability results for a Mars mission, where the systems scored 98.3% and 98.8% in reliability respectively using a developed tool called Reliability Environment for Life-Support System Simulation and Analysis (RELISSA) [39]. The main difference was found in the number of spare parts required to achieve those reliabilities where the ISS-like system had an Equivalent Size Mass (ESM) of 21.9 tons while the reduced mass system was 12.5 tons with 41.4% and 34.5% representing the number of spare parts in ESM needed for each system, respectively. This is key to understanding trade-offs between heritage, well-tested ECLSS subsystems and how they compare to lower TRL options with reduced mass, loop closure benefits, and reduced power consumption.

Using the existing Orbital Replacement Units (ORUs) as they are provides a baseline for understanding failure modes and corrective actions which inform repair and replace crew operations. To prepare for long-duration missions, current projects are addressing the need to design maintainability into fault-susceptible components as well as anticipate failures, spanning from independent recoverable faults to cascading total failure, by using data analytics like stochastic probabilistic modeling for diagnostics and prognostics [17]. Regarding maintainability, work has been done to develop a Maintenance Unit (MU) Method for ECLSS design that has the potential to replace the ORU method of ECLSS design. This work aimed to address maintainability requirements for ECLSS unit integration and repairability ease, concluding that the proposed MU method will enable easier and faster remove and replace operations, while keeping time-to-hazard constraints for out of service units in mind [18].

ECLSS autonomous functions and operations are critical for future missions that include dormancy periods. NASA plans for crew to inhabit Gateway, for example, for 30-day missions

in a yearly cadence, so that 11 months of the year the spacecraft would be dormant. According to Badger et. al., most spacecraft systems like guidance, navigation, control, power, and propulsion will remain the same state between crewed and uncrewed periods. However, ECLSS is expected to power down a substantial amount of its subsystems like carbon dioxide removal and water processing (to an extent). The main considerations for the ECLSS onboard a deep space habitat, such as Gateway, are ramp-up testing in preparation for crew arrival, robotic maintenance for component repairs and reconfiguration operations, and improvement of the state of the art for ECLSS system health management. In addition, three trade studies were described that can be addressed in relation to critical ECLSS components: (1) sensor array versus mobile sensors, (2) self-actuation versus mobile (robotic) manipulation, and (3) in-place redundancy versus “repair and replace” spares philosophy. [28], [42]

Spares logistics is an essential part of ECLSS design and maintenance. Based on work by Owens et. al., modeling spares logistics using deterministic failure rate estimates with aleatory and epistemic uncertainty provides a better idea of what the probability density function of the estimated service life of an ECLSS component could be. It is not just a number - its a probability. The idea of buying down uncertainty to get to the true value of the failure rate of any component leads to spares calculations that can increase overall reliability, reduce required spares mass, and inform engineers and analysts of additional testing time needed for current or future ECLSS components. This method is especially useful when we take all factors and parameters that characterize the reliability of a component or system and boil it down to one number, i.e. time to failure. Degradation of ECLSS components is a complex factor in this method, but it can be better understood (reducing uncertainty) with simulations and testing as recommended by this thesis. [43]–[45]

2.4 Defining Degradation in ECLSS

Degradation is a phenomenon that affects all materials. It is the wearing down and aging of materials which change its properties and performance over time. Degradation in ECLSS is a major issue that prompts analysts and engineers to measure and understand the lifetime of various units and hardware. NASA has collected reports and data on maintenance tasks in the ISS MADS and PRACA systems, among others, from ECLSS start-up in the ISS to present-day operations ranging from major repair and replace operations, known as “R&R”, to minor servicing tasks scheduled into an astronaut’s day. From the 2021 overview by Broyan et. al, NASA intends “to establish component-level testing capability to enable direct reliability testing for wear-out based components such as pumps and valves which may be due to reduced pressures, higher temperatures, or degraded modes to obtain diagnostics data signatures” [32]. Furthermore, reliability testing of other critical components like packed beds are in alignment with NASA’s efforts.

The purpose of understanding degradation of critical components is to have higher certainty and confidence in the robustness, reliability, and resilience of the system. Survivability and sufficiency of ECLSS and space habitats are also of high importance and have been defined and studied in other works related to future habitat and ECLSS design. Based on work by Escobar et.al. regarding ECLSS robustness, the term was defined as the “ability to maintain habitable conditions for crew survival and productivity over the mission lifetime under a wide range of conditions” [2]. Degradation rates can change and propagate forward in time in different ways based on varying conditions. Some of the conditions that must be accounted for are ordinary usage, temporary environmental disturbances or disruptions (expected and unforeseen), and sustained changes in the system (i.e. physical or control reconfigurations).

Based on work done by Matelli et. al., ECLSS resilience was defined as “the ability of the system to 1) withstand a major disruption within acceptable degradation parameters and 2) to recover within an acceptable time and composite costs and risks” which aligns with part of the previously mentioned robustness metric methodology by Escobar et. al. [46]. Regarding reliability, Owens et. al. defined the term as “concerned with prevention of failure, while resilience is concerned with optimization of performance in the presence of failure, to enable the graceful degradation of systems - that is the transition through a series of degraded but still partially functional states before complete system failure” [27]. Harry Jones described these three terms as the following: “Reliability, robustness, and resilience describe dependable performance under increasingly difficult conditions, first the specified environment, then a wider possible environment, and finally unanticipated damaging conditions. These three qualities are increasingly desirable and increasingly difficult to achieve” [47]. These definitions and past work are critical for understanding the impact degradation rates have on ECLSS design and the system’s ability to support the crew and the mission with utmost certainty and confidence. Lastly, degradation can be both deterministic and stochastic, so the impact of varying conditions and probabilities may open ECLSS design to various options regarding overall design, spares logistics, and reconfigurations for different mission types.

2.5 Degradation & Packed Beds (Air & Water)

Selecting hardware that close the ECLSS loop requires a great deal of resources, testing, insight, and review. One of the main factors assessed in hardware selection is service life, which ideally would be infinite for a closed loop system. However, all materials degrade at some rate and depending on their sensitivity to the magnitude and frequency of varying operational conditions and disturbances, these rates can fluctuate and make it difficult to anticipate failures

with certainty. An integral part of ECLSS subsystems is the class of components that resemble packed beds, akin to organs in the body, which scrub, separate, or generate life support components like CO₂, O₂, water, and more. Packed beds are large pipes, or any types of enclosed volumes, that are packed with adsorbent or absorbent material, typically solid pellets or meshes but can be a liquid solvent or a mixture of solids, gases, and/or liquids.

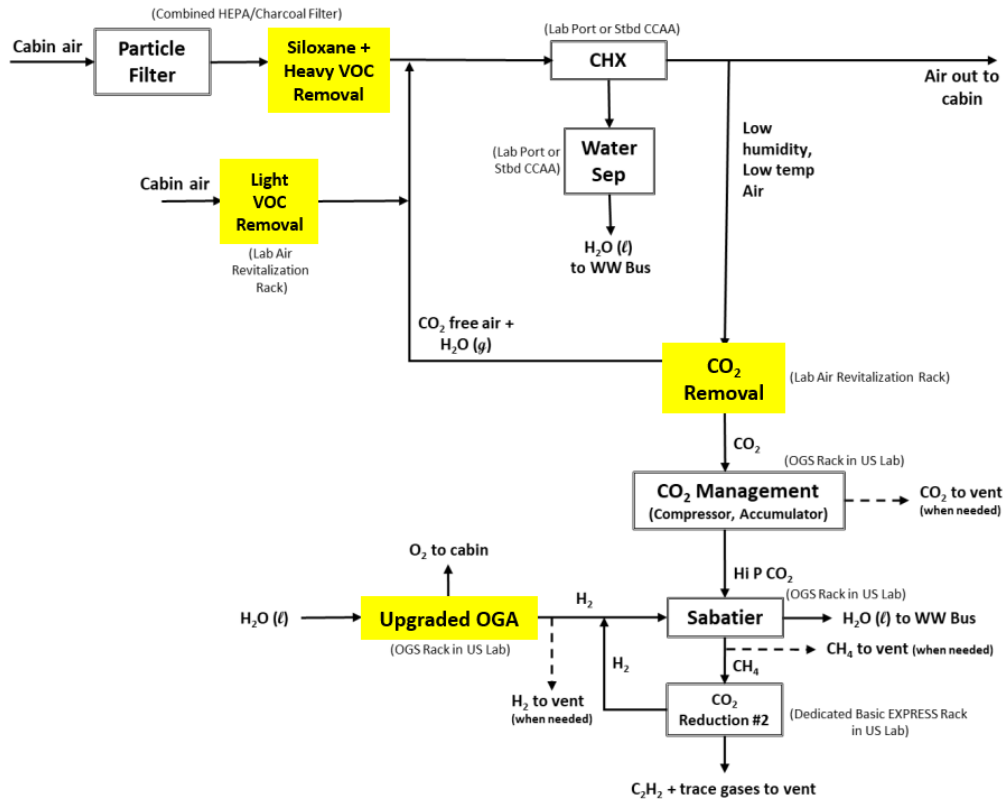


Figure 6. Air String Schematic with Packed Beds colored in yellow [48]

A sizable amount of volume and mass of ECLSS components are due to packed beds. For example, zeolite and silica gel packed beds are used for CO₂ scrubbing while activated carbon is used for trace contaminant control in the Air String. In the Water String, ion exchange beds are used in the water recovery system as well as the oxygen generation system, and multifiltration activated carbon beds are used in the water recovery system. Due to the integral role packed beds

play in current and future ECLSS, understanding degradation modes and learning to prevent failures is of utmost importance in a closed loop system. Failure and degradation modes of packed beds will be studied and analyzed to facilitate spacecraft self-awareness.

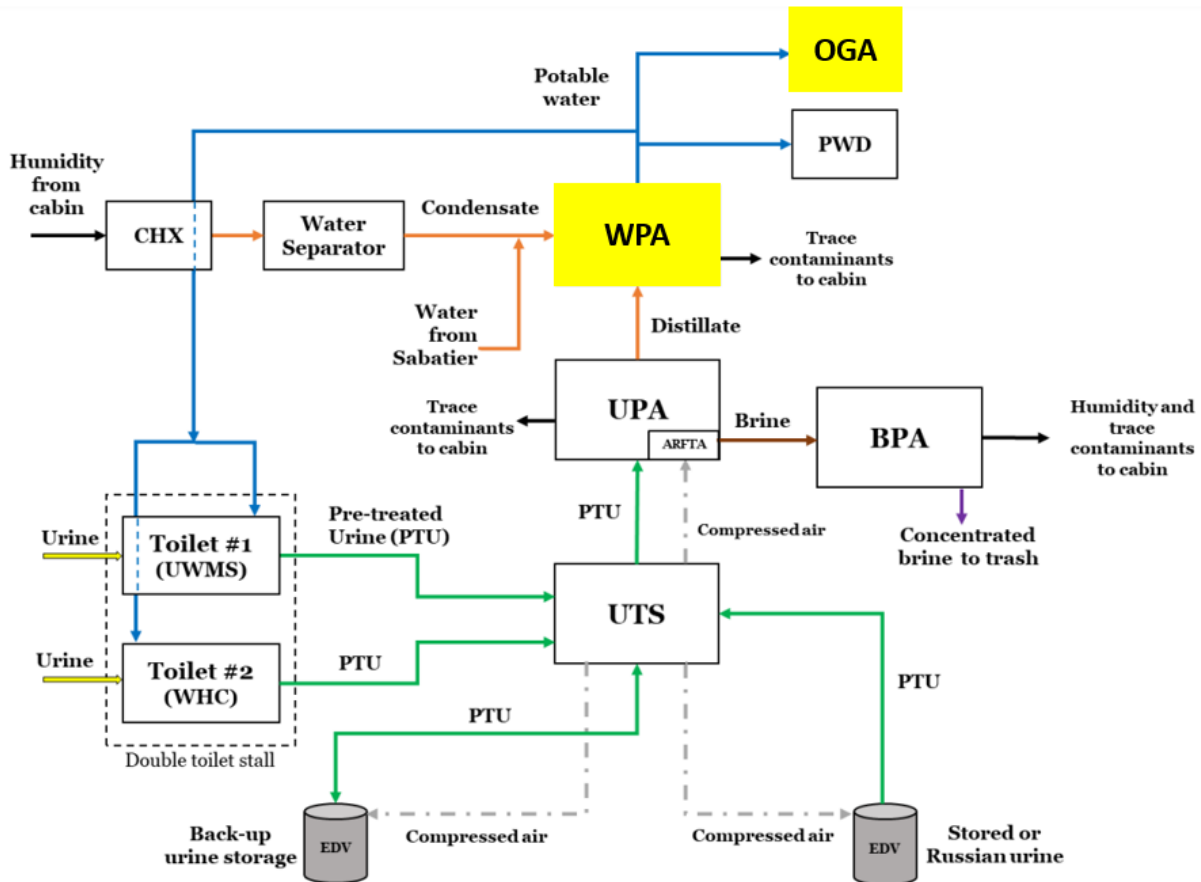


Figure 7. Water String Schematic with Packed Beds colored in yellow [48]

2.6 Packed Bed Service Life

Pre-flight and in-flight tests of ECLSS subsystems provide the necessary data to determine and certify service life. Service life is the sum of shelf life and operating life. Service life of ECLSS packed beds range from 1/3 of a year to 10 years, and it depends on many factors as detailed in the assessment of regenerative ECLSS beds done by Cloud et. al. [49]. Regardless of the type of packed bed and its inputs and constraints, all have failure rates and degradation

rates which inform overall service life. The more degradation mechanisms are understood, the more potential there is to not only anticipate failures but to also prevent failures and extend the life of these critical units.

The study by Cloud et. al. on ECLSS resin beds found that certain beds are robust and have operated far beyond their initial estimates for service life, improving maintenance schedules, launch costs, and spares logistics while other beds are highly dependent on crew usage and overall loading. For example, the microbial check valve beds in the WPA and OGA have an extended shelf life from 5 to 10 years while other beds containing ion exchange resin were not. It was found that charcoal does not generally degrade in storage. However, the industrial standard for ion exchange resin and microbial check valves shelf life is typically 2 years but can be extended with good storage, like limiting oxygen and light exposure in addition to regulated pressure, temperature, and humidity. This study conducted a 2-year test to determine resin degradation rates, and the resin capacity was found to have degraded by 8% and 12.7% in a parallel test conducted in two different locations. It was found that discrepancies in resin capacity may be due to different resin bed ages at the time of testing. Immediately after a resin bed has been manufactured, the highest degradation rate is seen initially and then decreases over time. Due to this finding, the WPA designers estimated a 6% degradation rate per year which is assumed to occur during both the shelf and operating life of the resin. Testing of 12 year old microbial check valve resin allowed the investigators to recommend an extension of shelf life from 5 to 10 years for resins of that family. This study highlights the need for rigorous testing of beds to determine degradation rates and operating life of critical WPA and OGA components and enabling baseline understanding of ECLSS health status [49]. However, it leaves short-term disturbances and their effects on degradation rates to modeling and simulation efforts.

The Carbon Dioxide Removal Assembly (CDRA), the primary CO₂ scrubber aboard the ISS, has had many issues since the beginning of its life in the station. There were also issues related to pair scrubbing of CO₂ by CDRA and Vozdukh, the amine-based scrubber provided by the Russian Space Agency. LiOH canisters were used as consumable CO₂ scrubbers that could be used for contingency situations or in highly saturated areas, like sleep areas. For inter-module ventilation during docked scenarios, dust accumulation was frequent and degraded scrubbing efficiency, especially since sleep areas were a long distance from the scrubber location. Cargo arrangement in various modules also blocked airflow and created localized CO₂ pockets. Since 2015, Vozdukh had degraded from utilizing 3 beds to only 2 and needed support from CDRA to fully scrub CO₂ onwards. In CDRA, zeolite occlusion due to dust accumulation led to excessive mechanical obstruction in downstream valves and pipes. Heater failures in CDRA have also occurred which prevented CO₂ from fully desorbing from the beds, but they have been resolved with troubleshooting and crew time. Degradation modes occur in the sorbent bed as well as in ancillary equipment that interface intimately with the sorbent beds [50].

The Water Processor Assembly (WPA) uses activated carbon and ion exchange resin beds for the bulk of water purification. Not only does the system provide potable water recycled from waste streams but it also supplies water, at a specified purity, to the Oxygen Generation Assembly (OGA) to revitalize the cabin atmosphere. The multifiltration beds contain activated carbon and ion exchange resin. The ion exchange bed uses ion exchange resin. The OGA Inlet de-ionizing bed uses de-ionizing resin. The microbial check valves used in the WPA and OGA use an iodine-based ion exchange resin. The OGA also uses an ACTEX bed which is made of a mixed resin and performs as a deionizer. Because these beds are meant to be consumed during the purification process where they saturate with impurities over time, some beds are replaced

regularly. Due to regular maintenance cycles for the WPA and OGA, resin bed life management for beds in use and in storage are monitored closely regarding storage environment, shelf-life requirements, microbial growth, and variations in the levels and types of impurities, or contaminants, flowing through the system. Given varying factors and operating conditions, a water model and spares traffic model are used by NASA to track water throughput and quality as well as operational logistics like service life and maintenance schedules. [51]

Degradation of ECLSS packed beds plays a big role in understanding ECLSS design for long duration human exploration missions. A study done by Bagdigian et. al. determined the reliability and fit of ISS ECLSS, specifically the Water Recovery System (WRS) and Oxygen Generation System (OGS), for future missions to Mars based on factors like equipment mass utilization rates, achieved hardware operating lifetimes, and crew time spent on maintenance tasks [8]. If there was a way to use existing systems for long duration transit habitats or surface habitats on the way to and on the Moon and Mars, the role of ISS as a testbed for future missions can be fulfilled. The study concluded that certain units (from the 2015 standpoint) were ready while others needed further technology development due to high failure rates and degradation.

2.7 Degradation & Spares Logistics

In preparing for future missions to the Moon and Mars, calculating failure rate estimates, in the component, subsystem, and system levels, and their relationship with spares logistics have been studied in relation to crewed versus uncrewed (dormant) operations. ECLSS management during dormant operations, like those proposed for Mars transit habitats that are on standby while crew descend and stay on the surface, have several options. However, most plans expect certain units to shutdown with potential for periodic maintenance cycling. If the ISS ECLSS units were to be outfitted for Mars transit, not all are currently ready for a 1000-day mission. If

the equivalent mass of the existing state of the art flight tested units were compared to the life support consumables needed for 1000 days, certain regenerable units are more beneficial to bring while others are not. For example, Harry Jones found that the recycling mass, the mass of each ECLSS recycling unit plus three of its spares, can be more or less than the supply mass, consumable units, gas, or liquid plus 10% margin for tank mass and 10% margin for spares, for a roundtrip to Mars within 450 days with 4 crew [52]. It was found that the Carbon Dioxide Removal Assembly and Water Recovery System are worthwhile to bring on a spacecraft because they are approximately 6 times and 3 times less than the amount of mass to bring consumable LiOH canisters and water, respectively. The Oxygen Generation System, on the other hand, is more than double the mass of oxygen supply needed for the trip, making it more beneficial to bring oxygen gas tanks on just a mass basis. There are many considerations around this analysis, but it paints a picture of what could be useful for Mars transit and how degradation of ECLSS recycling units still plays a large role in these missions.

2.8 ECLSS Maintenance and Resupply

ECLSS maintenance is a recurring part of an astronaut's monthly or even weekly plan. ECLSS maintenance is dependent on resupply, spares, storage, tools available, hardware complexity, and software controls. Depending on interconnectivity with other systems like the Electrical Power System and the human crew loading, the magnitude and frequency of maintenance tasks can be proportional to the effect of those systems. Maintenance can be scheduled or unscheduled, complex or simple, and extremely impactful or minor. Based on work done by Eshima et. al., a Failure Modes and Effects Analysis (FMEA) on the ISS ECLSS found that there are varying causes, effects, and degrees of failure seen in the life of the ISS ECLSS [12].

Certain degradation modes are unavoidable while others are not. Degradation relates to performance as well as material breakdown. Most degradation modes are unavoidable as most primary ECLSS units are consumed over time based on usage and service life. However, avoidable degradation are instances where corrective actions can sustain unit performance and remaining useful life (RUL) for longer, making the unit more robust, or even going as far as reclaiming and increasing unit performance and RUL. The goal of understanding degradation is to design a life support system that is better equipped to survive known and unknown conditions. Degradation of ECLSS is complex, interconnected, nonlinear, and at times, recoverable. For future ECLSS design, a smart system that determines health status as well as execute actions to maintain good health, must know how baseline degradation occurs, how different inputs impact degradation rate, how degradation can be reversed if possible, and how to anticipate and possibly prevent degradation in the future. These metrics can be found by extensive component testing, modeling and simulations, estimation, and machine learning.

2.9 ECLSS Anomaly Resolution

Data analysis for spacecraft involves telemetry downlink, data processing and archiving, and interpretation of data for nominal monitoring or off-nominal investigations. For ECLSS, hundreds of telemetry data channels are downlinked to Mission Control and dispersed to teams, internal and external to NASA, that monitor specific subsystems. Data analysis focuses on drift trends, point anomalies, or simply off-nominal behavior, whether intermittent or sustained, to detect faults or failure modes and rapidly execute corrective actions. In anticipation of faults and failure modes, NASA utilizes a tool called the Caution and Warning System aboard various spacecraft and subsystems to set bounds on expected sensor readings [53]. This allows data analysis teams to detect abnormal behavior and immediately conduct investigations.

Investigations are conducted by many entities internal and external to NASA like within the Safety Review Panel (SRP) and Mission Evaluation Room (MER) which brief, discuss, and report failures and subsequently generate recommendations, rationales, and corrective actions [33].

2.10 Current ISS Anomaly Resolution Process

The ISS ECLSS is a complex and dynamic system that is heavily supported by multiple entities and teams regarding anomaly response and resolution. Anomalies in spacecraft life support systems are defined as any hardware or software performance characteristic that is or may be inconsistent with design or operational conditions. The investigation process can be broken down into three main parts: (1) the Missions Operations Flight Director takes responsibility for real-time actions in response to anomalies and to safe the vehicle, (2) the Mission Evaluation Room (MER) initiates a near-real-time anomaly investigation handled by discipline experts who continually monitor and support flight operations to enable continued and safe operations until the anomaly is resolved, and (3) corrective actions are executed, whether Mission Control sends commands up to the station or astronauts perform repair and replace (R&R) tasks, and the anomaly investigation is transitioned to the appropriate Subsystem Problem Resolution Team (SPRT), co-led by NASA and prime contractor subsystem managers [54]. All this diagnosis and prognosis work can't be done without database infrastructure to disseminate telemetry for near-real-time analyses, modeling and simulation capabilities to determine root cause of faults and failures, and subsystem design and operation information in the form of subject matter expertise, reports, blueprints, protocols, and flight rules.

2.11 Considerations for Future Life Support Anomaly Resolution

Anomaly resolution for life support systems of future exploration class vehicles may benefit from modifications and additions to the current process used for ISS ECLSS. Beyond the information and expertise provided by the Mission Flight Directorate and MER, advanced planning and control, higher fidelity fault trees, and additional Fault, Detection, Isolation, and Recovery (FDIR) reports may bring the vehicle management system closer to having the awareness and autonomy necessary to be self-sufficient beyond LEO. In accordance with the HOME objective for smart habitation in deep space, low technology readiness (TRL) research and development in system modeling, estimation, diagnosis, and prognosis may be combined with subject matter expertise and current spacecraft databases to create data-richness and further enable self-awareness and autonomy [55] [56] [57]. Other considerations include the inference of system state by sensor prioritization and criticality, the use of sensor arrays and mobile sensors, the use of self-actuation versus mobile manipulation, and finally the choice between in-place redundancy versus a repair and replace (R&R) strategy for fault tolerant subsystem design. Finally, degradation modeling and simulation can be utilized to determine nuanced effects of operational conditions, anomalies, and faults that can cause varying rates of degradation.

Chapter 3 Carbon Dioxide Removal Model Using Aspen Adsorption

3.1 ECLSS Simulations and Modeling Purpose & Objectives

To generate data for smart habitat modeling and low-TRL research into the application of machine learning for ECLSS diagnostics, prognostics, and control, the work presented here describes the development, set up, and use of simulation models for a carbon dioxide removal system using Aspen Adsorption, a chemical process simulator program, and MATLAB, a widely-used computing program. The carbon dioxide removal system was chosen based on work by members of HOME at CU Boulder who found that CO₂ Removal on the ISS has historically had the highest frequency of problems in operation and was therefore an appropriate candidate for fault and degradation focused smart habitat research for HOME [12].

The resulting CO₂ Removal testbed that was funded and built for HOME is a one-bed zeolite 13X CO₂ removal system that has the capability to test different faults and generate data for various types of failure modes. More information about the testbed is provided in the next section. The failure data signatures, in large amounts and replicates, are critical for training algorithms that can then provide diagnostics and prognostics to monitor the health of various systems and potentially recommend and execute corrective actions. Unfortunately, testbed start-up and operation can take multiple days to complete one test. Generating data from the testbed is extremely valuable, but it takes a long time. To combat this, models were developed to generate copious amounts of simulation data, i.e. nominal and off-nominal sensor data. Models require verification and validation; therefore, the testbed serves to validate simulation data.

3.2 STEVE Testbed

The Simulation Testbed for Exploration Vehicle ECLSS (STEVE), a physical testbed operated at CU Boulder, is shown below. The STEVE testbed comprises a single sorbent bed for batch removal of CO₂ laden air which is pressure fed using compressed gas cylinders and mass flow controllers, unlike CDRA which uses a blower. The sorbent bed is packed with 13X zeolite pellets, but it can also be packed with other sorbent materials. The CO₂ sorbent bed either removes CO₂ from the provided air flow (adsorption) or releases CO₂ under thermal vacuum (desorption). This alternating function is typical of scrubbing systems that work with pairs of beds that adsorb and desorb at the same time – allowing constant CO₂ removal of the cabin air stream the way CDRA operates.

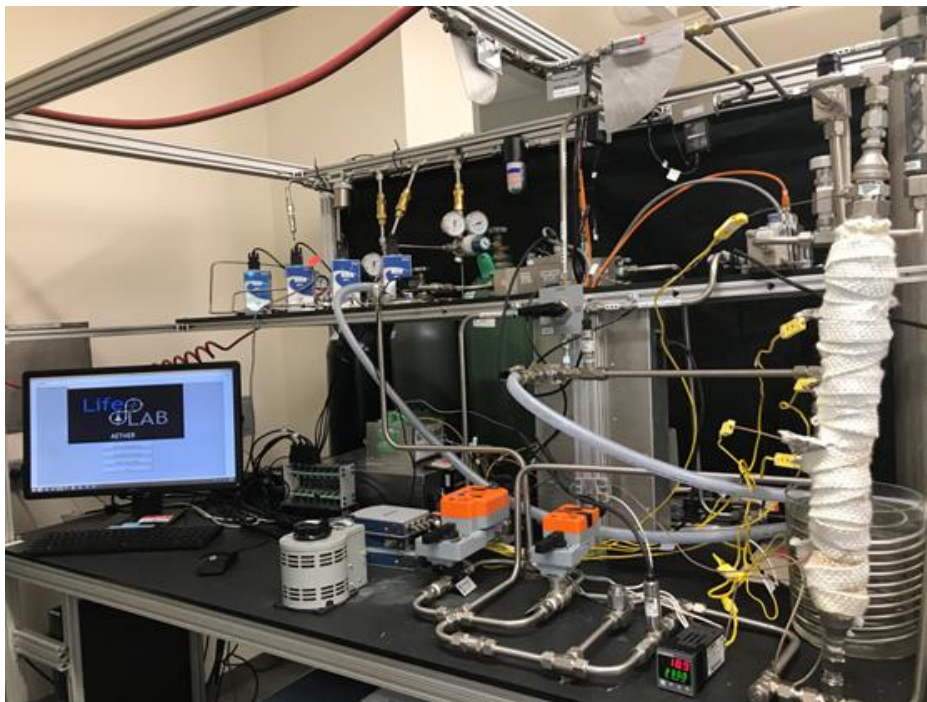


Figure 8. STEVE Testbed

During adsorption, the apparatus supplies a specified flow of CO₂-laden air to the sorbent bed. Nominally, STEVE provides a gas mixture with 78.86% nitrogen, 20.84% oxygen, 0.3%

carbon dioxide, and dew point of approximately -50°C which is achieved with a desiccant bed packed with Drierite beads. At this concentration, the CO_2 partial pressure is approximately 2.1 mmHg. An automated LabVIEW system commands the flow, valve positions, heater, and vacuum pump from their setpoints for CO_2 adsorption to those needed for desorption. A rope heater raises the insulated bed temperature to approximately 200°C and a vacuum pump reduces pressure to below 20 mmHg for CO_2 desorption and regeneration of the pellets via thermal-pressure swing. The adsorption/desorption cycle can be repeated for a specified number of cycles [23].

3.3 STEVE Aspen Model

This section focuses on the use of Aspen Adsorption V10, an extension of the Aspen Plus software, to simulate the scrubbing process of the STEVE testbed. To model the testbed, each major component is added as a block, configured with the appropriate test settings, and connected via fluid streams or control streams. Test settings include material properties, flow rates, temperatures, and pressures to name a few. The bed model block, which is the heart of the system, includes the governing equations for the mass, momentum and energy balances as well as the adsorption isotherm model for the sorbent material used.

Adsorption is a process where molecules move from a bulk fluid phase (liquid or gas) towards the surface of a solid material, in other words diffusing into the pores of a solid particle and binding to the surface at specific sites. The driving force behind the desorption, or regeneration, step following adsorption is achieved by pressure-swing adsorption (PSA), temperature-swing adsorption (TSA), or a combination of the two, i.e. thermal-pressure or thermal-vacuum swing. The adsorption process for the STEVE testbed is thermal-pressure swing, where the adsorption stage occurs at ambient temperature and pressure and desorption

occurs at high temperature and low pressure. It is typical to use isotherm model parameters, generated empirically, to model the effects of varying concentrations, flow rates, pressures, and temperatures with different materials. They are called isotherm models because they capture the amount of adsorbed gas at varying partial pressures at a constant temperature. Typically, the isotherm model has varying forms and amounts of terms which are dependent on the type of material under test and best fit to experimental data. The terms represent different types of adsorption sites for that material and typically contain a saturation capacity which is the maximum allowable adsorbed amount at that site and an affinity coefficient, typically temperature dependent, which is multiplied by the gas partial pressure or concentration in the sorbent bed. The isotherm model used here is the Dual-Site Langmuir model for zeolite 13X, an empirically determined and recommended model based on best-fit compared to other models [31], [58], [59]:

$$q = \sum_{j=1,2} \frac{a_j b_j P}{1 + b_j P}$$

$$b_j = b_o \exp\left(\frac{E_j}{RT}\right)$$

, where j represents parameters for site 1 and 2, q is the adsorbed molar amount of the gas component per mass of sorbent, a_j is the saturation capacity parameter, b_j is the affinity parameter, P is partial pressure of the gas component, E_j the energy term, R is the ideal gas constant, and T is temperature of the sorbent.

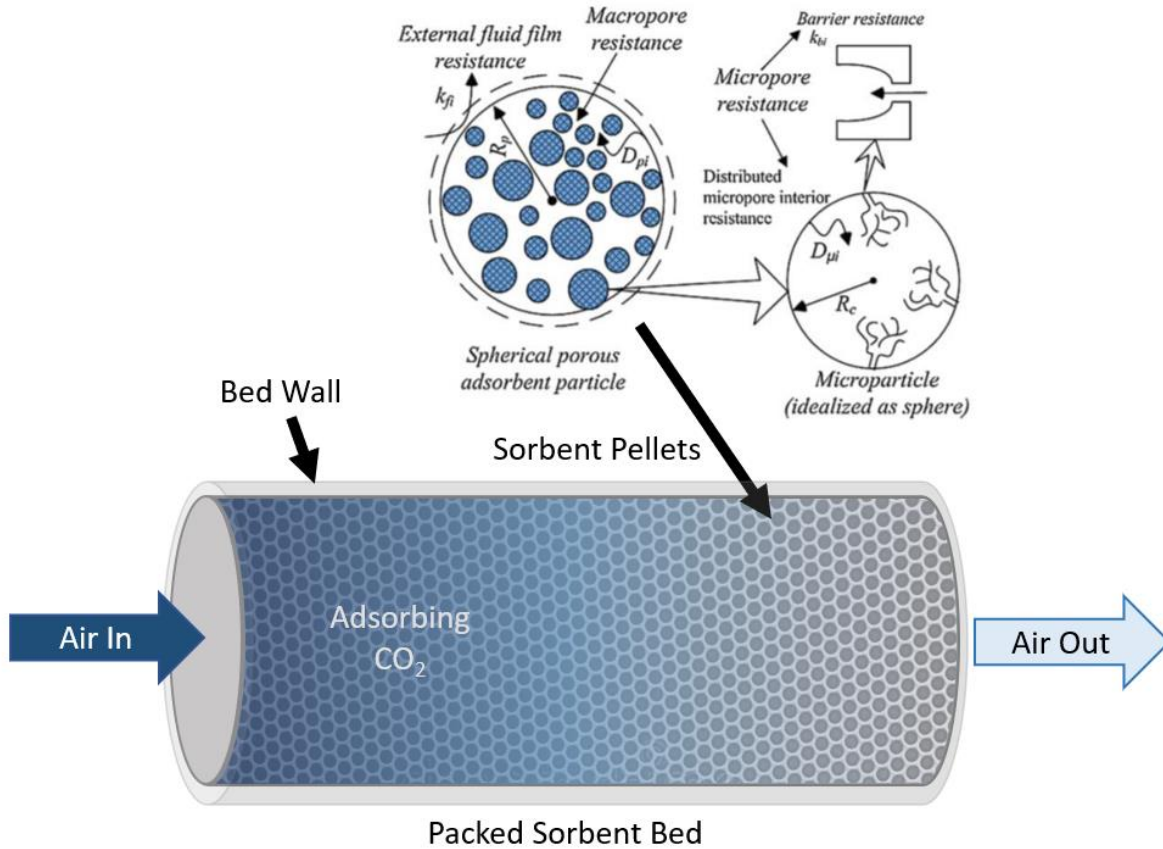


Figure 9. Diagram of a Sorbent Packed Bed with a Close-Up of a Spherical Porous Adsorbent Particle [60]

Modeling packed beds typically require other parameters like gas, solid, and wall density as well as void fraction. Since the solid adsorbent comes in the form of porous beads, density and void fraction helps to simulate the free flow area of the gas flowing through the packed bed. Void fractions, or porosities, of a packed bed is the total of external (inter-) and internal (intra-) particle voids within a packed bed over the total volume. Internal voids are the pockets and pores within pellet that gaseous components can attach to while external voids are the interstitial spaces between pellets. In addition, pellet shape, such as cylinders and spheres, can affect porosity. The behavior of gasses in a packed bed are characterized by equations for pressure drop and compressibility as well. When gas flows through a packed bed, it has a decrease in pressure

from the immense source of friction due to impacting beads, or particles, in the bed. Here, the Ergun equation is used, which handles both laminar and turbulent flow through a packed bed [61].

3.4 Aspen Adsorption Model

STEVE is composed of pressurized gas cylinders, inlet mass flow controllers, one sorbent bed, upstream and downstream sensors, upstream and downstream valves, an electric rope heater wrapped around the bed, and a vacuum pump. These components are modeled in the STEVE Aspen Adsorption model detailed below.

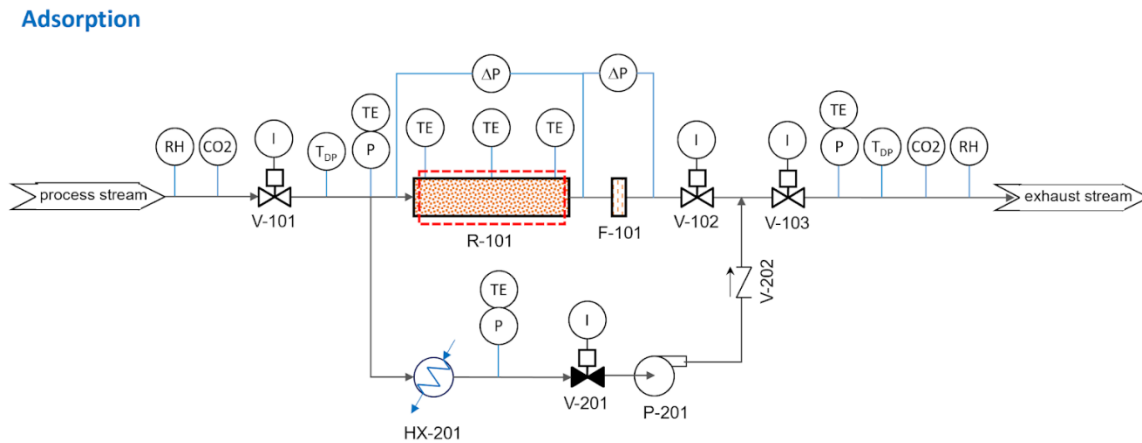


Figure 10. STEVE Schematic [23]

The Aspen Adsorption model is a virtual replicate of the STEVE testbed. The schematic is pictured below with the blue dotted line marking gas flow during adsorption and red dotted line marking gas flow during desorption. The GasFeed block sets the inlet composition of air entering the system at a specified pressure. Following the STEVE testbed CO₂ amount, the Aspen model inlet gas stream is set to 0.3% CO₂ and 99.7% N₂. The adsorption effects of O₂ was not considered as the adsorption is negligible and removing it does not affect the operation of the system. In addition to composition, the inlet pressure is set to ambient, approximately 100 kPa or

1 bar. Next, the air stream travels through valve VI (I for inlet), representing the mass flow controller, which sets the flow rate of the air stream to any specified range. The STEVE tests are typically run at 8 SLPM, so any flow rate between 1 to 10 SLPM can be simulated. Then the air stream enters through the bottom of the sorbent bed which is capped on the top, B5, and bottom, B4 with voids that allow for multiple inlet and outlet streams to the sorbent bed block.

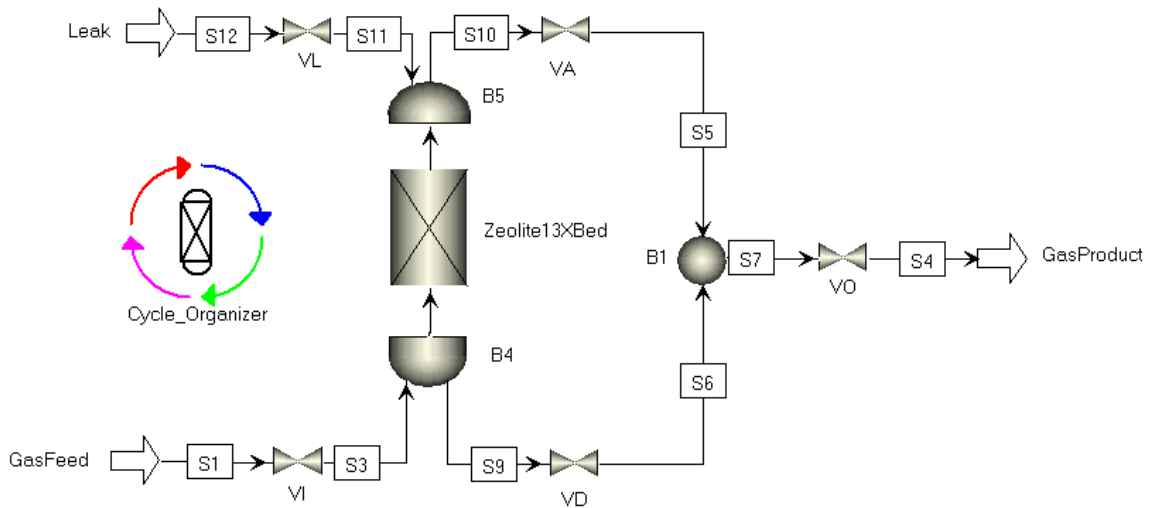


Figure 11. Aspen Adsorption Model of the STEVE Testbed

During adsorption, valve VD (D for desorption) is closed while valve VA (A for adsorption) is open. The air stream travels through the sorbent bed block which handles all mass, momentum, and energy balance equations and solves for adsorbed carbon dioxide over time. Then the air stream flows through the tee junction at B1 which is a void block with multiple inlet and outlet capability. Finally, the air stream flows through valve VO (O for outlet) which acts as the filter downstream of the STEVE sorbent bed before flowing out of the GasProduct block, the exhaust. During desorption, VI and VA are closed, the sorbent bed jacket heater is activated to a set point temperature, VD is opened, and GasProduct is commanded to pull a vacuum with a low pressure and act as a vacuum pump.

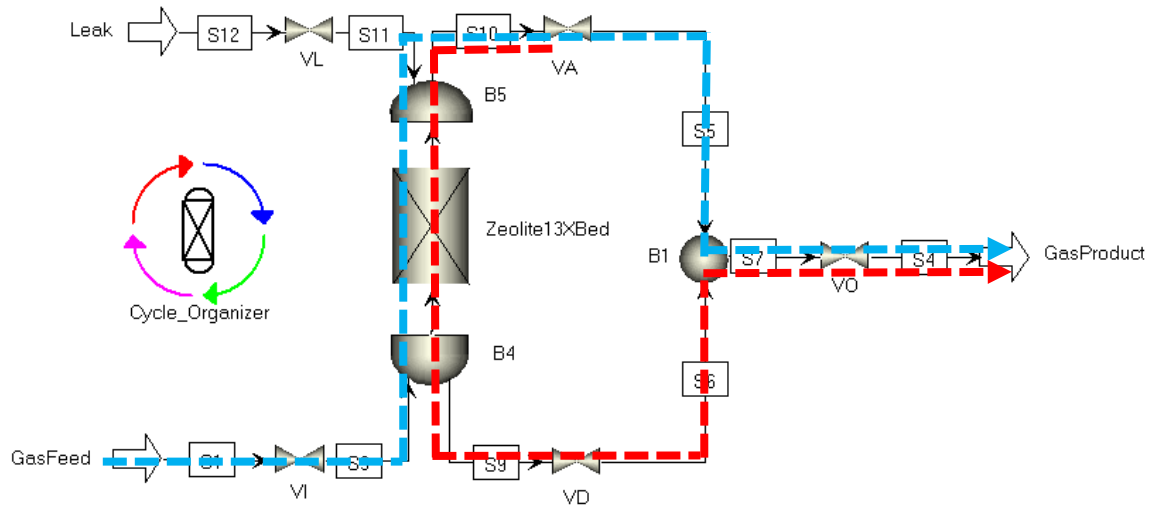


Figure 12. Aspen Adsorption Model of the STEVE Testbed where the blue dotted line is the Adsorption flow and the red dotted line is the Desorption flow.

All controls for cyclic operation, alternating between adsorption and desorption, is done using the Cycle_Organizer tool. Aspen Adsorption has the benefit of reporting all stream results for each block in the schematic as well as all stream connections. Data that would otherwise be recorded by a sensor can be recorded and extracted from the model by selecting the variable from the block and plotting it over time. Therefore, no sensor blocks were added to the model. To implement noise to signals, the Aspen Adsorption file can be opened in Aspen Custom Modeler where a noise block can be applied to a variable of choice such as outlet concentration of carbon dioxide.

The purpose of this model is to simulate nominal and off-nominal operation. Nominal operation follows the STEVE testbed procedure without any failure injections. For off-nominal simulations, faults are injected as listed in the table below.

Table 3. Failure Modes that can be simulated in Aspen Adsorption [23]

Failure Mode	Physical Test Method	Possible Root cause
Valve Failure	Commanding valve position to partially open or closed	<ul style="list-style-type: none"> ▪ Dusting ▪ Actuator failure
	Slow valve actuation by commanding a different speed of rotation	<ul style="list-style-type: none"> ▪ Dusting ▪ Actuator failure
	Cause valve to operate incorrectly (ON when OFF)	<ul style="list-style-type: none"> ▪ Multiplexer failure
Leak	Loosen a tube connection	<ul style="list-style-type: none"> ▪ Wear and tear ▪ Human error during maintenance
Sensor Failure	Use a biased (i.e. uncalibrated) sensor	<ul style="list-style-type: none"> ▪ Sensor degradation
	Incorrect excitation voltage to the sensor	<ul style="list-style-type: none"> ▪ Power system failure
	Loss of sensor signal (e.g. zero out in the data file)	<ul style="list-style-type: none"> ▪ Sensor failure
Blower Failure	Use a biased (i.e. uncalibrated) mass flow controller	<ul style="list-style-type: none"> ▪ Sensor degradation
	Change flow rate during simulation	<ul style="list-style-type: none"> ▪ Bad current to blower
Heater Failure	Change the temperature setpoint	<ul style="list-style-type: none"> ▪ Power system failure ▪ Heater control failure

3.5 Aspen Adsorption Model Set Up

Introduction tutorials exist for Aspen Adsorption, but the information and guides are not specific to carbon dioxide removal and can be challenging to follow, especially with regard to nuances in running simulations successfully and understanding errors [62], [63]. The following steps were documented to create and run an Aspen Adsorption CO₂ removal system model:

1. Open a new file and save with a filename like “CO₂ Removal System”.
2. Set up the main fluid components of your system.
3. In the simulation explorer, click “Component Lists”.
4. In the Component Lists folder, double-click on “Configure Properties”.
5. In the pop-up Physical Properties Configuration box, click on “Use Aspen properties system” then click on “Edit using Aspen Properties”.

6. Aspen properties will automatically open. Add components under Component ID – in this case, “CO₂” for carbon dioxide and “N₂” for nitrogen. Oxygen and water vapor can be added as well.
7. Click on the “Next” button.
8. This opens the Methods - Specification tab. Within the Global tab for Method Filter choose “COMMON” and for Base Method choose “Ideal Gas”.
9. Now click on the “Run” button and save the file when prompted.
10. Now go back to Aspen Adsorption and find the green box next to “Configured using Embedded Aspen Properties”. Click “OK”.
11. In the Build Components list box, choose CO₂ and N₂ and click on the right-facing button to add the gas properties into the Aspen Adsorption model. Click “OK”.
12. Next, drag and drop physical components of interest to the flowsheet.
13. Ensure that the Model Library tab is visible at the bottom of the screen. If not, go to the View tab and click on “Model Libraries” to enable and display it.
14. In the drop down menu in the library, choose “Adsim”. Then click on the “Gas: Dynamic” tab.
15. Drag and drop the following components into the workspace: bed, valves, “pump” valve, feed source, and product endpoint.
16. Afterwards, click on “Connections” and choose “gas_material_connection”. Then click once for the starting point, making sure to click on a blue arrow on the source object, and click a second time on a blue arrow on the end object. You may drag the blue arrow to your desired location on the object for visual ease. Then the arrow resets to source. Repeat for all components in the system.
17. Set up the feed source with the inlet flow rate and composition of interest.
18. Set up the product endpoint properties and reverse composition.
19. Set up the valves with the appropriate Active Specification and parameter values: open (1), closed (0), operating with a specific Cv (2), or operating at a specified flow rate (3).
20. Lastly, set up the bed with the appropriate parameters and settings. Refer to the Block Descriptions in the next section for more information.
21. Note, signal noise and control modules can be added to data streams using Aspen Custom Modeler.

3.6 Aspen Adsorption Model Block Descriptions

The following model blocks represent hardware components in the STEVE testbed.

Inlet

The GasFeed block is the inlet to the system. This block is used to set the gas composition, temperature, and pressure of the air stream that will enter the sorbent bed. The inlet is a reversible pressure setter with reporting enabled. Because this block represents the gas into

the system, flow rate is not specified and set to “Free”. Flow rate is set in the following block in the diagram. The gas composition is specified as a fraction of 1 where 1 is 100%. Thus, CO₂ is set to 0.003 kmol of CO₂/ kmol which is equal to 0.30% of the total gas stream, and the rest is N₂. Temperature is set to 289.15 K which is room temperature. Pressure is set to ambient at 1.1 bar.

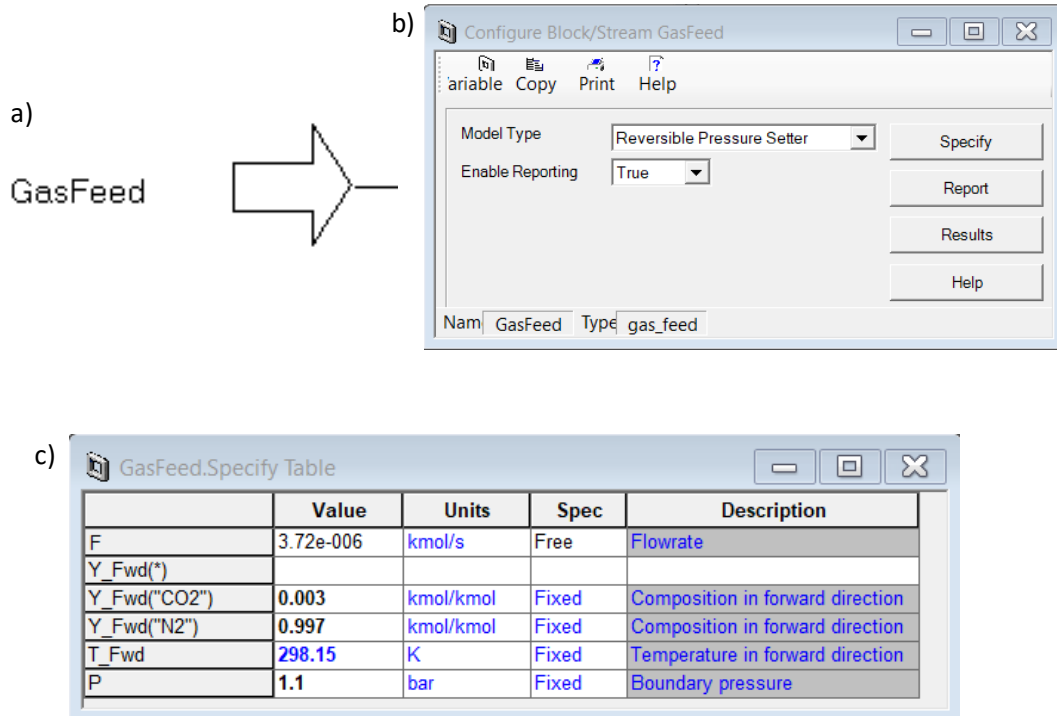


Figure 13. Images of the a) GasFeed block, b) GasFeed configure screen and c) the GasFeed Specification table.

Sorbent Bed

The sorbent bed, called “Zeolite13Xbed” in the diagram, is the main component in this system and relies on the adsorption properties of the zeolite 13X material and physical properties of the STEVE packed bed. The bed is set to Vertical because STEVE is vertically placed (as of March 2022). The 1-phase jacket type heater was selected to mimic the electrical rope heater

used for STEVE. In the General tab, the discretization method was set as USD1, the Upwind Differencing Scheme, and the number of nodes, or slices, was set to 20, the default value. For the Material/Momentum Balance, the Ergun equation was used as advised by literature and for ease of simulation, the assumption was set to “convection only”. This was later changed to include dispersion as well – given parameter values from literature review of a similar packed bed [31]. For the kinetic model, the film model assumption was set to solid since the sorbent is solid zeolite beads. As advised by literature, the kinetic model was set to use a linear lumped resistance model [58]. The mass transfer coefficient was set to constant as provided by literature as well. The default setting was set to apply cyclic correction and was not changed for this model. Based on literature applied to research on zeolite 13X and CDRA, the Dual-site Langmuir model was selected which uses Partial Pressure (rather than concentration) and does not use a fugacity term [64]. For the energy balance, we assume a non-isothermal balance with gas and solid conduction, meaning temperature change is dependent on the environment and is affected by the gas, heater, and sorbent solid temperatures. Coefficients, conductivities, and capacities provided in literature were set to constant and the rigorous wall model was selected for heat transfer to the environment [58]. Lastly, no reactions are taking place and no additional user procedures were added.

Under specify, all necessary values were set as seen in the Specify Table in Figure 20. All values are based on the physical STEVE testbed and literature values for the zeolite 13X sorbent bead, CO₂ mass transfer with the sorbent, and steel piping. It is important to note that the isotherm parameters, specifically for CO₂ not N₂, were slightly modified from literature to better match STEVE operation through sensitivity analyses. It is not important to match N₂

breakthrough as it is not currently being measured in STEVE and exhibits negligible adsorption in the sorbent bed.

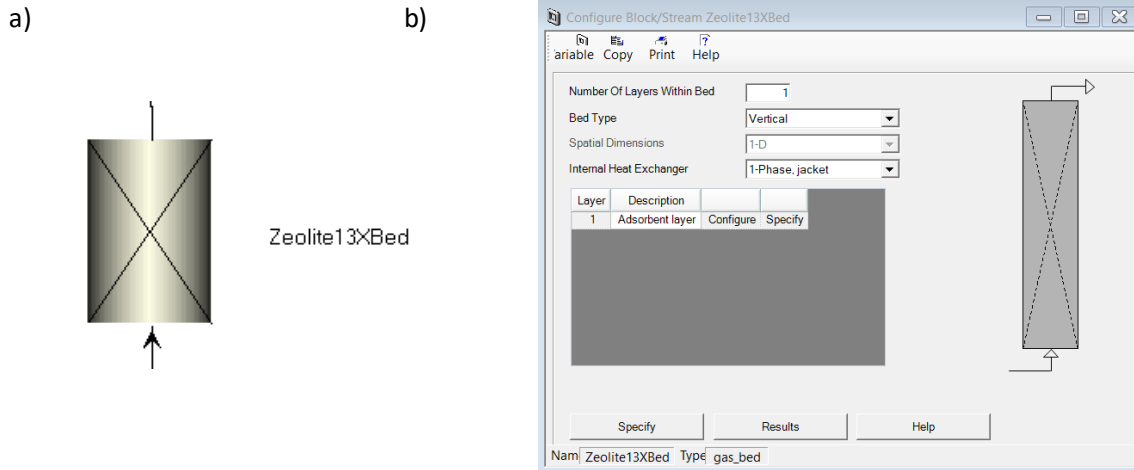


Figure 14. Images of the a) reactor block labeled “Zeolite13XBed” and b) the main configure screen where orientation and heater options are selected.

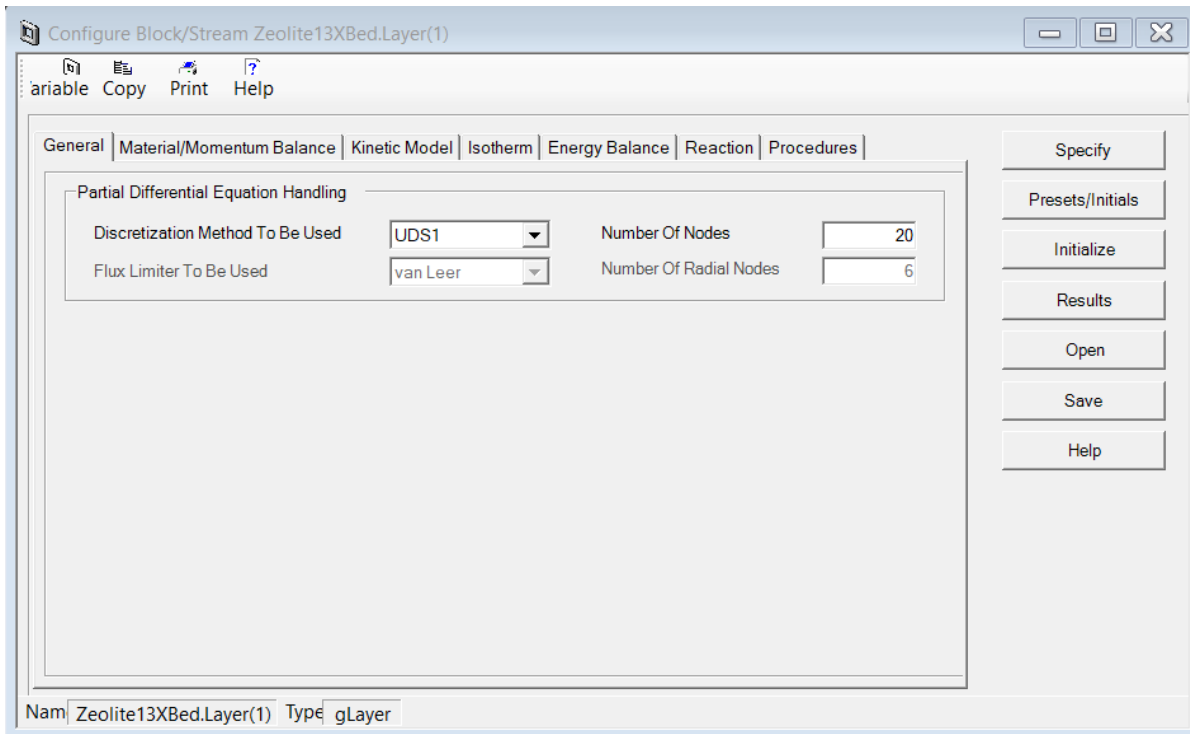


Figure 15. Image of the reactor block General tab where the discretization method and number of nodes are selected. This screen appears when clicking on the diagram of the reactor in the previous figure.

The screenshot shows the 'General' tab of a reactor block configuration. The tabs at the top are: General, Material/Momentum Balance, Kinetic Model, Isotherm, Energy Balance, Reaction, and Procedures. The 'General' tab is active. It contains three dropdown menus: 'Material Balance Assumption' set to 'Convection Only', 'Momentum Balance Assumption' set to 'Ergun Equation', and '2-D Dispersive Properties' set to 'Fixed'.

Figure 16. Image of the Material/Momentum Balance tab where the material and momentum balance assumption options are selected.

The screenshot shows the 'Material/Momentum Balance' tab of a reactor block configuration. The tabs at the top are: General, Material/Momentum Balance, Kinetic Model, Isotherm, Energy Balance, Reaction, and Procedures. The 'Material/Momentum Balance' tab is active. It contains several settings: 'Film Model Assumption' set to 'Solid', 'Kinetic Model Assumption' set to 'Lumped Resistance', 'Form Of Lumped Resistance Model' set to 'Linear', 'Molecular Diffusivities' set to 'Fixed', 'Form Of Mass Transfer Coefficient' set to 'Constant', 'Apply Cyclic Correction' set to 'Yes', 'Estimated Mass Transfer Coefficient Assumption' set to 'Macropore Only', 'Number Of Nodes' set to '5', and 'Effective Diffusivity' set to 'Fixed'.

Figure 17. Image of the Kinetic Model tab where the kinetic model and mass transfer options are selected.

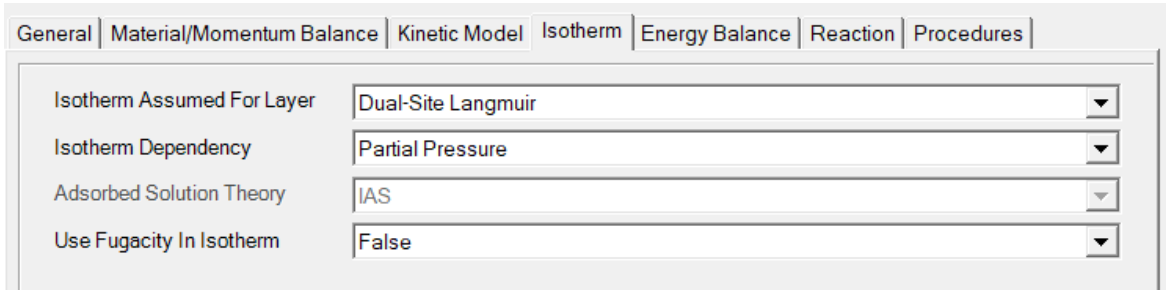


Figure 18. Image of the Isotherm tab where the isotherm model and dependency options are selected.

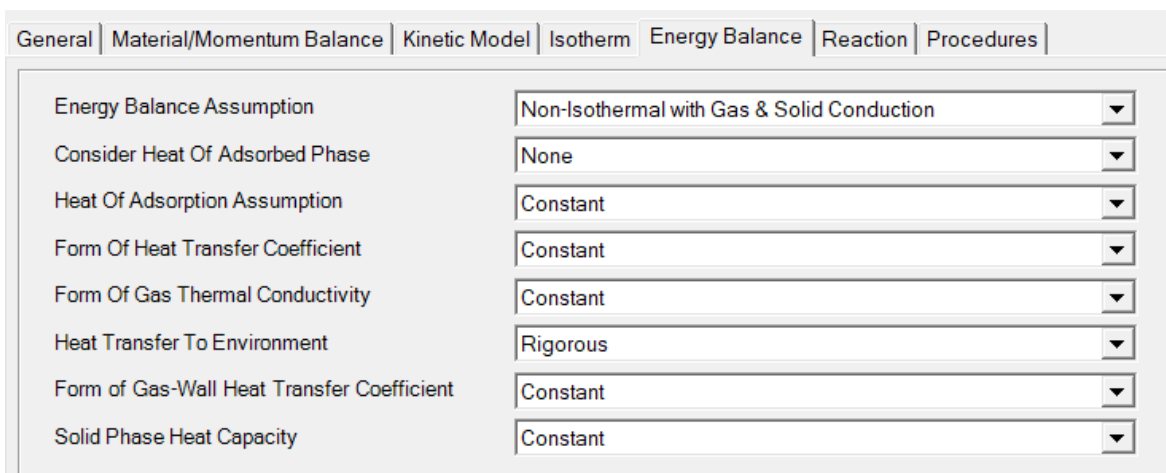


Figure 19. Image of the Material/Momentum Balance tab where the material and momentum balance assumption options are selected.

Zeolite13XBed.Layer(1).Specify Table			
	Value	Units	Description
Hb	20.0	in	Height of adsorbent layer
Wt	0.005	m	Wall thickness used of bed
Db	0.87	in	Internal diameter of adsorbent layer
Ei	0.41	m ³ void/m ³ bed	Inter-particle voidage
Ep	0.21	m ³ void/m ³ bead	Intra-particle voidage
RHOs	756.0	kg/m ³	Bulk solid density of adsorbent
Rp	8.e-004	m	Adsorbent particle radius
SFac	1.0	n/a	Adsorbent shape factor
MTC(*)			
MTC("CO2")	0.065	1/s	Constant mass transfer coefficients
MTC("N2")	0.02	1/s	Constant mass transfer coefficients
IP(*)			
IP(1,"CO2")	5.21e-009	n/a	Isotherm parameter
IP(1,"N2")	1.e-009	n/a	Isotherm parameter
IP(2,"CO2")	5401.0	n/a	Isotherm parameter
IP(2,"N2")	3000.0	n/a	Isotherm parameter
IP(3,"CO2")	2.35e-006	n/a	Isotherm parameter
IP(3,"N2")	1.e-006	n/a	Isotherm parameter
IP(4,"CO2")	5401.0	n/a	Isotherm parameter
IP(4,"N2")	3000.0	n/a	Isotherm parameter
IP(5,"CO2")	6.39e-008	n/a	Isotherm parameter
IP(5,"N2")	1.e-008	n/a	Isotherm parameter
IP(6,"CO2")	4197.0	n/a	Isotherm parameter
IP(6,"N2")	3000.0	n/a	Isotherm parameter
IP(7,"CO2")	1.77e-006	n/a	Isotherm parameter
IP(7,"N2")	1.e-006	n/a	Isotherm parameter
IP(8,"CO2")	4197.0	n/a	Isotherm parameter
IP(8,"N2")	3000.0	n/a	Isotherm parameter
Direction	0.0	n/a	Specified flow direction (self determined: 0, forward: 1)
Cps	980.0	J/kg/K	Adsorbent specific heat capacity
Cpw	475.0	J/kg/K	Wall specific heat capacity
DH(*)			
DH("CO2")	40.0	MJ/kmol	Constant for heat of adsorption
DH("N2")	0.0	MJ/kmol	Constant for heat of adsorption
Hamb	3.0	W/m ² /K	Heat transfer coefficient between wall and ambient
HTC	128.0	W/m ² /K	Constant for the heat transfer coefficient
Hw	16.0	W/m ² /K	Constant heat transfer coefficient between gas and wall
Kg	0.015	W/m/K	Constant for the gas phase heat conductivity
Ks	0.152	W/m/K	Adsorbent thermal conductivity
Kw	14.2	W/m/K	Wall thermal conductivity
Rhow	7800.0	kg/m ³	Wall density
Tamb	300.0	K	Ambient temperature
ap	2212.5	1/m	Specific surface area of adsorbent
aHx	2000.0	1/m	External specific surface area of heat exchanger
UHx	10.0	W/m ² /K	Overall (gas to medium) heat transfer coefficient

Figure 20. Image of the Specifications Table where all appropriate parameter values are populated such as physical, mass transfer, and heat transfer properties.

The specifications for the physical properties of the bed were aligned with STEVE values [23]. The mass transfer and heat transfer coefficients were set based on literature values [31], [64], [65]. The isotherm parameters were taken from literature as well but modified to fit the equation

form used in Aspen Adsorption [64]. Equation 1 describes the Dual Site Langmuir equation used in literature and equation 4 describes the same equation in a different form in Aspen Adsorption and the transformed parameters following:

$$n = \frac{a_1 b_1 P}{1 + b_1 P} + \frac{a_2 b_2 P}{1 + b_2 P} \quad (1)$$

$$a_1 = a_{01} + c_{01}/T \text{ and } a_2 = a_{02} + c_{02}/T \quad (2)$$

$$b_1 = b_{01} \exp \left[\frac{E_1}{RT} \right] \text{ and } b_2 = b_{02} \exp \left[\frac{E_2}{RT} \right] \quad (3)$$

, where n is the amount of gas adsorbed in mol per kg of sorbent, a is the saturation capacity, b is the affinity parameter and P is the partial pressure of the gas, which can be interchanged with concentration. a_0 , b_0 , c_0 , and E are fitted parameters and T is the temperature of the sorbent. In general, the two terms represent two different types of temperature and partial pressure dependent adsorption sites on the porous surface of the sorbent pellets, where one or the other may have stronger capacity or affinity for the adsorbate.

$$W = \frac{IP_1 e^{IP_2/T} P}{1 + IP_3 e^{IP_4/T} P} + \frac{IP_5 e^{IP_6/T} P}{1 + IP_7 e^{IP_8/T} P} \quad (4)$$

, where W is the same as n , the amount of gas adsorbed and IP stands for ‘‘Isotherm Parameter’’. The following table provides the conversions between the parameters in equation 1-3 to the IP parameters needed for the model in equation 4.

Table 4. Conversion of Dual-Site Langmuir Parameters from Literature to Aspen Adsorption

Aspen Adsorption	Literature [64]
IP_1	$a_1 b_{01} = (a_{01} + c_{01}/T) b_{01}$
IP_2	E_1
IP_3	b_{01}
IP_4	E_1
IP_5	$a_2 b_{02} = (a_{02} + c_{02}/T) b_{02}$
IP_6	E_2
IP_7	b_{02}

IP_8	E_2
--------	-------

	Value	Units	Spec	Derivative	Description
ProfileType	Constant				Is the bed initially specified with constant o
Y_First_Node(*)					
Y_First_Node("CO2")	0.0	kmol/kmol	Initial		Mole fraction within first element
Y_First_Node("N2")	1.0	kmol/kmol	Initial		Mole fraction within first element
Vg_First_Node	0.24	m/s	Initial		Gas velocity within first element
W_First_Node(*)					
W_First_Node("CO2")	0.0	kmol/kg	Ratelinitial	0.0	Solid loading within first element
W_First_Node("N2")	0.0	kmol/kg	Ratelinitial	0.0	Solid loading within first element
Tg_First_Node	298.0	K	Initial		Gas temperature within first element
Ts_First_Node	298.0	K	Initial		Solid temperature within first element
Tw_First_Node(1)	300.0	K	Initial		Wall temperature

Figure 21. Image of the Presets/Initials where the initial conditions for gas and solid phase compositions as well as velocity and temperatures are populated.

Voids

The voids are used to allow multiple stream inputs and outputs to the sorbent bed block to mimic STEVE operation, here labeled B5 for the upper void and B4 for the lower void. The sorbent bed block does not allow for more than one input or output stream, so voids are typically used to allow for multiple ports. They are set to default settings: reversible pressure setters, uses compression term, and are adiabatic. Both voids are set to a very small, or negligible, volume of 1e-5 cubic meters since it acts as a small tee junction. In Presets/Initials, both are set to have no CO₂ and only N₂ present initially at a starting temperature of 298.15 K, room temperature. The only difference is pressure. For ease of simulation, the pressure of the upstream block B4 is set slightly lower than B5 to induce the direction of flow from the bottom to the top, mimicking STEVE operation. The pressure setting is only an initial setting and will change as the simulation runs.

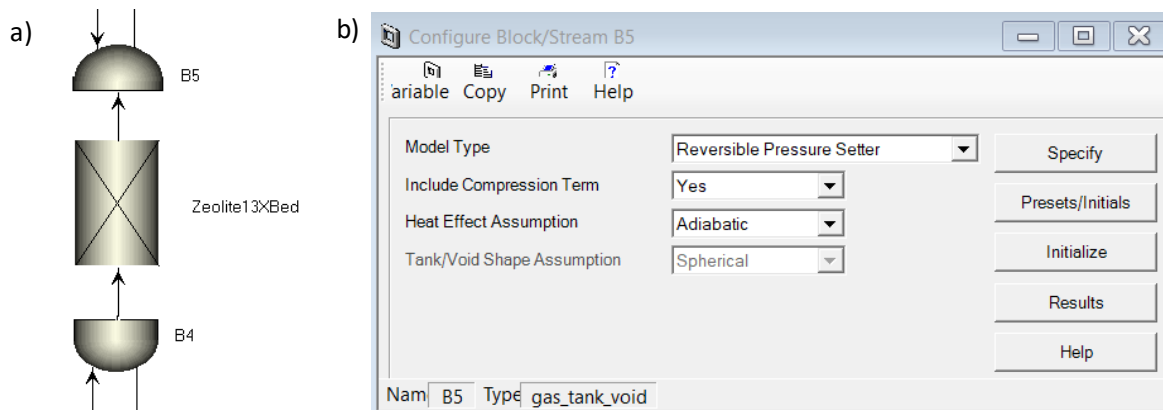


Figure 22. Images of the a) void blocks labeled “B4” and “B5” and b) the main configure screen.

	Value	Units	Spec	Description
Tank_Volume	1.e-005	m3	Fixed	Total volume of tank/void

Figure 23. Image of the void block specification for volume.

	Value	Units	Spec	Derivative	Description
Y(*)					
Y("CO2")	0.0	kmol/kmol	Free		Composition within tank/void
Y("N2")	1.0	kmol/kmol	Initial		Composition within tank/void
T	298.15	K	Initial		Temperature within tank/void
P	0.9	bar	Initial		Pressure within tank/void

Figure 24. Image of the Presets/Initials for the downstream void block “B5” where the initial conditions for gas phase compositions as well as pressure and temperatures are populated.

	Value	Units	Spec	Derivative	Description
Y(*)					
Y("CO2")	0.0	kmol/kmol	Initial		Composition within tank/void
Y("N2")	1.0	kmol/kmol	Free		Composition within tank/void
T	298.15	K	Initial		Temperature within tank/void
P	0.95	bar	Initial		Pressure within tank/void

Figure 25. Image of the Presets/Initials for the downstream void block “B4” where the initial conditions for gas phase compositions as well as pressure and temperatures are populated.

Valves

The valve blocks act as valves or mass flow controllers depending on their settings. To follow STEVE operation, VI, I for inlet, acts as a mass flow controller with a specified flow rate, VL, L for leak, is a hole or leak with a specified Cv or flow rate, VA, A for adsorption, and VD, D for desorption, act as shutoff valves (fully open/closed) or partial open valves with specified Cv values, and VO, O for outlet, is always set to ON or fully open and can have a modified Cv value to mimic filter dust accumulation at the outlet of the bed. All valves are set as Reversible Pressure Setters with linear valve characteristics, no stop action applied, Flow/Cv specifications made available, and temperature calculated from the energy balance of each valve. Cv stands for coefficient of variation and is used for sizing valves. All values are specified according to their configuration/role in a cycle phase, i.e. adsorption vs desorption, etc. Refer to the Valve Settings table below. For nominal operation (i.e. no leak or any faults), VL will be set to 0, fully closed.

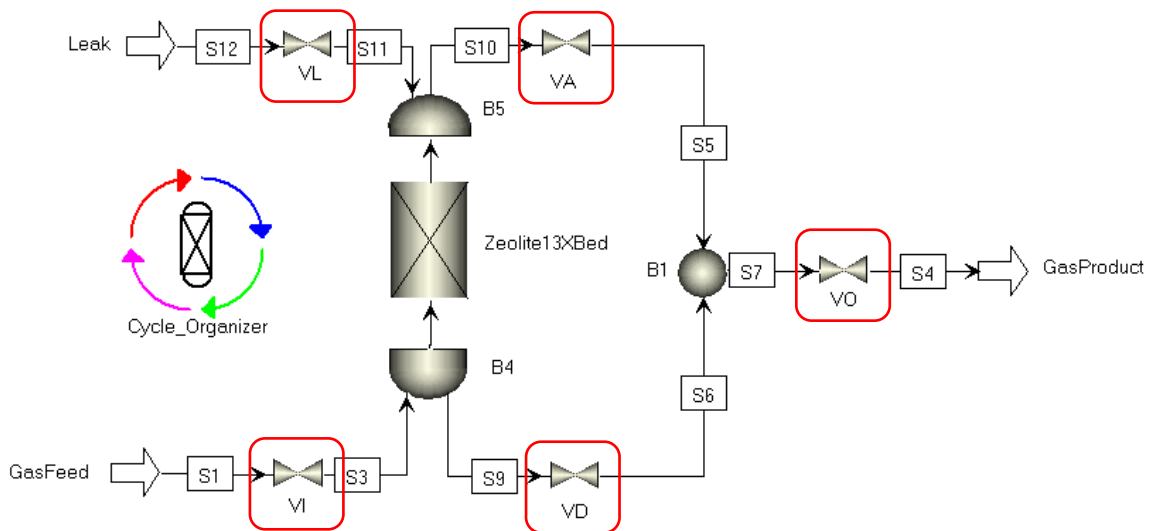
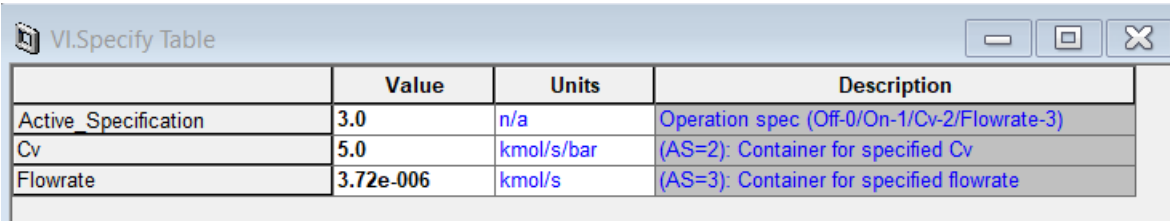


Figure 26. Image of the valve blocks labeled “VI”, “VL”, “VA”, “VO”, and “VD”.



	Value	Units	Description
Active Specification	3.0	n/a	Operation spec (Off-0/On-1/Cv-2/Flowrate-3)
Cv	5.0	kmol/s/bar	(AS=2): Container for specified Cv
Flowrate	3.72e-006	kmol/s	(AS=3): Container for specified flowrate

Figure 27. Image of the Specifications table for the inlet valve block “VI” which acts as a mass flow controller.

Table 5. Valve Settings

Label	Valve ID	Adsorption			Desorption		
		Active Spec.	Cv (2)	Flowrate (3)	Active Spec.	Cv (2)	Flowrate (3)
Inlet	VI	3	-	5.56e-6 kmol/s*	3	-	5.56e-6 kmol/s*
Leak	VL	2	1e-5 kmol/s/bar**	-	2	1e-5 kmol/s/bar**	-
Adsorption	VA	1	-	-	0	-	-
Desorption	VD	0	-	-	1	-	-
Outlet	VO	1	-	-	1	-	-

*Calculated based on density of air and 8 SLPM flowrate.

**Guesstimate based on pressure drop across that leak location, 8SLPM flowrate assumed, and specific gravity of air.

Key: 1 – fully open, 0 – fully closed, 2 – based on Cv, 3 – based on flowrate

Leak Inlet

A leak was simulated using another inlet block and a valve block. The leak inlet block was set to have the same gas composition as the lab environment of the STEVE testbed at 0.04% CO₂ and the rest N₂. The temperature and pressure were set to ambient - the same as the GasFeed block. The leak valve block was set to act as a hole/leak. Therefore, the active specification when there is a leak is 2 or 3 and the active specification when there is no leak is 0.

The Cv was calculated based on an assumed 8 SLPM flowrate at the leak location with a pressure drop of approximately 0.3 bar and a specific gravity of 1 for air. The Cv can be tuned based on the assumed pressure drop and flowrate used in the calculation. The leak can also be specified by a flow rate, positive for incoming air or negative for exiting gas.

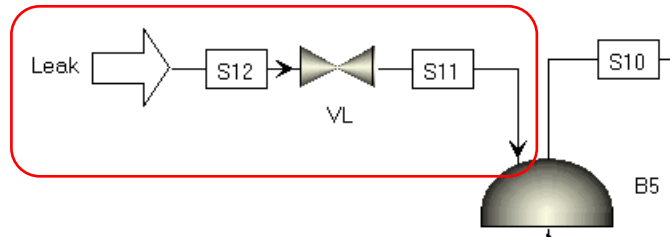


Figure 28. Image of the leak blocks which include another GasFeed block labeled “Leak” and a valve to command the leak labeled “VL” which is located at the outlet downstream portion of the sorbent bed at “B5”.

	Value	Units	Spec	Description
F	0.0	kmol/s	Free	Flowrate
Y_Fwd(*)				
Y_Fwd("CO2")	4.e-004	kmol/kmol	Fixed	Composition in forward direction
Y_Fwd("N2")	0.9996	kmol/kmol	Fixed	Composition in forward direction
T_Fwd	298.0	K	Fixed	Temperature in forward direction
P	1.1	bar	Fixed	Boundary pressure

Figure 29. Image of the Specification table for the GasFeed block labeled “Leak” where gas composition, pressure, and temperature are populated.

	Value	Units	Description
Active_Specification	0.0	n/a	Operation spec (Off-0/On-1/Cv-2/Flowrate-3)
Cv	6.79e-006	kmol/s/bar	(AS=2): Container for specified Cv
Flowrate	0.0	kmol/s	(AS=3): Container for specified flowrate

Figure 30. Image of the Specification table for the valve block labeled “VL” where the valve operation, Cv, and flow rate can be set.

Junction

The void block is used as the junction labeled B1. It acts as a tee or 3-way connection and is set to have a negligible void volume. Refer to the Voids section above for more details. It is configured with default settings: reversible pressure setter, includes a compression term, and is adiabatic. It is initialized with only N₂, no CO₂, at ambient temperature and a slightly higher pressure than the outlet which was set to 0.8 bar in this case. The pressure is set to be slightly higher, to induce pressure-driven flow from upstream to downstream, than the measurement value of the pressure at the outlet of the STEVE testbed.

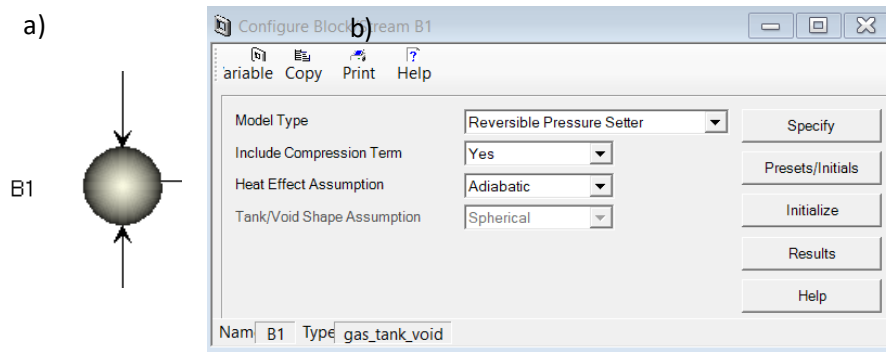


Figure 31. Images of the a) junction void block labeled “B1” and b) the main configure screen.

Figure 32 is a screenshot of the 'B1.Specify Table' window. It contains the following table:

	Value	Units	Spec	Description
Tank_Volume	1.e-005	m3	Fixed	Total volume of tank/void

Figure 32. Image of the void block specification for volume.

Figure 32 also includes the 'B1.Initials Table' window, which contains the following table:

	Value	Units	Spec	Derivative	Description
Y(*)					
Y("CO2")	0.0	kmol/kmol	Initial		Composition within tank/void
Y("N2")	1.0	kmol/kmol	Free		Composition within tank/void
T	298.15	K	Initial		Temperature within tank/void
P	0.85	bar	Initial		Pressure within tank/void

Figure 33. Image of the Presets/Initials for the junction void block “B1” where the initial conditions for gas phase compositions as well as pressure and temperature are populated.

Outlet

The GasProduct block is the outlet of the system, or exhaust/waste/product stream, as well as the vacuum pump during the desorption phase of a cycle. The flow rate is set to “Free” and is dependent on upstream components and the specified pressure of the outlet. If the exhaust were to simulate reversed operation, i.e. air is coming into the system from the outlet, the composition of gas is set to be 100% N₂, no CO₂. The temperature in the reverse direction is set to ambient. For adsorption, the pressure is set to a slightly lower value than ambient like 0.8 bar while for desorption the vacuum pressure is set to a vacuum pressure like 0.1 bar.

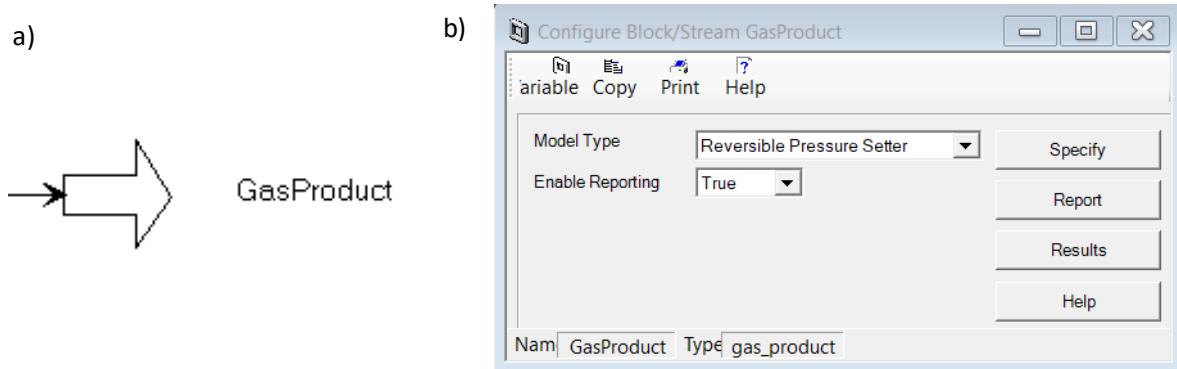


Figure 34. Images of the a) GasProduct block and b) the main configure screen.

Figure 35 is a screenshot of the 'GasProduct.Specify Table' window. It displays a table with the following data:

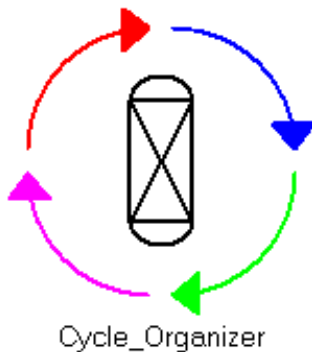
	Value	Units	Spec	Description
F	0.0	kmol/s	Free	Flowrate
Y_Rev(*)				
Y_Rev("CO2")	0.0	kmol/kmol	Fixed	Composition in reverse direction
Y_Rev("N2")	1.0	kmol/kmol	Fixed	Composition in reverse direction
T_Rev	298.15	K	Fixed	Temperature in reverse direction
P	0.8	bar	Fixed	Boundary pressure

Figure 35. Image of the Specification table for the GasProduct block where the reverse gas composition, pressure, and temperature can be set.

Cycle Organizer

The cycle organizer is the main interface to use for running the model simulation in nominal or off-nominal operation. The user can set or change values for all variables in the model. In cycle options, the maximum number of cycles can be set to a desired value such as 10. Each step in the cycle is set to be time-driven. Therefore, adsorption (1 and all other odd numbered steps) and desorption (2 and all other even numbered steps) are set to be 80 minutes or 4800 seconds following STEVE operation. Based on the type of adsorption or desorption step, refer to the figures below for the values of manipulated variables. There are several ways to simulate this model using the Cycle Organizer. Many failure injections can be implemented here as well. Some examples are heater malfunction (changing the temperature setpoints), valve stiction (changing the valve Cv or flow rate), sorbent degradation (adding humidity isotherm parameters), and blower failure (changing inlet flow rate).

a)



b)

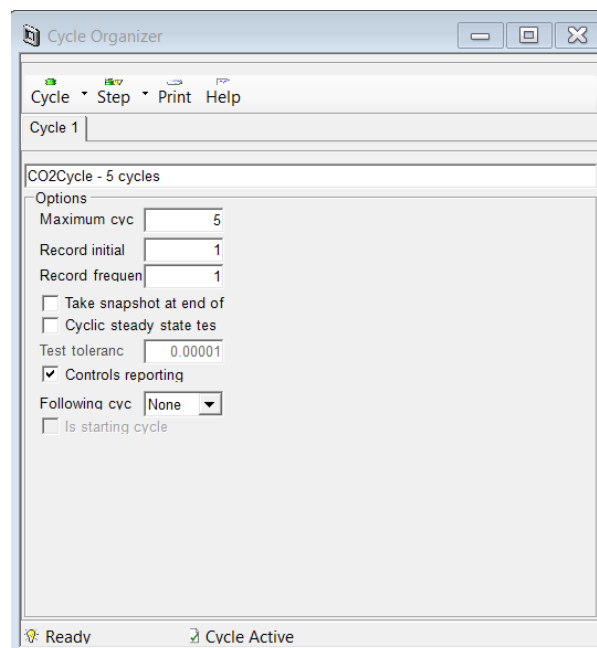


Figure 36. Images of the a) Cycle Organizer and b) the main Cycle configure screen.

Cycle Options

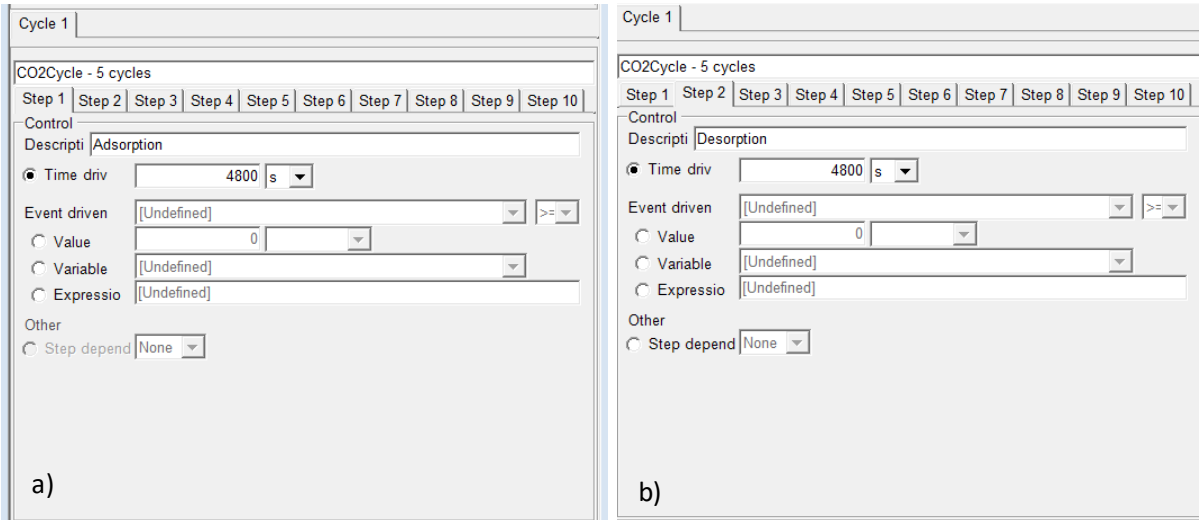


Figure 37. Images of the Cycle Control screens for a) step 1 - adsorption and b) step 2 – desorption with time-driven setpoints.

Figure 38 shows two screenshots of the initial values for the manipulated variables. Screenshot (a) is for Step 1 (adsorption) and screenshot (b) is for Step 2 (desorption). Both screenshots show a table of manipulated variables with columns for Variable, Value, Units, Spec, Ramped, Target, and Time (s).

Variable	Value	Units	Spec	Ramped	Target	Time (s)
GasFeed.P	1.1	bar	Fixed	No		
GasProduct.P	0.8	bar	Fixed	No		
VA.Active_Specification	1	n/a	Fixed	No		
VD.Active_Specification	0.0	n/a	Fixed	No		
VI.Active_Specification	3	n/a	Fixed	No		
VL.Active_Specification	0.0	n/a	Fixed	No		
Zeolite13XBed.cp	0.01	J/kg/K	Fixed	No		
Zeolite13XBed.MFlow	100	kg/s	Fixed	No		
Zeolite13XBed.Taux_In	298	K	Fixed	No		

Variable	Value	Units	Spec	Ramped	Target	Time (s)
GasFeed.P	1.1	bar	Fixed	No		
GasProduct.P	0.8	bar	Fixed	Linear	0.1	1.000e+3
VA.Active_Specification	0.0	n/a	Fixed	No		
VD.Active_Specification	1	n/a	Fixed	No		
VI.Active_Specification	0.0	n/a	Fixed	No		
VL.Active_Specification	0.0	n/a	Fixed	No		
Zeolite13XBed.cp	0.01	J/kg/K	Fixed	No		
Zeolite13XBed.MFlow	100	kg/s	Fixed	No		
Zeolite13XBed.Taux_In	298	K	Fixed	Linear	498	1.000e+3

Figure 38. Images of the initial values for the manipulated variables for a) step 1 - adsorption and b) step 2 – desorption.

Cycle 1								Cycle 1												
CO2Cycle - 5 cycles								CO2Cycle - 5 cycles												
Step 1	Step 2	Step 3	Step 4	Step 5	Step 6	Step 7	Step 8	Step 9	Step 10	Step 1	Step 2	Step 3	Step 4	Step 5	Step 6	Step 7	Step 8	Step 9	Step 10	
Manipulated Variables								Manipulated Variables												
Variable	Value	Units	Spec	Ramped	Target	Time (s)	Variable	Value	Units	Spec	Ramped	Target	Time (s)	Variable	Value	Units	Spec	Ramped	Target	Time (s)
GasFeed.P	1.1	bar	Fixed	No			GasFeed.P	1.1	bar	Fixed	No			GasFeed.P	1.1	bar	Fixed	No		
GasProduct.P	0.1	bar	Fixed	Linear	0.8	1.000e+3	GasProduct.P	0.8	bar	Fixed	Linear	0.1	1.000e+3	GasProduct.P	0.8	bar	Fixed	Linear	0.1	1.000e+3
VA.Active_Specification	1	n/a	Fixed	No			VA.Active_Specification	0.0	n/a	Fixed	No			VA.Active_Specification	0.0	n/a	Fixed	No		
VD.Active_Specification	0.0	n/a	Fixed	No			VD.Active_Specification	1	n/a	Fixed	No			VD.Active_Specification	1	n/a	Fixed	No		
VI.Active_Specification	3	n/a	Fixed	No			VI.Active_Specification	0.0	n/a	Fixed	No			VI.Active_Specification	0.0	n/a	Fixed	No		
VL.Active_Specification	0.0	n/a	Fixed	No			VL.Active_Specification	0.0	n/a	Fixed	No			VL.Active_Specification	0.0	n/a	Fixed	No		
Zeolite13XBed.cp	0.01	J/kg/K	Fixed	No			Zeolite13XBed.cp	0.01	J/kg/K	Fixed	No			Zeolite13XBed.cp	0.01	J/kg/K	Fixed	No		
Zeolite13XBed.MFlow	100	kg/s	Fixed	No			Zeolite13XBed.MFlow	100	kg/s	Fixed	No			Zeolite13XBed.MFlow	100	kg/s	Fixed	No		
Zeolite13XBed.Taux_In	498	K	Fixed	Linear	298	2.000e+3	Zeolite13XBed.Taux_In	298	K	Fixed	Linear	498	1.000e+3	Zeolite13XBed.Taux_In	298	K	Fixed	Linear	498	1.000e+3

Figure 39. Images of the values for the manipulated variables for subsequent a) adsorption and b) desorption steps. The main difference is that the jacket heater temperature and exhaust pressure are set to linearly decrease or increase from its hot to cold or ambient to vacuum (and vice versa) states at a specified rate.

3.7 Simulation Experiment Design

This model aims to simulate what-if scenarios, particularly faults, and study the system’s performance based on varying conditions and mission types. The test plan below describes the simulation tests conducted to provide sensitivity analysis in nominal operation of the system, determine key indicators of varying fault types in off-nominal operation to ultimately provide recommendations for diagnostics and prognostics. At the end of the list is a randomized test which combined various faults to see how the system was affected and provide insight into how to mitigate faults with specialized corrective action sequences. The test plan is broken down into 10 test types. The first test focuses on nominal operation, then there are 6 different component-focused faults, then stability, dormancy, and finally randomized multi-fault tests. The test results will output the expected outcomes tailored to the test type. However, additional results metrics will be determined such as performance deviation compared to baseline in the context of spacecraft life support and crew safety. The goal of this test plan is to provide faulty data signatures that would provide insight and features that facilitate and improve diagnostics and prognostics – working towards a fault-tolerant system for future deep space habitation.

Table 6. Aspen Adsorption Simulation Test Plan

Test #	Test Type	Manipulated Variables	Expected Outcome
1	Nominal Operation	Crew size, bed length, flow rate	Sensitivity analysis of key variables
2	Valve Faults	Valve stiction, V1 vs V2 (partial)	Determine key indicators against nominal operation, amount of removal loss
3	Heater Faults	Low vs high, wrong command	Determine key indicators against nominal operation, amount of removal loss
4	Vacuum Fault	Not enough vacuum	Determine key indicators against nominal operation, amount of removal loss
5	Leak Faults	During adsorption or desorption or sustained (with water)	Determine key indicators against nominal operation, amount of removal loss
6	Blower Fault	Low or high or off	Determine key indicators against nominal operation, amount of removal loss
7	Filter Fault	Clogged filter	Determine key indicators against nominal operation, amount of removal loss
9	Dormancy Test	Water preloading	Determine key indicators and insights
10	Multi-fault	Combination of faults	Determine key indicators and insights

Note: Test 2-7 will use the same properties and test conditions as STEVE.

STEVE Conditions: 8 SLPM, 0.25% CO₂ in air, ambient/225C, ambient/0.1 torr

3.8 Simulation Results

Simulation results using the Aspen Adsorption CO₂ Removal Model built using the set-up procedure in the previous section is reported below. The objective of these tests is to determine data signatures of various faults to facilitate identification and detection of anomalies that indicate faults which lead to specific failure. The final table describes the faults tested as well as the overall effect and deviation from baseline (nominal) for each fault tested. All supporting data and additional information are provided.

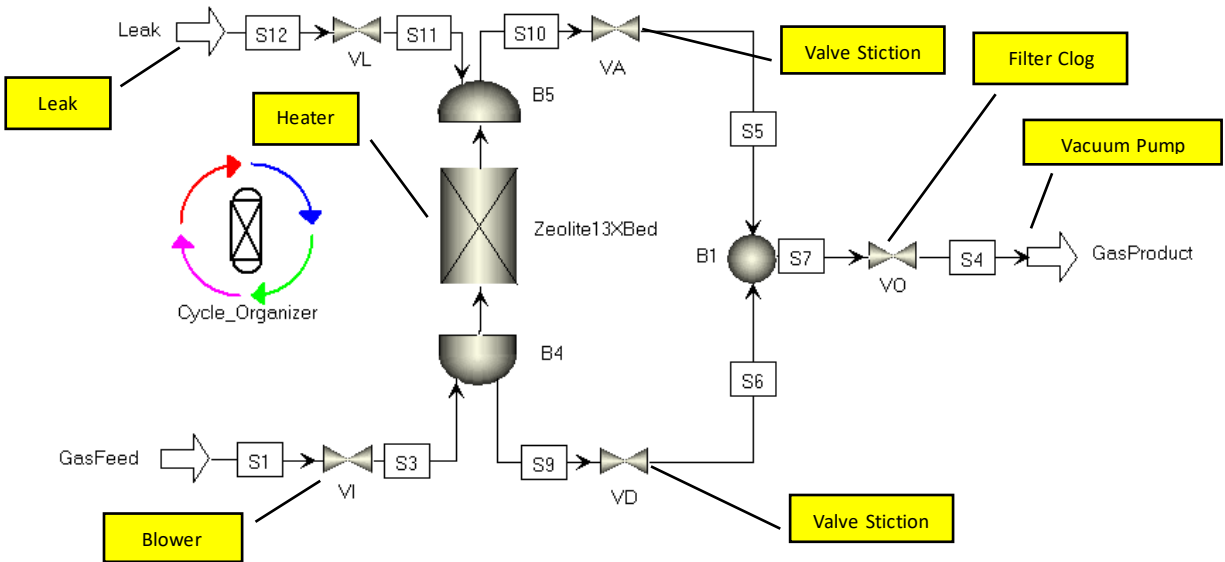


Figure 40. Fault Injection Schematic

The test plan uses the nominal STEVE test conditions as control for the tests simulating other faults. This will enable model validation against experimental data. The control (or nominal) test conditions are listed below:

Table 7. STEVE Control (Nominal) Test Conditions

Variable	Value	Units
Flow Rate	8	SLPM
CO ₂ Composition	0.30	%
Adsorption Upstream Pressure	95	kPa
Adsorption Downstream Pressure	92	kPa
Desorption Vacuum Pressure	10	kPa
Bed Length	20	In.
Bed Diameter	0.87	In.
Sorbent Material	Zeolite 13X	-
Adsorption Temperature	25	°C
Desorption Temperature	200	°C

3.9 Simulating Nominal Operations

Crew Size

Nominal simulation testing was done to create baseline (control) data for subsequent fault simulation tests. The following nominal operation tests display breakthrough curves and cyclic operation data for outlet CO₂ concentration, analogous to the outlet sensor of the STEVE testbed, and sorbent loading, a calculated amount of CO₂ adsorbed in the bed at each time step.

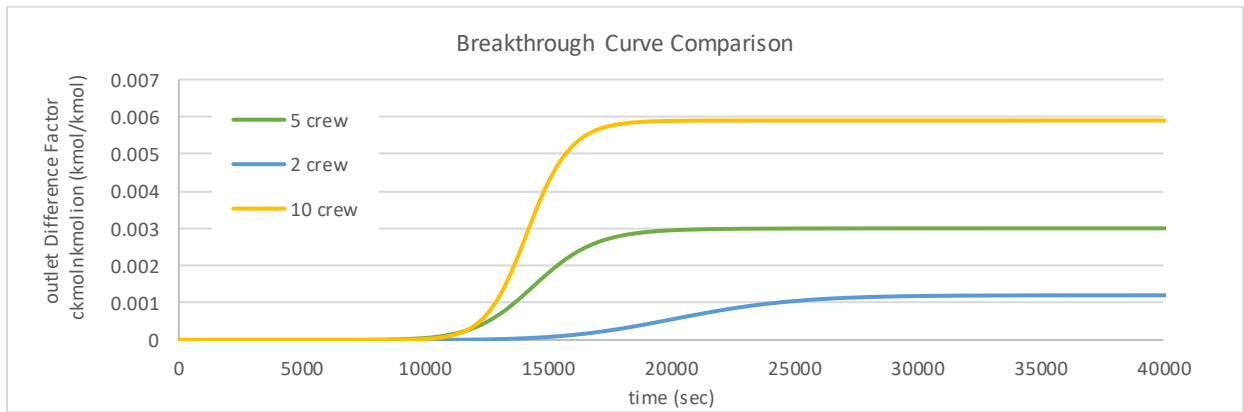


Figure 41. Breakthrough Curves with Varying Crew Size

Table 8. Crew Size Effect on Breakthrough Time

Crew Size	Production (kg CO ₂ /day) [10]	Partial Pressure (Pa)	PCO ₂ (ppm)	CO ₂ Percent (%)	t _b (hr)
1	1.04	57.44	566.88	0.06	-
2	2.08	114.88	1133.77	0.11	4.17
3	3.12	172.32	1700.65	0.17	-
4	4.16	229.80	2267.92	0.23	-
5	5.2	287.20	2834.42	0.28	3.89
10	10.4	574.40	5668.85	0.57	3.33

t_b is breakthrough time (5% to saturation).

There are considerable differences in breakthrough time, outlet concentration, and loading for varying crew size. For a given control volume and constant input parameters, CO₂

mole fraction was set to a range of 0.12% to 0.59% in air which equates to a range of 1177 to 5886 ppm. STEVE operates with 0.30% CO₂ in air. Breakthrough time, the time at which 5% of the feed concentration is reached at the outlet, was found to be 4.17 hours, 3.89 hours, and 3.33 hours for a crew size of 2, 4, and 10 with the standard test parameters listed in Table 7. These values facilitate sizing and design for systems or vehicles that may have variable crew sizes for the duration of its mission to find optimal factors for parameters like bed length, mass, power, and operational performance.

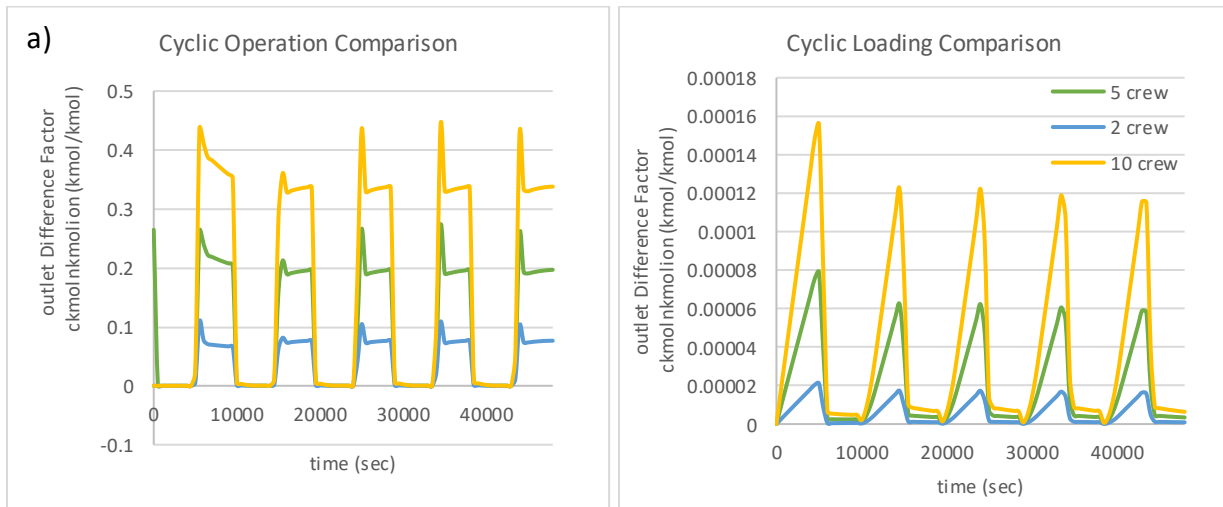


Figure 42. a) Outlet CO₂ Concentration and b) Sorbent Loading with varying Crew Size

The same crew sizes were used to determine changes in CO₂ outlet concentration and loading in cyclic operation. Here, higher crew numbers output higher outlet concentration of CO₂ and loading in the zeolite bed. The increase in outlet concentration is 150% greater for 5 crew than for 2 crew with the same sorbent bed and conditions while 10 crew is 206% greater using the maximum outlet concentration. For loading in the sorbent bed, operating with 5 crew increases loading by 3.7 times than for 2 crew and 7.18 times with 10 crew using the total amount loaded.

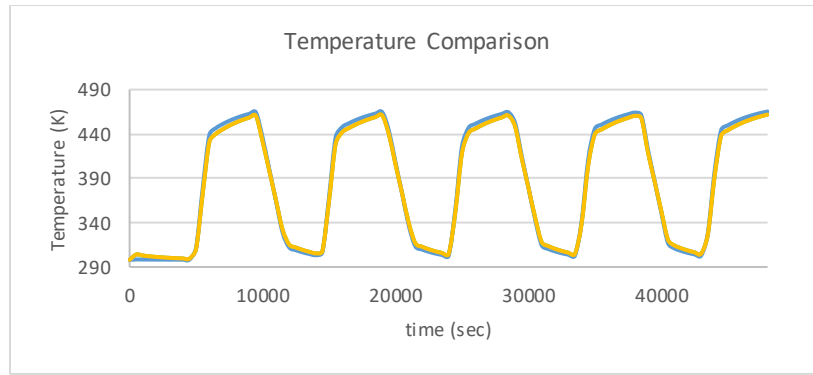


Figure 43. Gas Temperature in the Sorbent Bed with varying Crew Size

It was found that changing crew size did not significantly affect the gas temperature profiles in cyclic operation. With this finding, it can be noted that varying crew size within the reported range will not change the thermodynamics of the system significantly. Therefore, heater and power conditions may stay the same even with fluctuations in crew size.

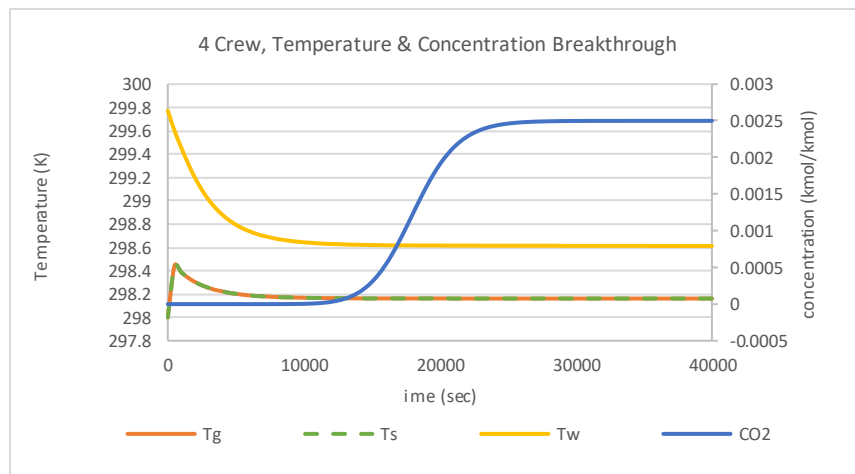


Figure 44. Breakthrough Curve and Temperatures for 4 Crew

The plot above shows the breakthrough curve and temperatures at the midpoint along the axial length of the sorbent bed for a crew size of 4. The gas and solid temperature trend with the same rate of change and the same initial temperatures while the wall temperature decreases to an

equilibrium temperature towards the equilibrium temperature of the gas and solid sorbent. This is the same trend in temperature change for varying crew size.

Bed Length

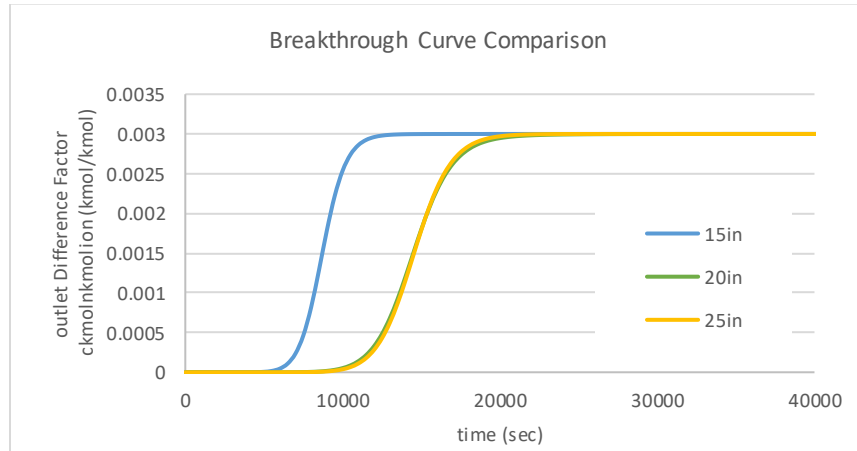


Figure 45. Breakthrough Curve with Varying Bed Length

Bed length was tested from a range of 15 to 25 inches where the STEVE sorbent bed is 20 inches long. The breakthrough curve displays very similar breakthrough time for the 20 and 25 inch beds indicating a limit on breakthrough time increase based on all other test conditions and a significant change with shorter beds. The shorter the bed, the faster breakthrough will occur, where the 15 in. bed exhibited 39% faster breakthrough time.

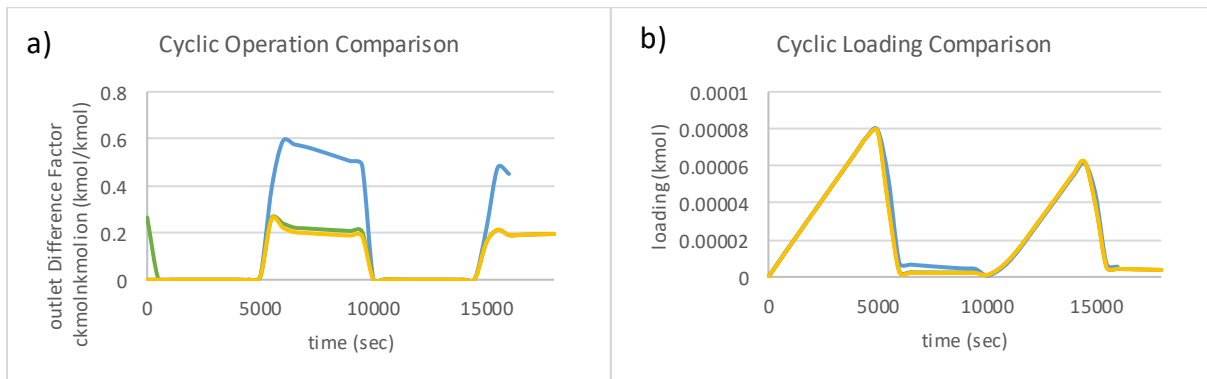


Figure 46. a) Outlet CO₂ Concentration and b) Sorbent Loading with varying Bed Length

Regarding cyclic operation, a significant difference can be seen for the outlet concentration but not for the loading. For outlet concentration, the 15 in. bed releases 2.23 times more CO₂ at the outlet than the 20 in and 25 in. beds which indicates a greater release attributed to better performance of the bed at that length. However, the loading for all three bed lengths have no significant difference, meaning loading capacity did not change for the range of bed length studied here.

For sizing sorbent beds, it is typical practice to determine and check against length to diameter ratio (L/D) as well as the column diameter (or bed diameter) to sorbent pellet diameter ratio. The L/D ratio is important for achieving acceptable residence time and space velocity for the sorbent used. It is also an important aspect for optimizing mass and volume for space applications. The diameter ration (D_{col}/D_{pel}) indicates potential impacts of wall channeling and is usually tuned to a value above 20 to avoid those effects and unpredictable behavior [31]. The L/D ratios are 17.2, 22.9, and 28.7 for the 15, 20, and 25 in beds, respectively. The diameter ratio is 49.10.

Flow Rate

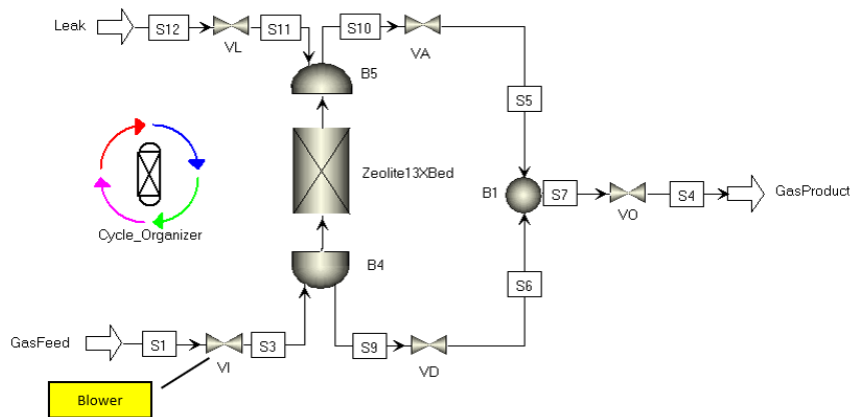


Figure 47. Diagram of Aspen Adsorption Model with Blower Flow Rate Control

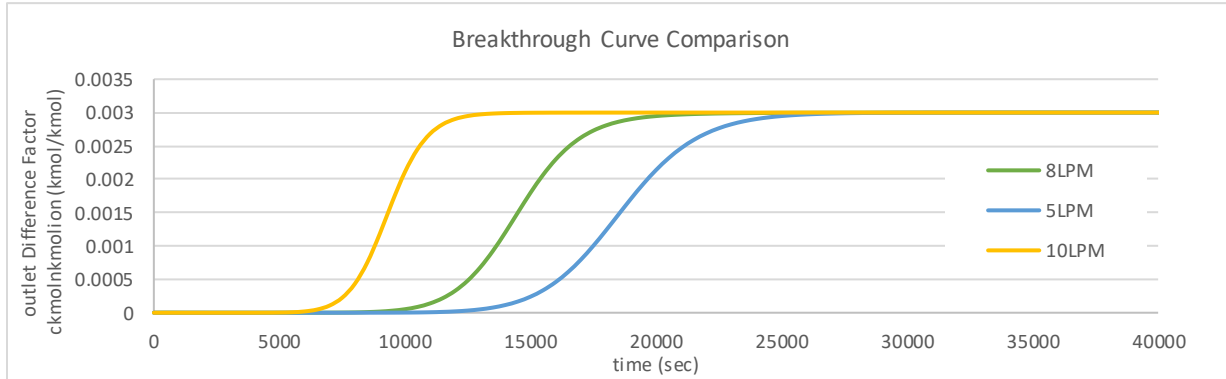


Figure 48. Breakthrough Curves with Varying Flow Rates

Flow rate has a significant effect on breakthrough and overall performance of the bed. The flow rate change is analogous to blower performance change. Here, the larger the flow rate, the shorter the breakthrough time. Flow rate has a critical impact on the interstitial velocity of the gas through the bed and thus the convection of gas around the sorbent. The breakthrough times are 4, 3.9, and 2.1 hours for 5, 8, and 10 LPM, respectively.

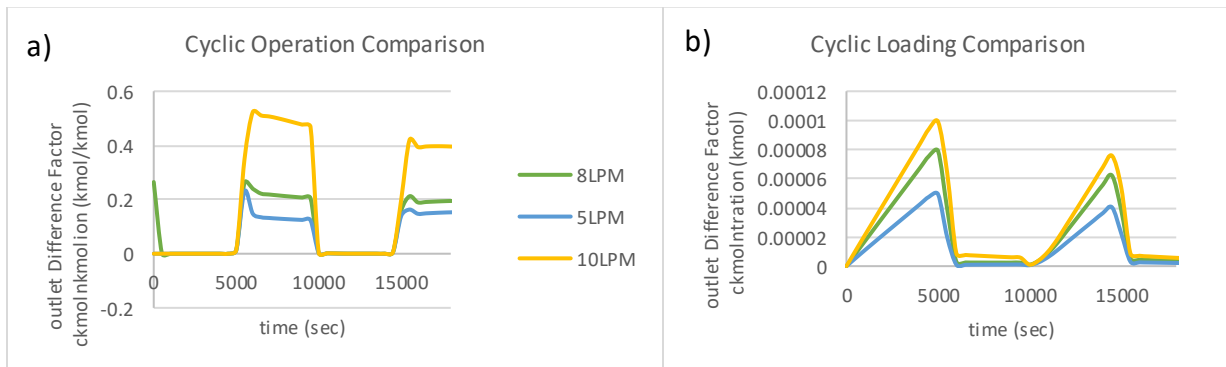


Figure 49. a) Outlet CO₂ Concentration and b) Sorbent Loading with varying Flow Rate

The change in flow rate was used to determine the change in CO₂ outlet concentration and loading in cyclic operation. Here, higher flow rate outputs higher outlet concentration of CO₂ and loading in the zeolite bed. The increase in outlet concentration is 1.15 times greater for a

flow rate of 8LPM compared to 5LPM and 2.27 times greater for 10 LPM using the maximum outlet concentration. For loading in the sorbent bed, operating with 10 LPM loads approximately 2.08 times more CO₂ than 5 LPM and 1.6 times greater with 8 LPM using the total amount loaded.

3.10 Simulating Off-Nominal (Faulty) Operation

Valve stiction

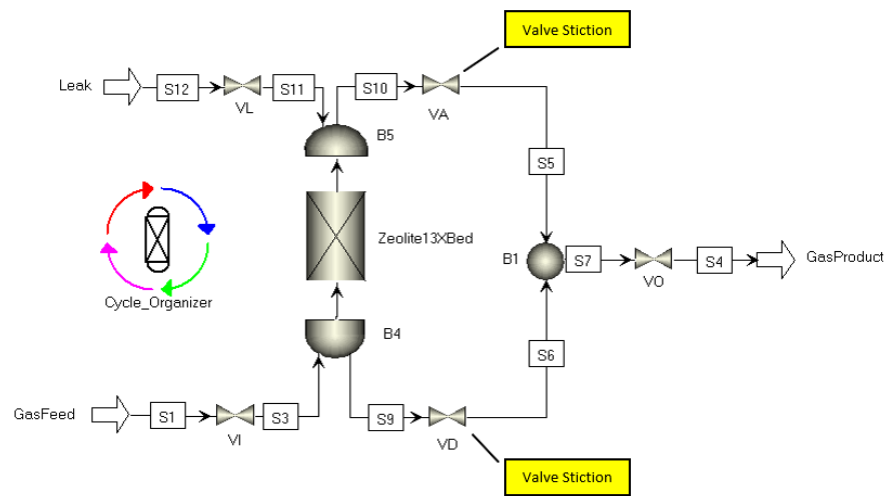


Figure 50. Diagram of Aspen Adsorption Model with Valve Stiction Fault Injection

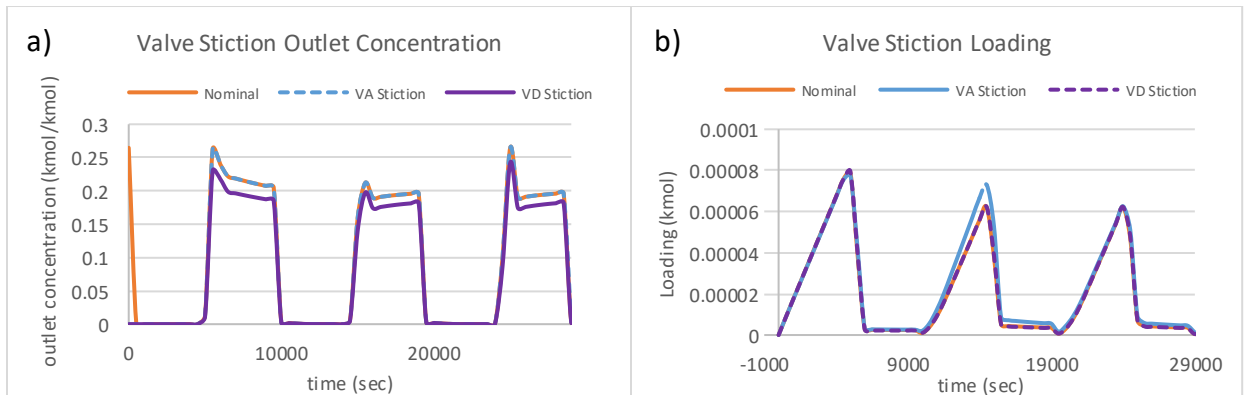


Figure 51. a) Outlet CO₂ Concentration and b) Sorbent Loading with Valve Stiction

Valve stiction is the phenomena in which a valve does not open or close properly due to some resistance in the internal valve seat or some external disturbance. Valve stiction is simulated by setting the flow coefficient of the valve, C_v , to a value that coincides with partial opening of the valve. In this case, the C_v was set to $1E-5$ kmol/s/bar for valves VA or VD, not simultaneously, while a fully open valve would have a C_v value of 1000. The concentration and loading were plotted to determine any change in the performance of the bed. There was no significant difference between nominal settings and VA stiction but a slight dip in outlet concentration with VD stiction. Loading was similar for nominal and VD stiction with a slight increase for VA stiction in the 2nd cycle; however, it is not clear if that is a simulation artifact or not. Further work is needed to advance the capabilities of the model to simulate valve stiction as model runtime could not be achieved beyond 3 cycles due to numerical instability.

Heater

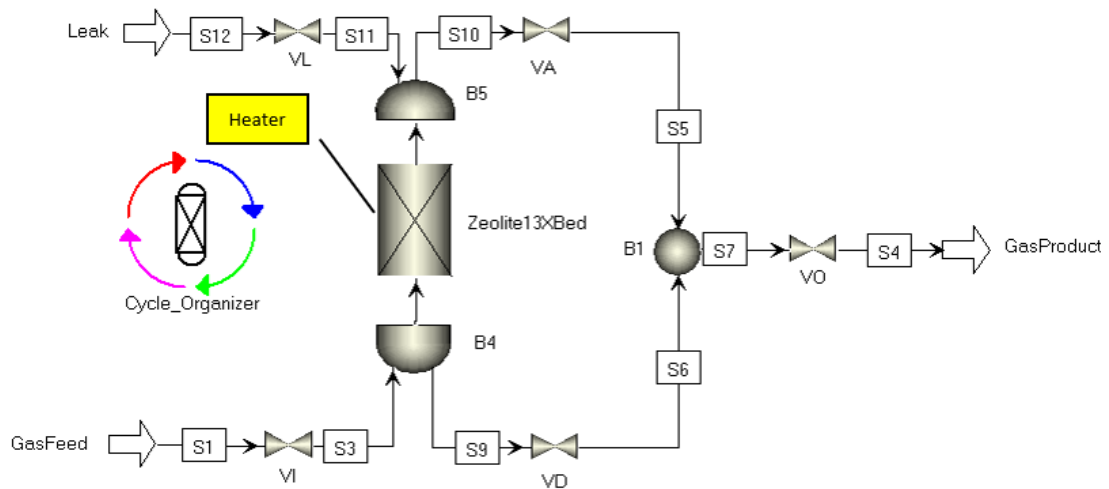


Figure 52. Diagram of Aspen Adsorption Model with Heater Fault Injection

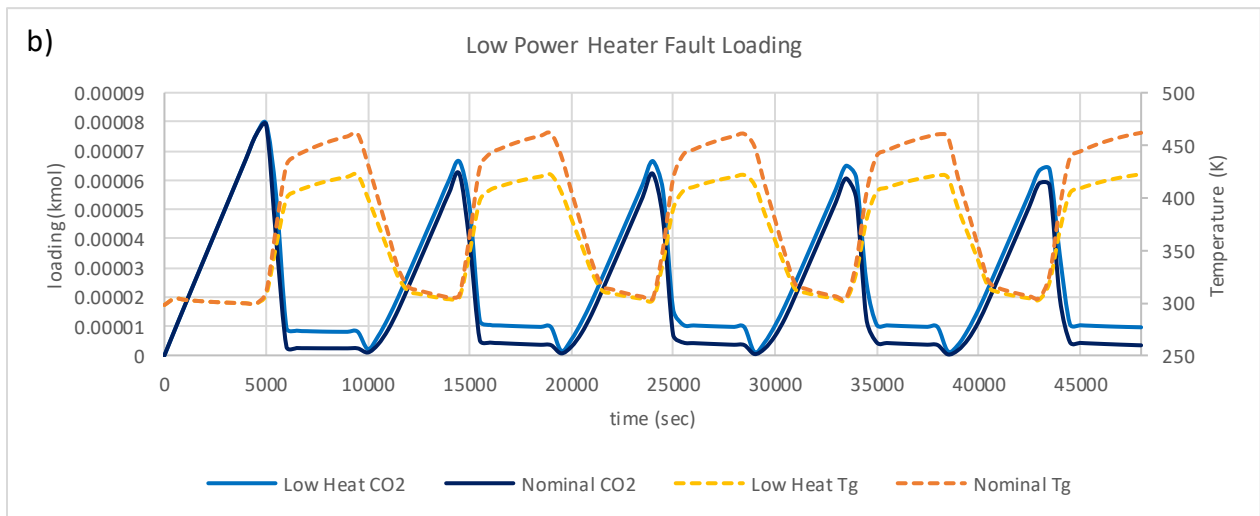
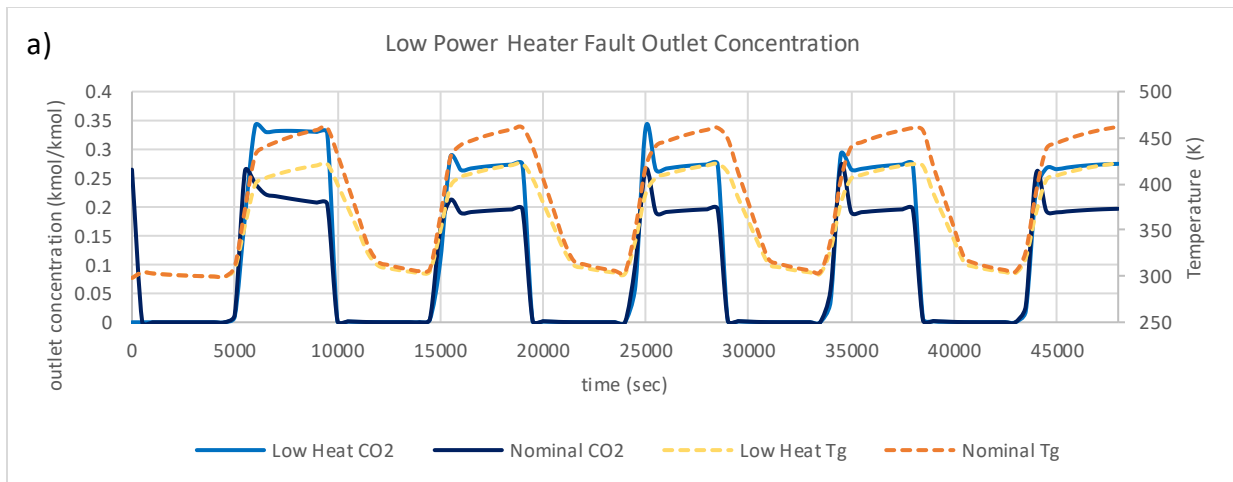


Figure 53. a) Outlet CO₂ Concentration and b) Sorbent Loading with Sustained Heater Fault

Heater faults can occur due to problems with the heater or power to the heater. The fault demonstrated here displays a low heater setting versus nominal heating temperature for the desorption and regeneration phase of the cycle. The temperature for nominal operation is 498K and the temperature for low heat is 450K. There is an increase between the low heat and nominal data sets for outlet concentration as well as in sorbent loading during the desorption steps. The outlet concentration and sorbent loading of the low heat setting is approximately 1.25 times larger than the nominal values. It is not an intuitive result, but more CO₂ would stay adsorbed in

the bed with lower desorption temperature. Thus, more CO₂ may leave the bed during desorption as indicated in the outlet CO₂ concentration plot.

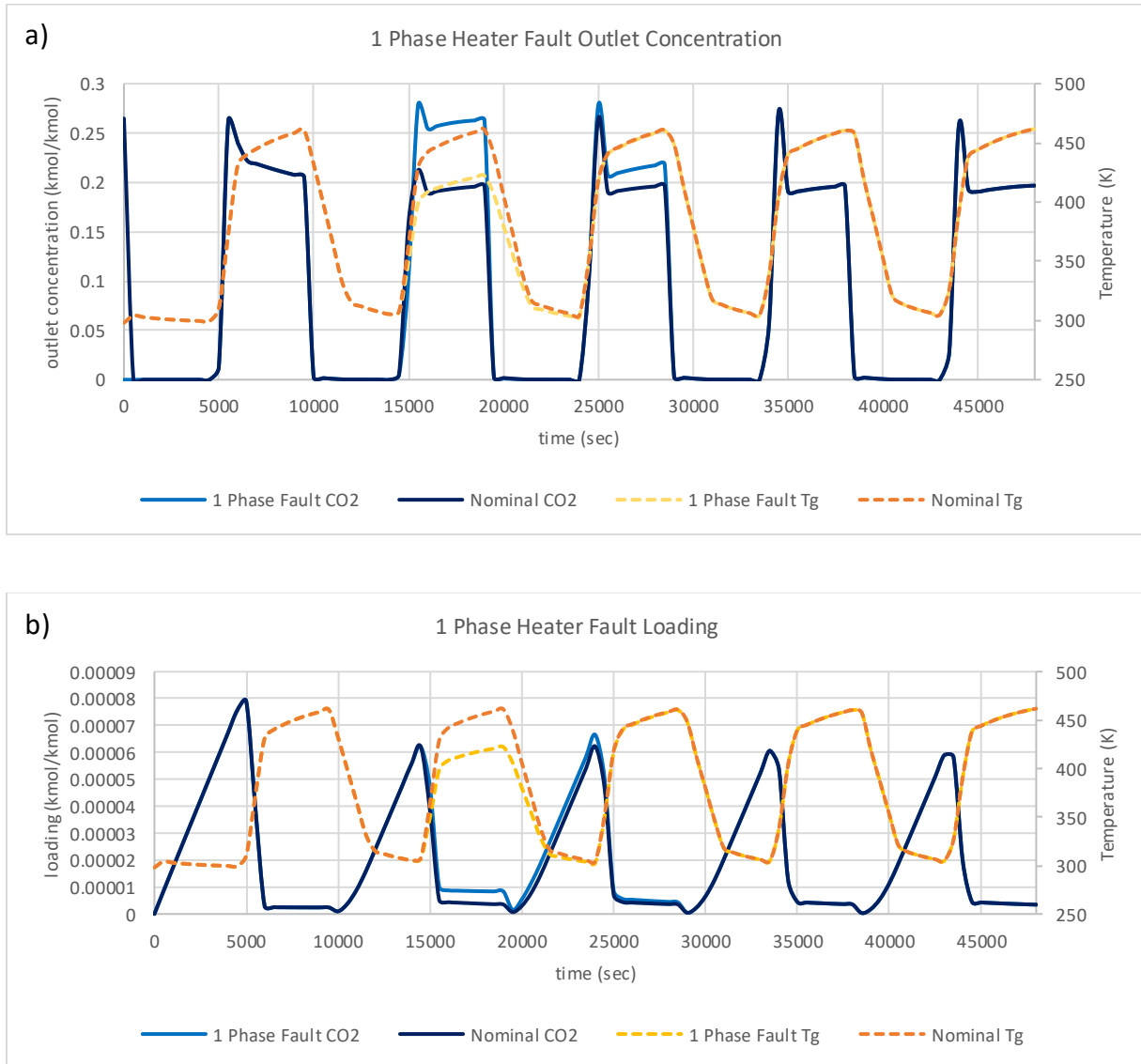


Figure 54. a) Outlet CO₂ Concentration and b) Sorbent Loading with Temporary Heater Fault

Temporary (or “1 phase” labeled in the plots above) heater faults may occur due to heater or power issues. The fault demonstrated here displays a low heater setting only in the desorption phase of the 2nd cycle of the simulation indicated by the dip in temperature to 450K from 498K. There is an increase between the 1 phase fault and nominal data sets for outlet concentration as

well as in sorbent loading during the desorption steps as was seen in the sustained low heat dataset. The outlet concentration and sorbent loading of the 2nd cycle is also approximately 1.25 times larger than the nominal values.

Vacuum

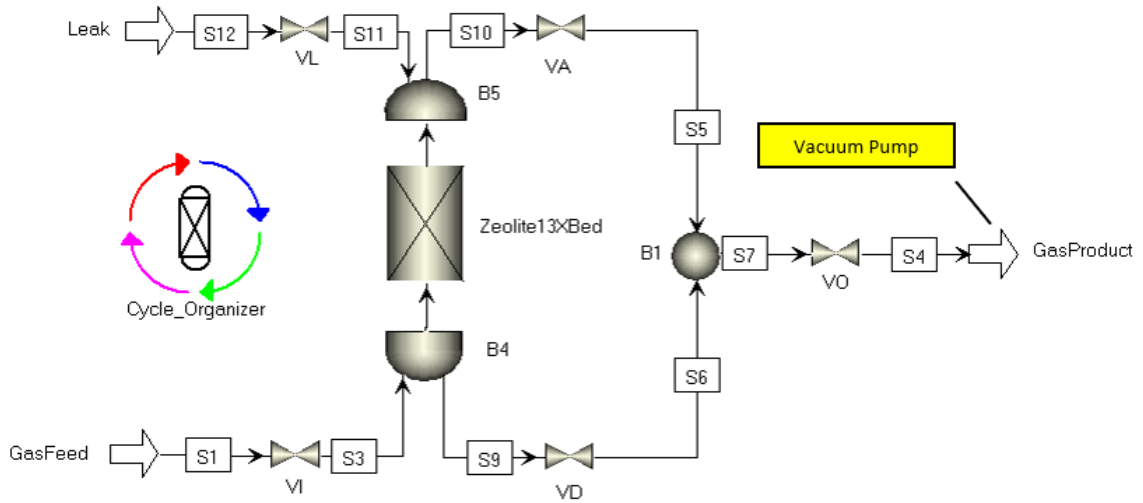


Figure 55. Diagram of Aspen Adsorption Model with Vacuum Pump Fault Injection

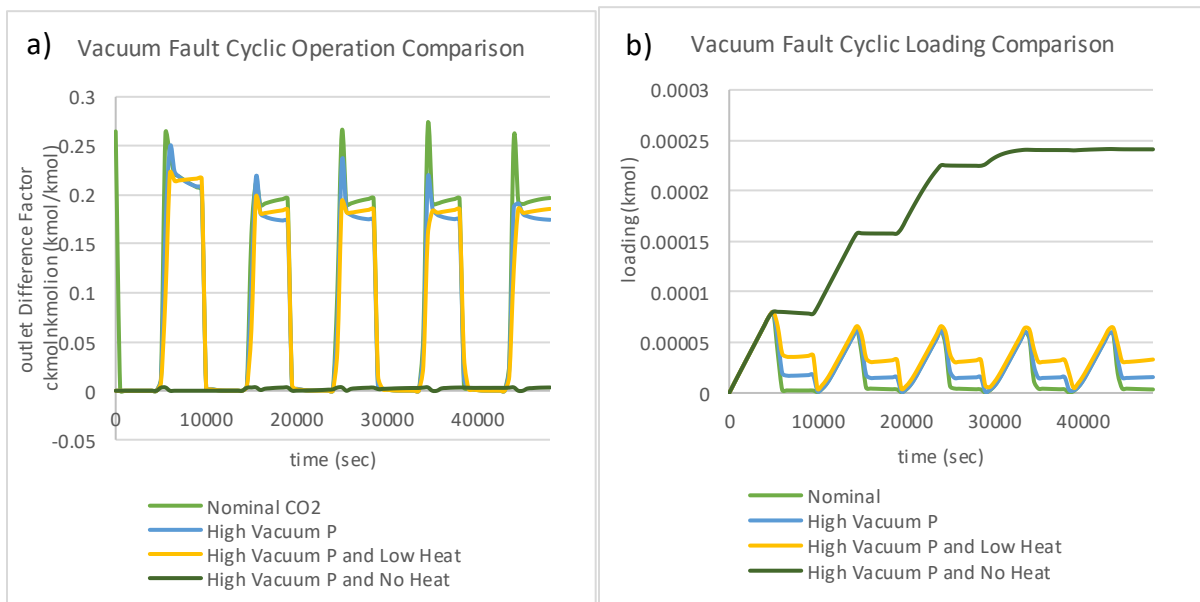


Figure 56. a) Outlet CO₂ Concentration and b) Sorbent Loading with varying Vacuum Faults

The vacuum faults were demonstrated in three different ways. The 1st vacuum fault may manifest as a low vacuum efficiency due to an anomaly downstream or a degraded vacuum pump at the outlet of the carbon dioxide removal system. The 2nd vacuum fault is tested with low heat which may arise in an overall low power setting where the vacuum pump and heater are not supplied enough power. The 3rd fault represents low power to the vacuum pump and no power supplied to the heater. There are differences in outlet CO₂ concentration and loading for the vacuum faults compared to nominal operation with the most drastic difference seen for the high vacuum pressure and no heat simulation – indicating the dominant effect of supplied to scrub CO₂ in the system. Although efficiency for scrubbing may go down with degraded vacuum, having no heat will have the largest impact on the system.

Leak

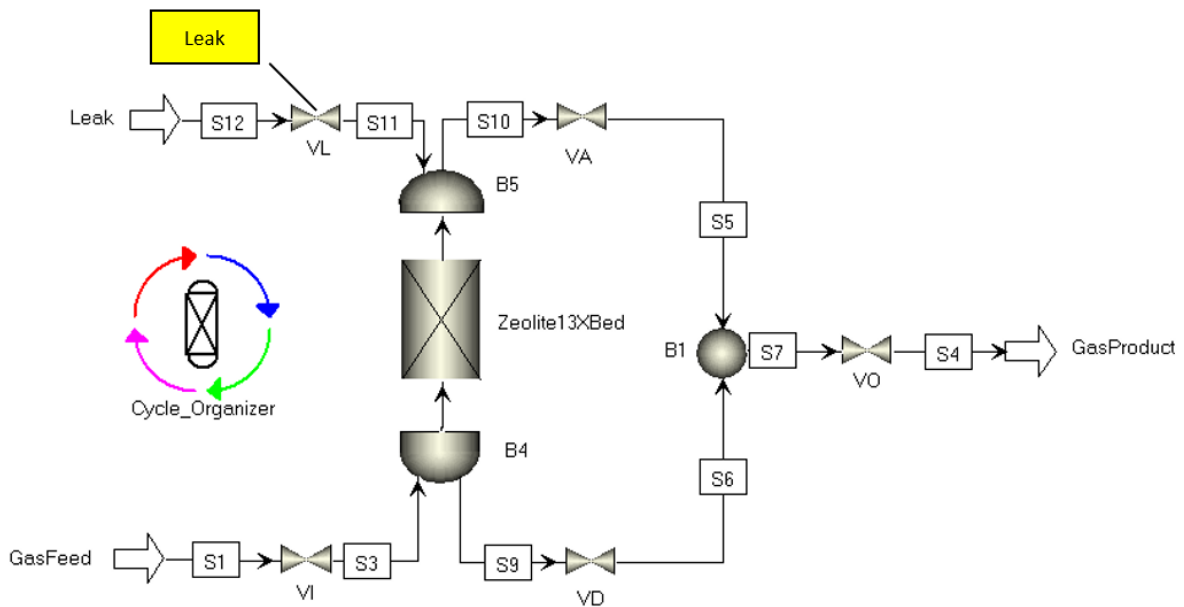


Figure 57. Aspen Adsorption Model with Leak Fault Injection

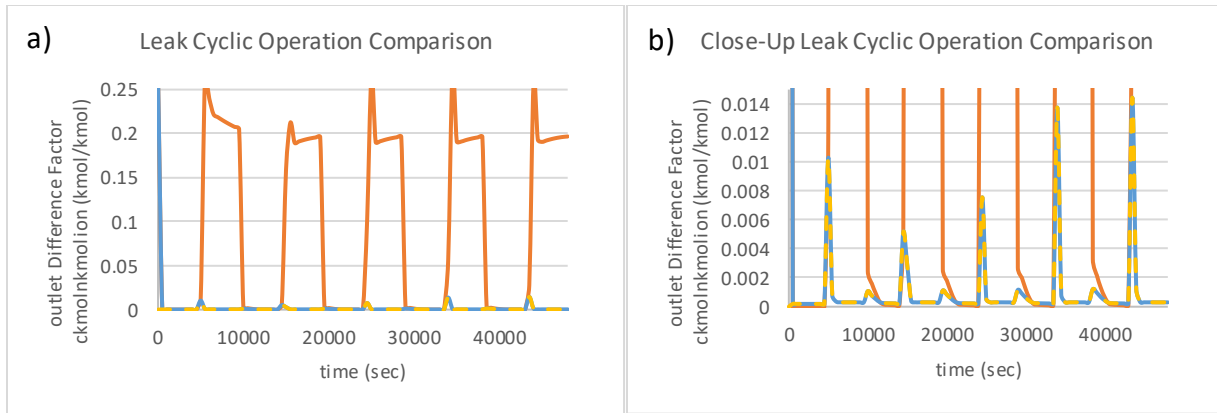


Figure 58. a) Outlet CO₂ Concentration with Leak and b) Close-Up

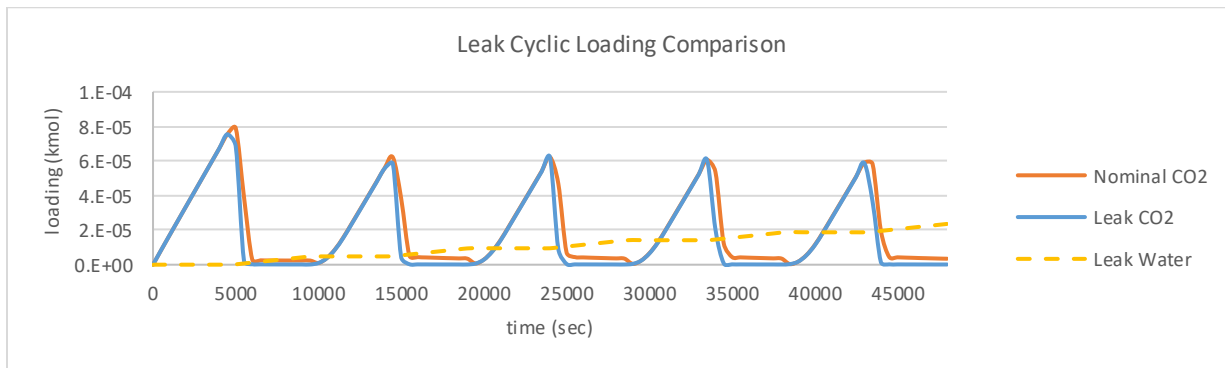


Figure 59. Sorbent Loading with Leak

Leaks in life support systems can be catastrophic to the mission and safety of the crew. Leaks can also occur in various places and be very hard to find even when detected. Here, a leak right outside of the outlet of the bed is simulated with water vapor input. Zeolite 13X is known to have strong adsorption of water and was tested in this simulation. The data signature of the leak from outlet concentration is drastic due to the severity of this leak. Sorbent loading does not show significant difference between nominal and leak CO₂ but there is significant rise in water loading as the leak persists with a constant inlet leak flow of 1 kmol/s of water vapor and nitrogen during both the adsorption and desorption phases. Other leak locations and severities can be tested.

Filter Clog

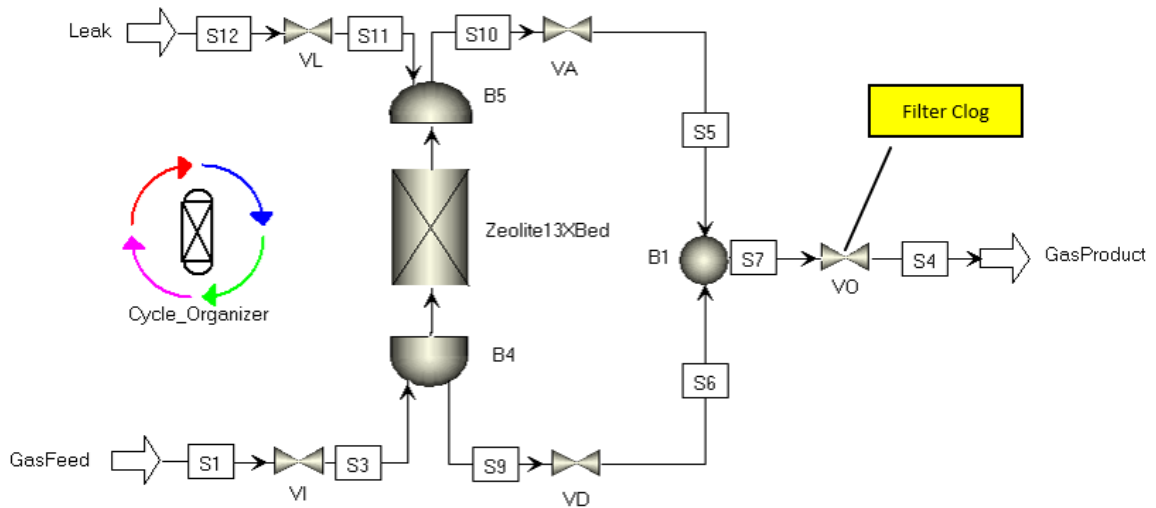


Figure 60. Aspen Adsorption Model with Filter Clog Fault Injection

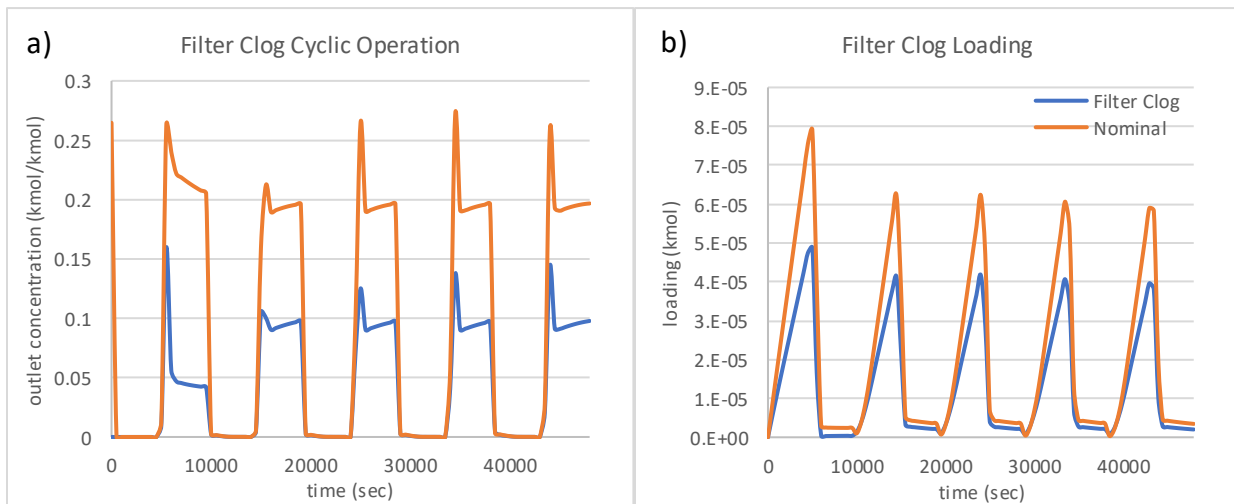


Figure 61. a) Outlet CO₂ Concentration and b) Sorbent Loading with Filter Clog

The outlet filter clog was simulated by commanding a low Cv value for the outlet valve in the model. The effect of a filter clog either by foreign debris or accumulation of dust and thus a rise in pressure drop shows significant deviation from nominal operation. The max outlet

concentration of nominal operation compared to the filter clog simulation is 1.7 times larger while the total sorbent loading was 1.52 times larger – indicating that this filter clog reduced the adsorption and therefore scrubbing efficiency of the system.

Dormancy

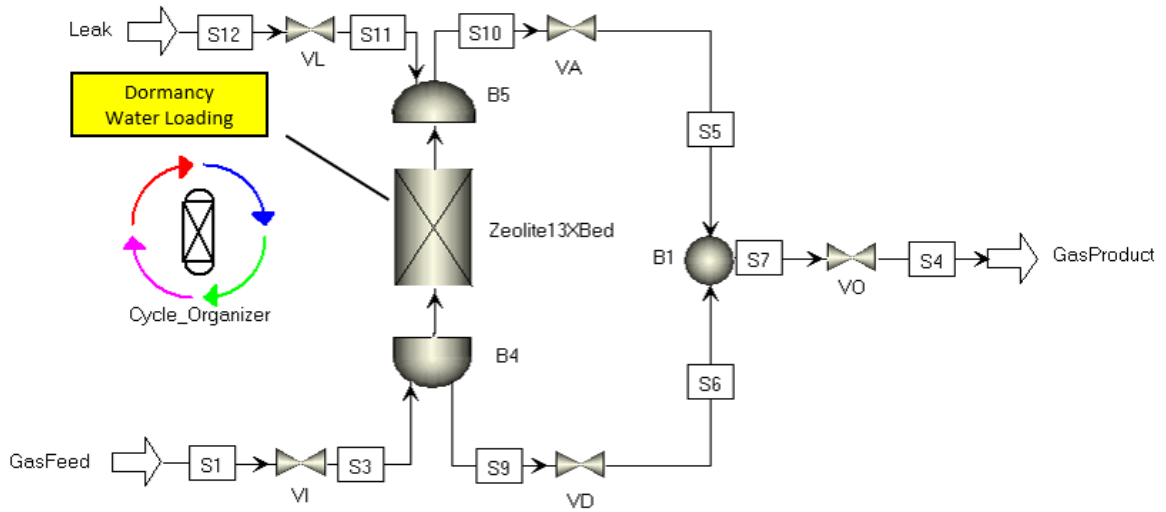


Figure 62. Aspen Adsorption Model with Dormancy Water Loading Fault Injection

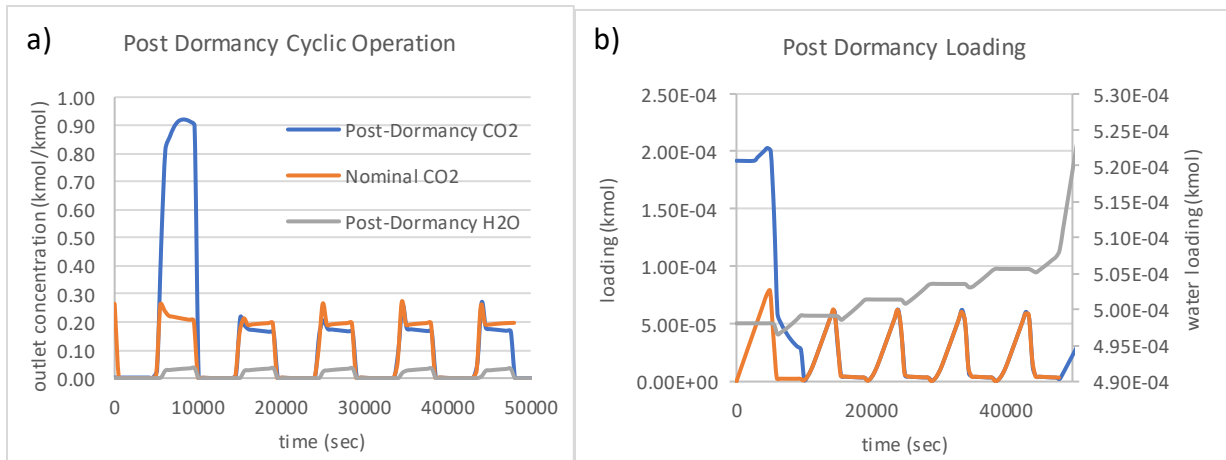


Figure 63. a) Outlet CO₂ Concentration and b) Sorbent Loading Post-Dormancy Water Loading

Dormancy for deep space habitats that are uncrewed for long periods of time may power down most if not all ECLSS subsystems like the carbon dioxide removal system. Shutting down does not seem to pose any problems but starting up from a long dormant period may introduce undesirable effects such as water loading from humidity during dormancy. Water vapor can come from many sources, and with a leak or open valve, the system can take on water before post-dormancy start-up. In this simulation, the sorbent bed was loaded with water for 24 hours at $1e-4$ kmol/kmol in a CO_2/N_2 gas stream at nominal flow to pre-load the bed with water. Next, the bed was initiated to operate with normal conditions with adsorption first. The data shows a significant difference in outlet concentration and sorbent loading for the first cycle only with slight difference in subsequent cycles for outlet concentration which may be attributed to the water vapor seen leaving the bed at the outlet. After the dormant phase, water is no longer entering the bed; however, water loading seems to increase over time at extremely small amounts for those 5 cycles. Loading increase for water seems to stop during the desorption phases only.

Multiple Faults

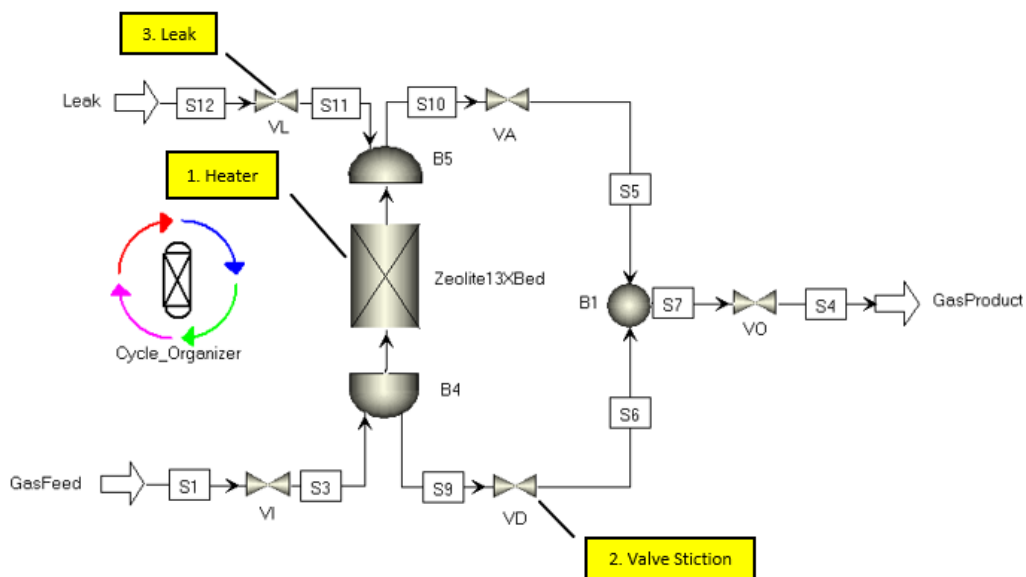


Figure 64. Aspen Adsorption Model with Multiple Fault Injections with (1) temporary low heat followed by (2) temporary valve stiction in VD and ending (3) with a sustained leak at the outlet of the bed.

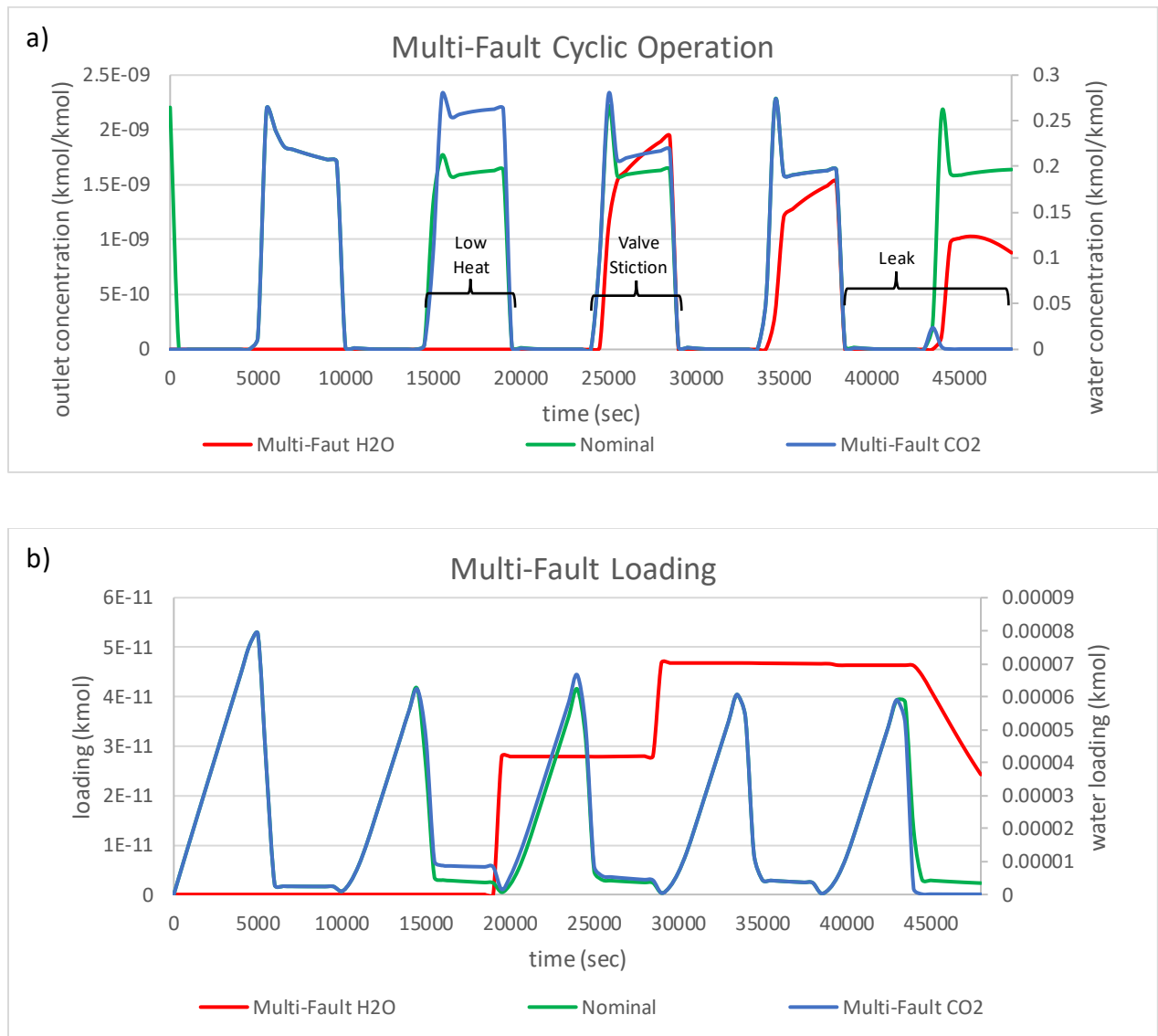


Figure 65. a) Outlet CO₂ Concentration and b) Sorbent Loading with Multiple Faults

Multiple fault injection is possible using Aspen Adsorption modeling. Here, a low heater fault was activated in the 2nd desorption step followed by valve stiction at VD on the 3rd desorption step and finally a leak at the outlet of the bed for the last adsorption and desorption steps. Low heat or power to the heater is indicated by the considerable increase in outlet

concentration and slight increase in sorbent loading. Valve stiction is indicated by the slight increase in outlet concentration of CO₂ compared to nominal and negligible increase in sorbent loading. Lastly, the leak is highly apparent due to the drop in the outlet concentration of CO₂. The water vapor outlet concentration and loading require further study. This multi-fault test serves to demonstrate the ability of the model to support further fault injection testing for data signature identification and detection.

3.11 Model Validation & Limitations

Model validation was done by comparing and correlating simulated data with experimental data. First, breakthrough curves were compared between the STEVE testbed and Aspen Adsorption model to determine baseline differences and similarities for adsorption behavior. Next, nominal to off-nominal cyclic operation of the STEVE testbed was compared to Aspen simulations to challenge the model and determine modeling gaps and discrepancies.

The breakthrough curves represent the base behavior of the testbed and model. It provides information on how long it takes for the carbon dioxide to saturate and reach the outlet of the sorbent bed. This is done by measuring the outlet carbon dioxide concentration. The slope of the concentration increase provides information on the mass transfer in the system while the timestamp provides information on the breakpoint of the carbon dioxide, when the concentration is 5% of the feed carbon dioxide concentration, as well as the time to saturation, when the outlet concentration matches the feed concentration. The model will also generate breakthrough curves with outlet concentration values as seen in the previous section.

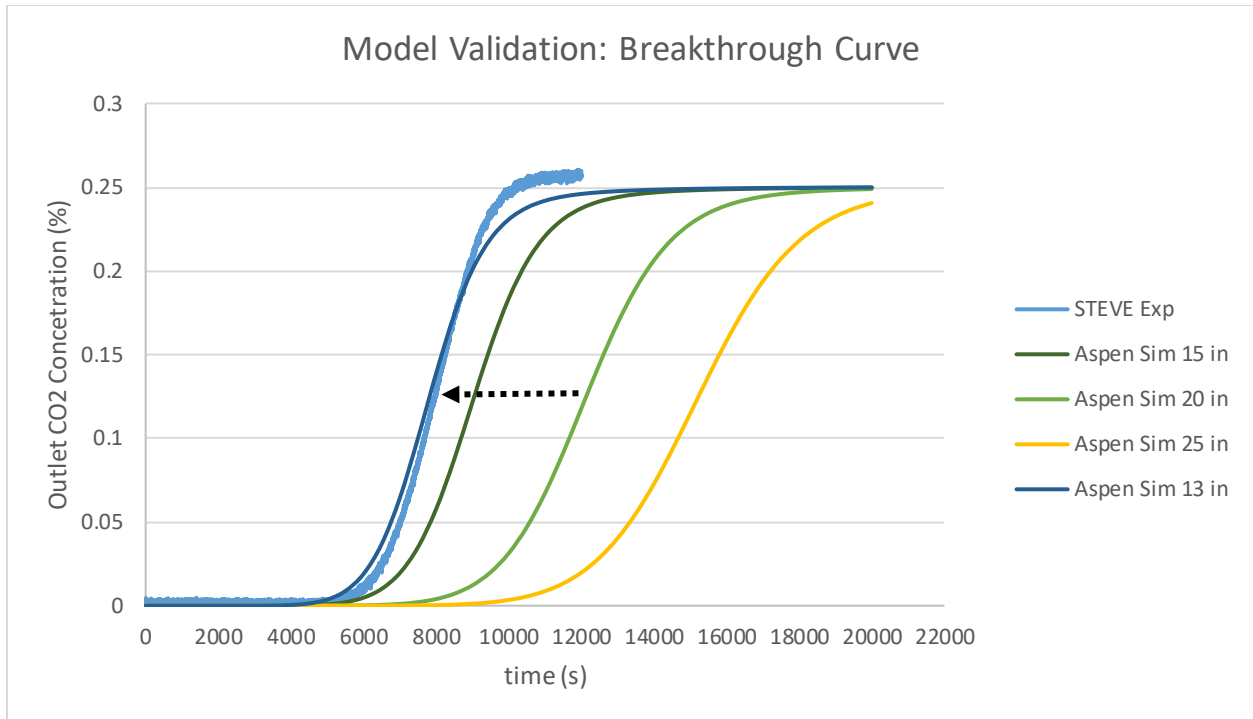


Figure 66. Model Validation with Breakthrough Curve Sensitivity Analysis by Varying Bed Length where the arrow indicates reduction of bed length to achieve correlation with STEVE experimental data.

In the plot above, there is discrepancy between the experimental data from the STEVE testbed and the simulated data from the Aspen Adsorption Model. The STEVE testbed uses a 20 inch bed with 0.87 inch inner diameter. The flow rate is set to 8 LPM and the carbon dioxide feed is set to approximately 0.25% CO₂. With the same parameter values set in Aspen Adsorption, the simulated results show a much later breakthrough curve than the experimental results. There can be many reasons for this discrepancy. To tune the parameters to correlate with experimental results, bed length was varied. In the plot above, reducing the bed length to 13 inches achieved good agreement. However, this implies that there is much less packing in the sorbent bed than reality.

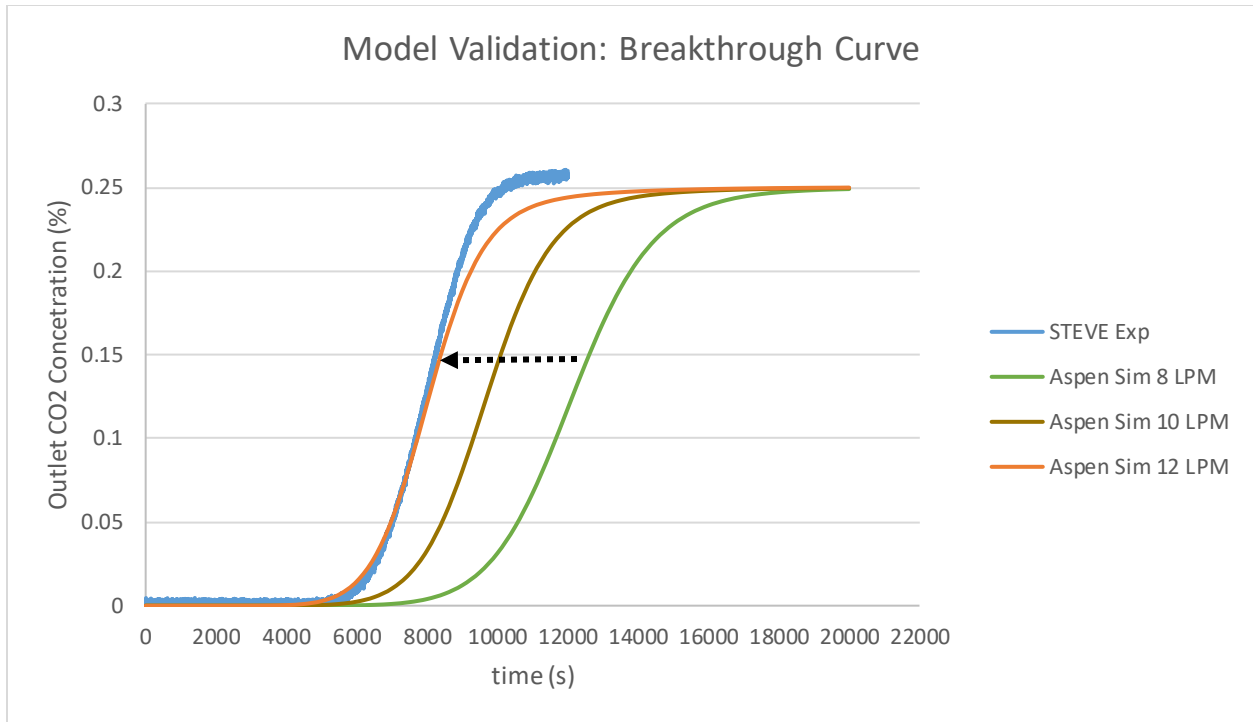


Figure 67. Model Validation with Breakthrough Curve Sensitivity Analysis by Varying Flow Rate where the arrow indicates increase of flow rate to achieve correlation with STEVE experimental data.

On the other hand, simulated flow rate may be varied to trend towards better correlation with experimental data. In the plot above, flow rate was increased to 12 LPM from the experimental setting of 8 LPM. This implies that the flow rate of the gas stream in the experiment may have been higher than what was measured and set in the experiment. However, this is unlikely.

There may be other more likely reasons for discrepancies. With all parameter values and conditions set the same between the testbed and the model, another reason may be that the isotherm model used in Aspen Adsorption could be slightly different for the STEVE testbed than testbeds from literature. The isotherm model was taken from several resources that studied zeolite 13X pellets extensively for carbon dioxide removal in life support systems for spacecraft

[31], [58], [59]. Although those parameter values are specifically for the same sorbent material used in the STEVE testbed, there is a possibility that the sorbent bead used in the STEVE testbed has slightly different material properties that altered or decreased its sorption capacity and therefore decreased overall breakthrough time. Another likely reason, if the isotherm model is correct and matches the behavior expected from the material used in the STEVE testbed, is that the sorbent beads may have water vapor loaded in adsorption sites in the beads, preventing some CO₂ from loading in the bed and thus causes the carbon dioxide to exit, or break through, the bed faster than anticipated.

The Aspen Adsorption model simulation results were also compared to cyclic operation of the STEVE testbed with alternating adsorption and desorption phases. Furthermore, the physical experiment injected a leak fault at the outlet of the bed at the beginning of the third adsorption phase in the experiment.

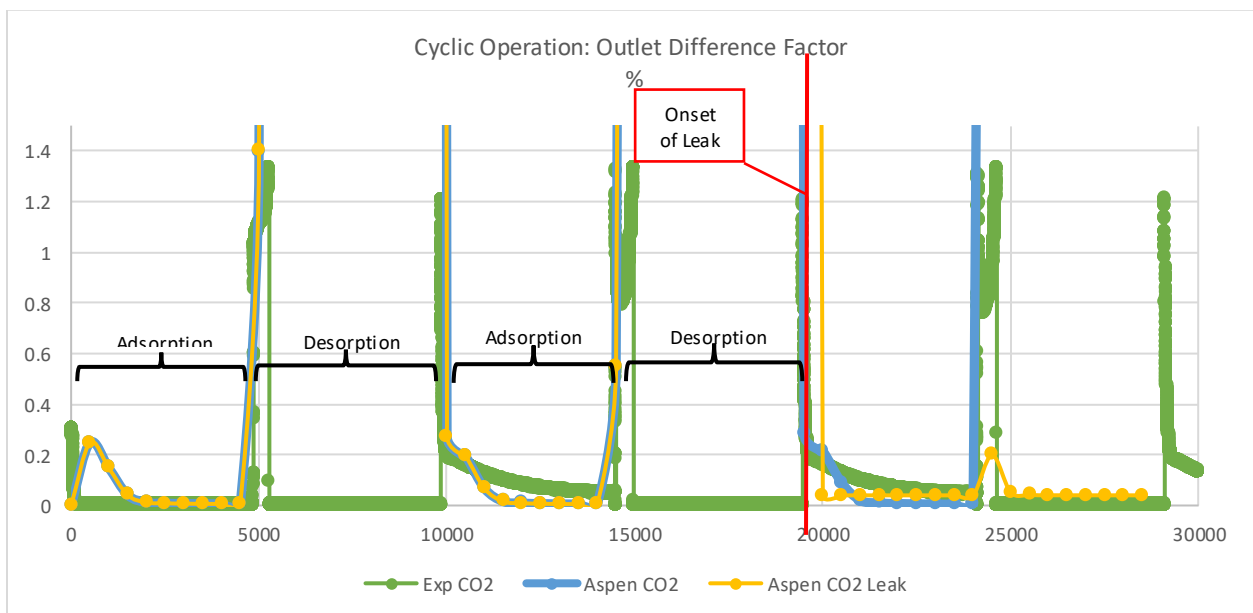


Figure 68. Outlet CO₂ Concentration with Leak Fault Injection Experimental and Simulation Correlation

The sensor readings tracked well except for the sensor saturation effect of the experimental data which automatically reads zero for sensor readings above its upper limit during desorption. A leak was introduced in the test during the third adsorption phase to see how the system performs and how well the model can fit to that test condition. The leak simulation was not able to track the leak behavior after onset, but it can be improved with further sensitivity testing with the testbed.

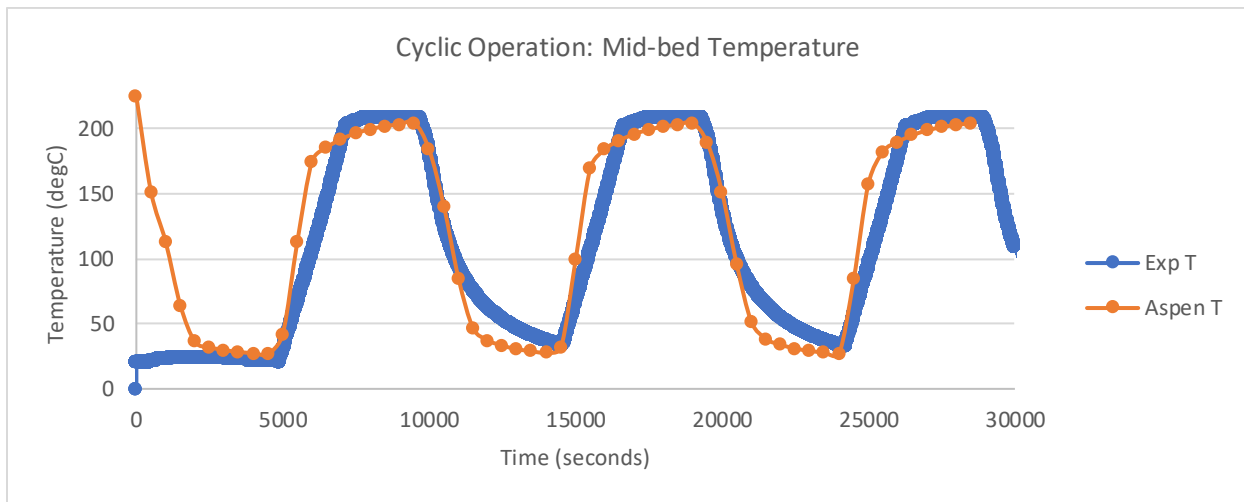


Figure 69. Sorbent Bed Temperature Experimental and Simulation Correlation

Model correlation was achieved for temperature in cyclic operation - displaying good agreement with experimental data. Tuning can be done to match the temperature rise more closely. The model uses steam jacket heaters rather than electrical tape type heaters so modeling the exact heater system was not possible [23], [66]. For the Aspen Adsorption model, a jacket heater with a fluid medium that transfers heat quickly and at high amounts showed the best correlation to electrical rope heater performance.

Due to the discrepancies found between experimental data and simulated data, further work can be done to confirm the nominal and baseline breakthrough curves for the STEVE

testbed to ensure that the simulation results do not correlate with the current baseline. STEVE testbed experiments can benefit from sensitivity analyses with varying bed lengths and flow rates to confirm effects on breakthrough curves as seen in the simulation results. In addition, the experiments should ensure that the sorbent and inlet gas stream is completely dry to prevent effects from humidity which decrease breakthrough time. The sorbent material should be confirmed to be the same as the material used in the references which provide the isotherm model [31]. If the sorbent is the same as referenced material, in this case zeolite 13X, then isotherm experiments may be needed to confirm the current isotherm parameter values or establish new parameter values that better fit the STEVE testbed.

Although there are discrepancies in the breakthrough curves, the data profiles for nominal (non-faulty) cyclic operation achieved good agreement with experimental data. Even if there is discrepancy, if the difference is in the order of minutes rather than hours for the carbon dioxide removal system, then there is less urgency and concern that the generated data is not useful for diagnostics and prognostics. Model validation is important for any modeling effort, but most models can only provide approximations and certain data features are more critical than others for diagnostics and prognostics. Data sets for fault detection and diagnostics should introduce new faults while data sets for prognostics benefit from repeated past faults. Detection and diagnostics benefit from data sets with detectable and isolated variation while prognostics benefit from data with gradual drifts or variation rate. Ultimately, diagnostics is concerned with faults, understanding isolated anomalous behavior, while prognostics is concerned with degradation, understanding nominal data and the onset and growth of off-nominal data. [23] There is a trade or cost analysis between achieving the highest fidelity model with the best match to physical systems and achieving flexibility and speed in generating anomalous data with reasonably

expected behavior. Ultimately, the data sets generated by the Aspen Adsorption model does not match experimental data exactly but it exhibits similar behavior and has the benefit of generating numerous data signatures that will be useful for future life support diagnostics and prognostics.

3.12 Discussion

The objective of this model is to generate nominal and off-nominal operation data that simulates performance, sensors readings, and other non-measured states to facilitate and improve diagnostics and prognostics for the system. The generated data sets simulate cyclic operation, i.e. alternating adsorption and desorption phases for each cycle, for test conditions at nominal operation of the STEVE testbed and fault injected conditions for off-nominal operation. Although the STEVE testbed has generated off-nominal data for leaky conditions and partial opening of valves, other fault injected tests should be conducted to further verify and validate simulations of all other faults such as multi-fault injection, low heat (sustained or temporary), filter clogging, and water loading due to dormancy. The summary of results is captured in the table below for the simulations reported in the previous section.

Table 9. Aspen Adsorption Test Results

Test #	Test Name	Manipulated Variables	Value	Units	Breakthrough Difference Factor	Loading Difference Factor
1	Nominal Operation	Crew size	5	-	1	1
			2		0.407407	0.2736
			10		1.666667	1.966943
		Bed Length	20	in	1	1
			15		2.23	0
			25		0	0
		Flow Rate	8	kmol/s	1	1
			5		0.869276	0.626643
			10		1.976057	1.30159
2	Sustained Valve Fault (Cv)	Nominal	1000	kmol/s/bar	1	1
		V _A Stiction	1e-5		0	1.098647
		V _D Stiction	1e-5		0.997578	0

3	Heater Fault	Nominal T _D	498	K	1	1
		Sustained Low T _D	450		1.288492	1.958614
		Temporary Low T _D	450		1.051267	1.658966
4	Vacuum Fault	Nominal P _D	10	kPa	1	1
		High vacuum P _D	80		0.917607	1.27095
		High vacuum P _D and Low T _D	80 450	kPa K	0.821548	1.739232
		High vacuum P _D and No T _D heat	80 298		0.012897	8.758971
5	Leak Fault	Nominal V _L	0	kmol/s	1	1
		V _L flow rate	1e-5		1	1.294704
6	Filter Clog Fault (C _v)	Nominal V _O	1000	kmol/s/bar	1	1
		V _O Clog	1e-5		0.602544	1.040286
7	Dormancy Water Preload	Nominal H ₂ O inlet	0 5.55e-6	kmol/kmol	1	1
		Preloaded Water inlet	1e-3 5.55e-6	kmol/s	3.475488	2.657253
8	Multi-Fault Combination	Nominal T _D	498	K Spec kmol/s	1	1
		Nominal V _D	1			
		Nominal V _L	0			
		Temporary Low T _D	450	K Spec kmol/s	1.026943	1.020825
Stiction V _D	2					
C _v Leak V _L flow	1e-5					

Note: Subscripts are A – adsorption, D – desorption, L – leak, O - outlet.

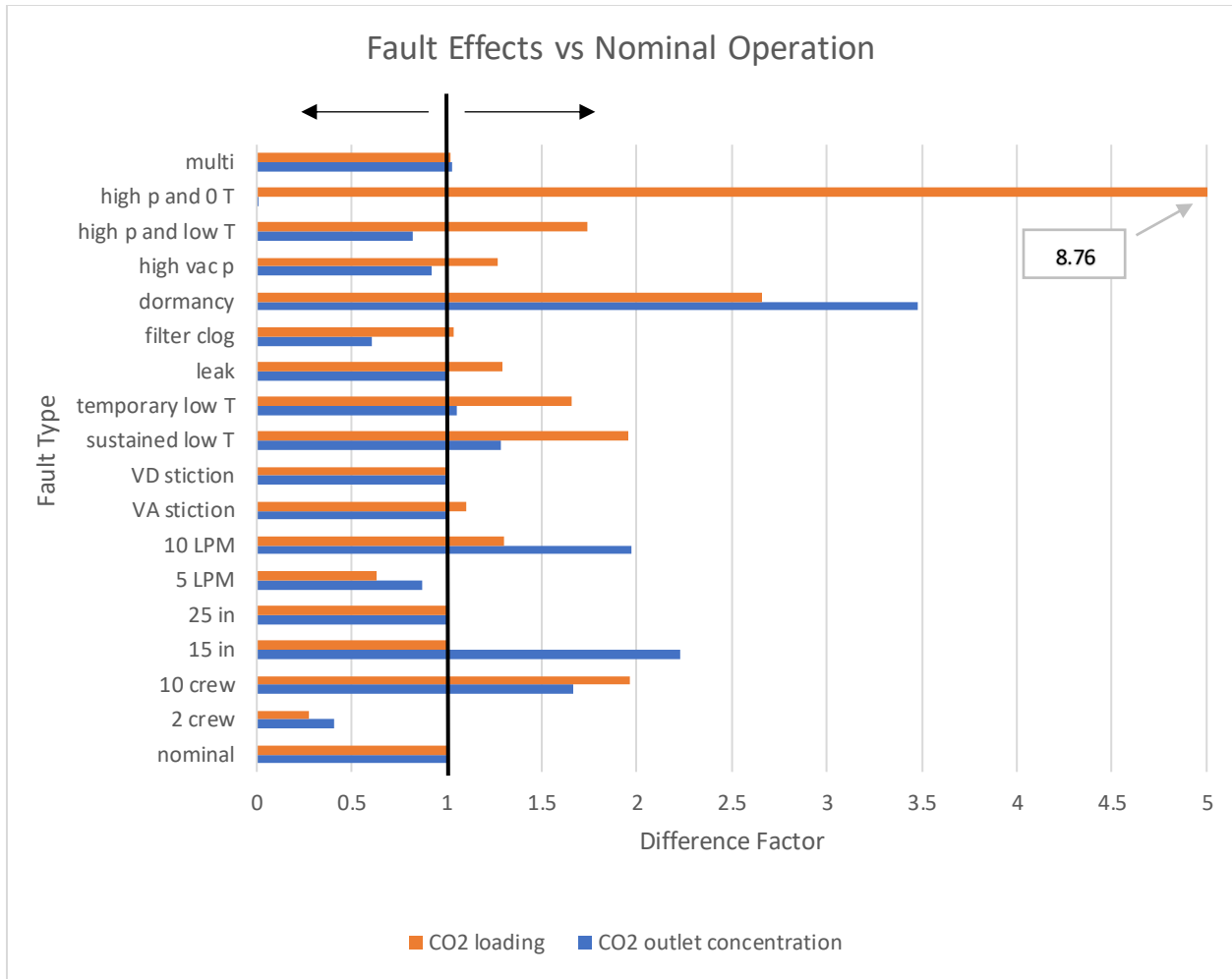


Figure 70. Outlet Concentration and Sorbent Loading Difference Factors for Nominal versus Off-Nominal Operation

The final test results show that CO₂ loading and outlet concentration increase or decrease in magnitude for the duration of the simulation based on the type of fault injected. Due to the design of the carbon dioxide removal system, higher outlet CO₂ concentration is not desirable while high sorbent loading is. High outlet concentration of CO₂ indicates the loss of scrubbing efficiency while high sorbent loading indicates desirable scrubbing performance and efficiency. Overall performance does depend on the initial conditions of the sorbent bed and the compositions of the inlet gas stream. Given the test results above, the sorbent loading was

increased from nominal due to all faults except lower flow rate at 5 LPM and operating with 2 crew CO₂ partial pressure. The outlet concentration decreased from nominal due to all faults except the multi-fault test, dormancy reloading, sustained and temporary low desorption temperature, low flow rate at 5 LPM and 2 crew. The faults injected in the model indicate anomalous behavior that must be corrected. A table of corrective actions and rationale are provided below:

Table 10. Faults, Key Indicators based on Simulation Results, and Corrective Actions

Test Name	Key Indicator(s)	Corrective Action(s)
Valve Stiction	No significant indicator except a slight increase in sorbent loading with VA stiction.	R&R valve with stiction
Heater Fault	Temperature and/or heater power sensor reads low. Slight increase in outlet CO ₂ concentration and significant increase in loading.	Repair the heater, power to the heater, or thermocouples
Vacuum Fault	Downstream pressure sensor reads higher than nominal during desorption. Increase in sorbent loading and slight decrease in outlet CO ₂ concentration. The prior effects become more severe as desorption temperature decreases from nominal.	Find and repair potential leaks or line configurations that prevent full vacuum pressure during desorption.
Leak Fault	Increase in outlet CO ₂ concentration.	Find and repair potential leaks.
Filter Clog Fault	Significant decrease in outlet CO ₂ concentration.	R&R filter with clog
Dormancy Water Preload	Significant increase in loading and outlet CO ₂ concentration.	Perform a long bakeout to purge water vapor from the bed
Multi-Fault Combination	Given the faults and sequence, no significant change was indicated.	Depends on the faults and sequence.

Future work is needed to further analyze the generated data signatures and extract unique data features that can be used as labels or flags for diagnostics and prognostics. Furthermore,

diagnostics and prognostics are used to monitor and maintain systems and can be affected by different fault types at varying degrees of impact and criticality.

Chapter 4 Carbon Dioxide Removal Model Using MATLAB

4.1 STEVE MATLAB Model & Estimation

As stated in previous sections, using MATLAB as a modeling program for carbon dioxide removal was done to compare model development and results using Aspen Adsorption. This parallel effort enables larger breadth of modeling capabilities for the HOME community. In addition, MATLAB offers increased flexibility and integration capabilities that proved useful for modeling carbon dioxide removal for diagnostics, in this case through the use of state estimation.

To promote increased self-awareness for deep space habitats, this MATLAB modeling effort has two objectives: modeling the physics of the STEVE testbed and estimating states based on measurements, uncertainty values, and the theoretical model of the testbed. This model combines data generated from the STEVE testbed, theoretical equations that represent the adsorption behavior of the bed, an estimation algorithm module, and applications to a digital twin framework to demonstrate the benefits of modeling and simulation deep space autonomous habitats [24].

Model development and state estimation in later sections mimic the components and operation of the STEVE testbed, described in more detail in the previous chapter. Parameters like sorbent bead radius and porosity, bed length and diameter, inlet gas composition, pressure, and temperature were used based on the nominal operation and test conditions of the STEVE testbed.

4.2 MATLAB Model Development

To estimate system performance parameters that cannot be readily measured in the lab or may have sensor uncertainties, a computational model of the CO₂ sorbent bed was developed. The sorbent bed is modeled as a tube packed with zeolite 13X pellets. It utilizes discretized nodes internal to a CO₂ removal system sorbent bed. The zeolite pellets have a designed porosity that enables CO₂ molecules to attach to the surface by physisorption. As cabin air flows through the

sorbent bed, CO₂ gas diffuses into the zeolite pellets and the scrubbed air is returned to the cabin as clean air. The scope of this MATLAB model is simulating only the adsorption phase. The switching mechanism and overall modeling of the desorption phase requires additional time and resources to complete and is recommended for future work.

The CO₂ sorbent bed model is comprised of classical mass balance equations. These equations include the packed-bed mass balance equation and an isotherm model, assuming an isothermal energy balance with constant temperature. The input and output measurements of the simulated testbed are CO₂ gas composition, mass flow rates, and gas pressure.

Packed Bed Mass Balance

The change in concentration of a gaseous species, in this case carbon dioxide, as it evolves over time and space is given by the spatial 1-D axial plug flow model in Equation 5 [31]:

$$\varepsilon_p + \frac{dC_i}{dt} + \frac{d(uC_i)}{dz} = \varepsilon_p D_L \frac{d^2 C_i}{dz^2} - (1 - \varepsilon_p) \rho_p \frac{d\bar{q}_i}{dt} \quad (5)$$

$$\frac{d\bar{q}_i}{dt} = K_L (q^* - \bar{q}) \quad (6)$$

Where ε_p is the particle porosity, u is the superficial velocity of the fluid, C_i is the concentration of component I, t is time, z is axial distance along the length of the bed, D_L is the axial dispersion coefficient, ρ_p is the particle density and $\frac{d\bar{q}_i}{dt}$ is the mass transfer rate of the gaseous species to the surface of the sorbent beads. The mass transfer term is calculated with K_L , the mass transfer coefficient, using the Linear Driving Force (LDF) model, q^* is the amount of gaseous species adsorbed onto the sorbent bead and \bar{q} the average adsorbed at equilibrium. To solve for concentration, equation (1) is rearranged to isolate $\frac{dC_i}{dt}$. Then the equation is discretized along the

length of the bed using the Finite Difference Method with n number of nodes, each node represented as k, and axial distance between nodes equal to dz. [31], [58]

$$\frac{dC_i}{dt} = D_L \frac{C_{k+1} - 2C_k + C_{k-1}}{dz^2} - \frac{u C_k - C_{k-1}}{\varepsilon_p dz} - \frac{(1 - \varepsilon_p)}{\varepsilon_p} \rho_p \frac{d\bar{q}_i}{dt} \quad (7)$$

Toth Isotherm Model

The Toth isotherm model governs the relationship between partial pressure of the gaseous species in a packed bed and the amount of that species that is adsorbed onto a solid surface or pore. There are many isotherm models to choose from [64], but Toth was selected based on good agreement with STEVE operation [67]. Other isotherm models can be used in future iterations of the model. The following Toth equation is solved for every time step and is the input for q^* in the mass transfer equation (7). q is the mean of the q^* values of the nodes in the bed at every time step.

$$q = \frac{q_m K_{eq} P}{[(1 + (K_{eq} P)^n)^{\frac{1}{n}}]} \quad (8)$$

$$K_{eq} = K_o \exp\left(\frac{-\Delta H}{RT}\right) \quad (9)$$

, where q is the adsorbed amount of the component, q_m is the maximum amount adsorbed at equilibrium, K_{eq} is an equilibrium constant, P is partial pressure of the adsorbed gaseous component, n is a Toth model parameter, K_o is the pre-exponential factor, ΔH is the heat of adsorption, R is the ideal gas constant, and T is temperature [67].

Finite Difference Method

The finite difference method is used to solve partial derivatives numerically. Due to the nature of the mass and energy balances of the 1-D axially dispersed plug flow model that represents the CO₂ removal sorbent bed, partial derivatives must be solved or approximated to determine the change of concentration and temperature of the gas and solid phase CO₂ over time and space. The finite difference method employed in this model are seen in equations 10-12:

$$\text{First Partial Derivative} \quad \frac{dc}{dz_i} = \frac{c_i - c_{i-1}}{z_i - z_{i-1}} \quad (10)$$

$$\text{Half Spatial Step} \quad \frac{dz_i}{2} = \frac{z_i + z_{i+1}}{2} \quad (11)$$

$$\text{Second Partial Derivative} \quad \frac{d^2c}{dz_i^2} = \frac{\frac{dz_i}{2} (c_{i+1} - c_i)}{(z_{i+1} - z_i)} - \frac{\frac{dz_{i-1}}{2} (c_i - c_{i-1})}{(z_i - z_{i-1})} \quad (12)$$

$$\left(\frac{dz_i}{2} - \frac{dz_{i-1}}{2} \right)$$

, where c is the gas phase concentration, z is the axial distance along the length of the bed and i denotes the spatial step. Future iterations of the model can utilize different difference methods. For examples, higher or lower order formulas can be used to reduce errors and enable better approximation of values at those discretization points. Furthermore, the difference method can also vary in direction with options for forward, backward, or central differencing [68]. Here, time is kept continuous while spatial steps are discretized into nodes as seen in the figure below.

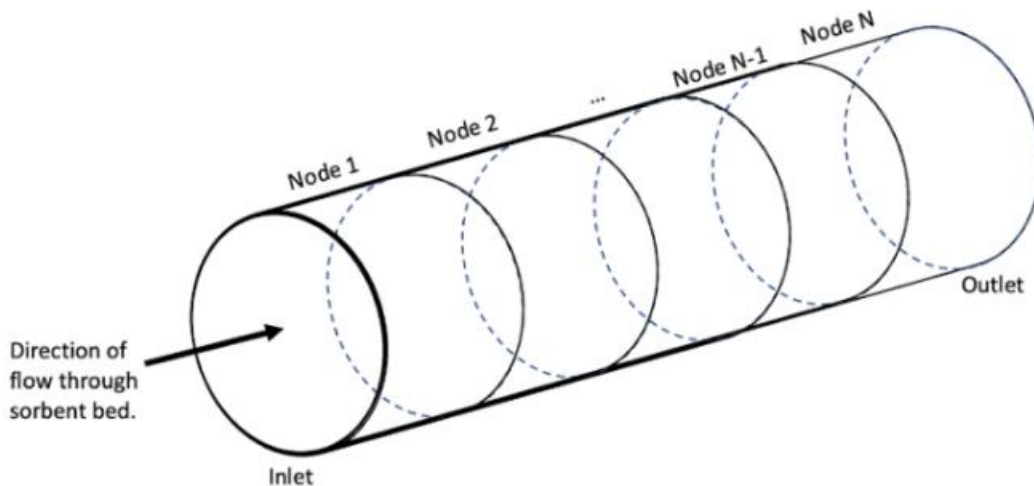


Figure 71. Spatial discretization along the length of the sorbent bed where N is the total number of nodes chosen for the calculation.

MATLAB Implementation

Carbon dioxide concentration, C_i , as it evolves in the sorbent bed is solved dynamically in MATLAB using the stiff ordinary differential equations solver function, ode15s. This solver was chosen due to its ability to integrate a system of stiff differential equations for a specified period of time and with specified initial conditions and handling of PDEs. Two functional MATLAB scripts were developed. The main script initialized concentration values and set initial conditions for CO₂ mole fraction in the incoming air stream and the simulation time. Then, the ode15s solver is called to solve the partial differential equations based on equations (7) to (9) written as one function in the second script. The main script initializes all variables and sets parameters first. Next, the process is broken down into several for loops to calculate the change in concentration from node 2 to node n-1 in the bed (the second term in (7)), the concentration at the boundary $z=L$ (the first term in (7)), loading based on the Toth isotherm model (equation (8)), and finally the concentration at each node at each time step as seen in equation (7). This result is used as a check and visualization of CO₂ loading within the sorbent bed along the axial distance and simulation time-space. In the main script after solving for simulated CO₂ mole fraction, all variables and parameters are initialized for state estimation followed by solving for state estimates which will be further described in the next section.

4.3 Estimation of System States

Among the options of estimation algorithms that can be applied to this use case, the Kalman filter was determined to be a good fit for this system. Other filter and estimation algorithms are good fits for a more complex suite of ECLSS subsystems such as the Particle Filter. Here, the Extended Kalman Filter was selected due to the nonlinear nature of the cyclic operation of the

STEVE testbed and due to the complex system of equations that represent the sorbent bed during adsorption and desorption cycling. The equations used are as follows:

$$\hat{x}_{k|k-1} = f_k(\hat{x}_{k-1|k-1}, u_{k-1}, 0) \quad (13) \quad A'_{k-1} = \frac{\partial f_k}{\partial x_k} \Big|_{\hat{x}_{k-1|k-1}} \quad (18)$$

$$P_{k|k-1} = A'_{k-1} P_{k-1|k-1} A'^T_{k-1} + E'_{k-1} Q_{k-1} E'^T_{k-1} \quad (14) \quad E'_{k-1} = \frac{\partial f_k}{\partial w_k} \Big|_{\hat{x}_{k-1|k-1}} \quad (19)$$

$$\hat{x}_{k|k} = \hat{x}_{k|k-1} + L_k (y_k - h_k(\hat{x}_{k|k-1}, u_k, 0)) \quad (15) \quad C'_k = \frac{\partial h_k}{\partial x_k} \Big|_{\hat{x}_{k|k-1}} \quad (20)$$

$$L_k = P_{k|k-1} C'^T_k (C'_k P_{k|k-1} C'^T_k + F'_k R_k F'^T_k)^{-1} \quad (16) \quad F'_k = \frac{\partial h_k}{\partial v_k} \Big|_{\hat{x}_{k|k-1}} \quad (21)$$

$$P_{k|k} = P_{k|k-1} - L_k C'_k P_{k|k-1} \quad (17)$$

, where Eq. (13) solves for the predicted state estimate (a priori), $\hat{x}_{k|k-1}$, based on the state transition model which utilizes the theoretically deduced state estimate, $\hat{x}_{k-1|k-1}$, and the previous time step data input, u_{k-1} , Eq. (14) calculates the covariance, $P_{k|k-1}$, based on the previous time step value and the covariance of the model noise, Q, Eq. (15) and Eq. (16) solve for the updated state value at the current time step using the Kalman gain, L_k , which utilizes the covariance of the measurement noise, R, and the measurement, y_k . Using the estimated state based on theoretical deduction, $\hat{x}_{k-1|k-1}$, as the input, A'_{k-1} is the solved derivative of $\frac{\partial f_k}{\partial x_k}$ and $E'_{k,i}$ is the solved derivative of $\frac{\partial f_k}{\partial w_k}$, where f_k is the state transition model and w_k is the process noise. Using the predicted state estimate, $\hat{x}_{k|k-1}$, as the input, C'_k is the solved derivative of $\frac{\partial h_k}{\partial x_k}$ and F'_k is the solved derivative of $\frac{\partial h_k}{\partial v_k}$, where h_k is the observation model and v_k is the observation noise. [69], [70]

Next, the above equations were applied to the mass transfer equations for the sorbent bed as can be seen in equations (22) to (25). The state x_k is the concentration of CO₂ in the last node and will be estimated using the extended Kalman filter, where x is the concentration of the gas component, k is the timestep and i is the denotation for specific gas component in a gas mixture. It is here forward assumed that x_k is for the carbon dioxide gas component in a mixture of CO₂ and N₂. The outlet measured concentration of CO₂ is $y_k = x_k$. The algorithm below is broken up into model prediction, then output, and followed by measurement update as shown below. It is important to note that k denotes the time step while z denotes the spatial step.

Model Prediction

$$\hat{x}_{k|k-1} = \hat{x}_{k|k} + \frac{dx_{k,i}}{dt} dt \quad (22)$$

$$\frac{dx_{k,i}}{dt} = D_L \frac{x_{z-1,i} - 2x_{z,i} + x_{z+1,i}}{dz^2} - \frac{u(x_{z,i} - x_{z-1,i})}{\varepsilon_p dz} - \frac{(1 - \varepsilon_p)}{\varepsilon_p} \rho_p \frac{d\bar{q}_{k,i}}{dt} \quad (23)$$

$$\frac{d\bar{q}_{k,i}}{dt} = K_L \left(\frac{q_m K_{eq} x_{k,i}}{[(1 + (K_{eq} x_{k,i})^n)^{\frac{1}{n}}]} - \bar{q} \right) \quad (24)$$

$$A'_{k,i} = 1 + \left(\frac{D_L}{dz^2} - \frac{u}{\varepsilon_p dz} - \frac{K_L(1 - \varepsilon_p)\rho_p}{\varepsilon_p} \left(\frac{q_m K_{eq} x_{k,i}}{[(1 + (K_{eq} x_{k,i})^n)^{\frac{1}{n}}]} - 1 \right) \right) dt \quad (25)$$

$$E'_{k,i} = 1 \quad (26)$$

$$P_{k|k-1} = A'_{k-1} P_{k-1|k-1} A'^T_{k-1} + E'_{k-1} Q_{k-1} E'^T_{k-1} \quad (27)$$

Output

$$y_{k,i} = x_{k,i} \quad (28)$$

$$h_{k,i} = x_{k,i} \quad (29)$$

Measurement Update

$$C'_{k,i=1} \quad (30)$$

$$F'_{k,i=1} \quad (31)$$

$$L_k = P_{k|k-1} C_k'^T (C_k' P_{k|k-1} C_k'^T + F_k' R_k F_k'^T)^{-1} \quad (32)$$

$$\hat{x}_{k|k} = \hat{x}_{k|k-1} + L_{k,i} (y_{k,i} - h_{k,i}) \quad (33)$$

$$P_{k|k} = P_{k|k-1} - L_k C_k' P_{k|k-1} \quad (34)$$

4.4 Estimation of 1-Phase Operation

In developing a self-aware space habitat, it is important to note the difference between using a physics-based versus a data-based model. The model described in this section is a first principles and physics-based model of a one-bed sorbent system for carbon dioxide removal. As seen in multiple past studies that have developed tools and models of spacecraft, physics-based models can be useful for test and system design for new products, prototypes, and systems (including reconfigurations). In the early stages of habitat development, there is little to no data that can be used to generate a robust data-based model. For example, data signatures for healthy operation of a carbon dioxide removal system will look smooth and cyclic while unhealthy data signatures may drift, spike, or go missing intermittently or for sustained periods of time. As time passes, the amount of data logs and signatures increase for a system which makes the data repository increasingly more useful in understanding how a product or system works in the field or under stochastic conditions. Early deep-space habitat design may use physics-based models to ensure self-awareness and autonomy in the beginning, but it has the potential to benefit more from data-based models as it ages.

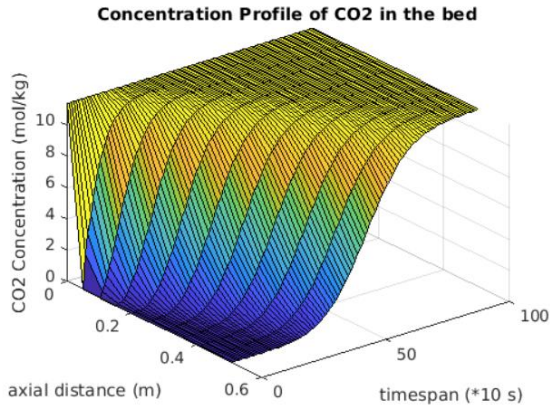


Figure 72. Concentration profile of CO₂ in the gas phase along the length of the bed and over time.

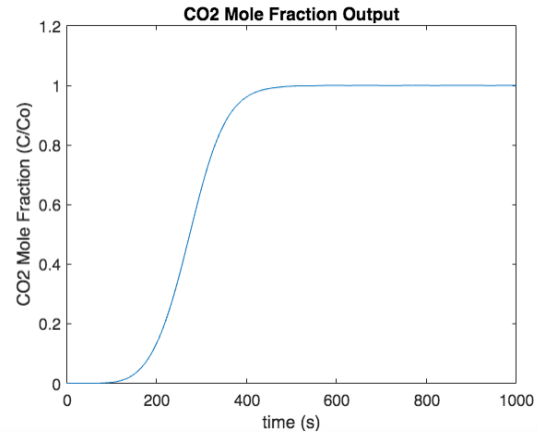


Figure 373. Theoretical measurement data for mole fraction of CO₂ in the exhaust stream of the bed.

States were modeled for CO₂ mole fraction in the gas phase at discretized nodes along the length of the sorbent bed which were updated by measured CO₂ concentration in the outlet gas stream. This parameter, amongst many others, must be estimated due to difficulty of adding internal sensors to various systems, such as the ISS CDRA, or even the CU Boulder STEVE apparatus. To create a robust and informed Digital Twin, a validated system model allows an infinite number of location-specific states to be estimated. However, only a finite number of sensors can be physically implemented into a system, such as that of the ECLSS of any spacecraft which is comprised of multiple similarly packed beds. In the use case considered here, CO₂ mole fraction at the exhaust of the sorbent bed can be measured and estimated concurrently. Understanding of current state relies on real-time sensing and historical investigations. We increase our understanding of system state using models. State estimations can be made from past, present, and simulated future datasets – demonstrating the power of system health monitoring that “learns” from past data and makes “educated” recommendations for future anticipated failures based on any number of operational conditions.

The model was verified by comparing the STEVE experimental data with the model-simulated data. The error and covariance were plotted to determine the accuracy of the simulation and estimation algorithm. Although this is one small set of data representing state estimation for a single adsorption phase, this demonstrates the ability to employ state estimation algorithms to measured experimental data, thereby displaying how first principles-based computation with known measurement and model uncertainty tracks physical data – uncertainty or noise factors can be tuned based on preference or engineering judgement on model versus sensor accuracy.

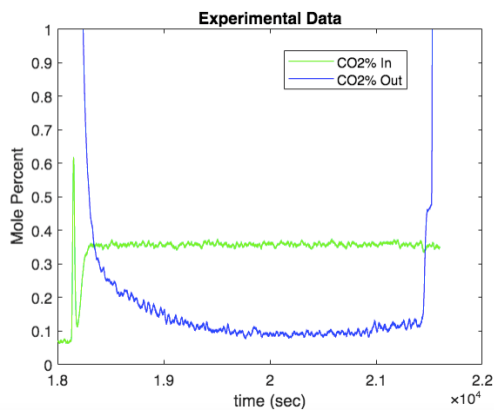


Figure 74. Experimental Measurement Data of CO₂ Mole Percent from the STEVE test bed.

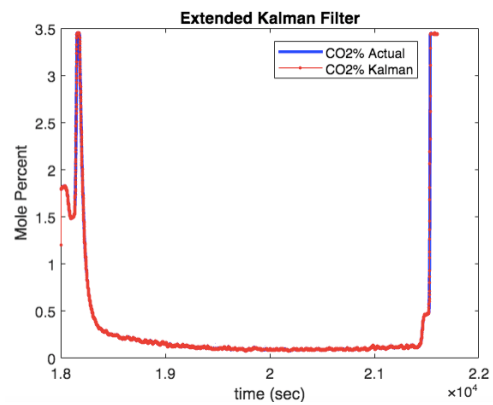


Figure 75. Comparison of Actual Data and Kalman Filter Estimation of CO₂ Mole Percent

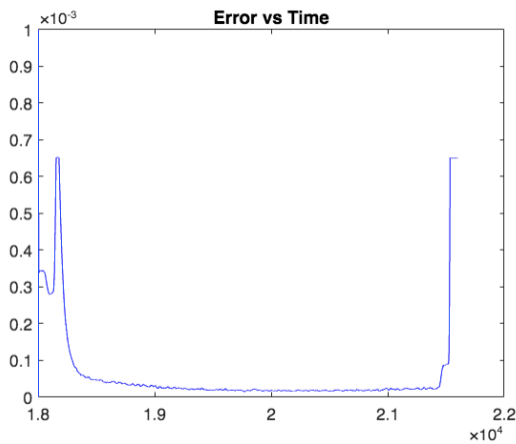


Figure 76. Error of CO₂ Mole Percent

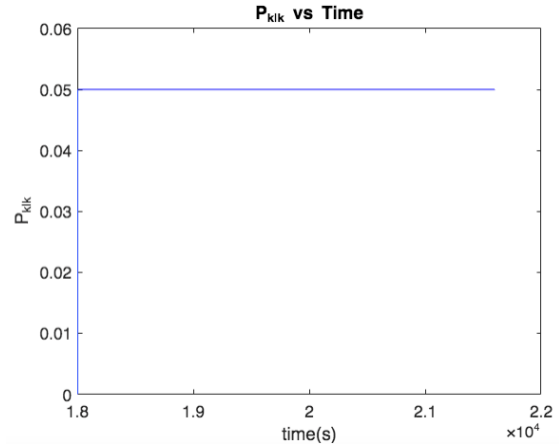


Figure 77. Covariance of CO₂ Mole Percent

There are several benefits to state estimation and implementing this type of module in a Digital Twin. If for example, internal or external sensors are not present, missing, or faulty, a state

estimator module, or “agent”, is able to calculate a more realistic value for certain parameters where sensor uncertainty is too high. Therefore, with a validated system model, self-awareness and autonomy of a spacecraft remains strong even in the face of sensor reduction.

4.5 Estimation for Cyclic Operation

Given an $E'_{k,i}$ set to 1 with process noise set to 0.1 and measurement noise set to 0.05, we get the results below. Error is $1e-3$ at most, and the Kalman Filter Estimation seems to track exactly with the sensor readings. In this case, analyses of this estimation and sensor data indicate no error in the sensor readings or any detection of something wrong in the system.

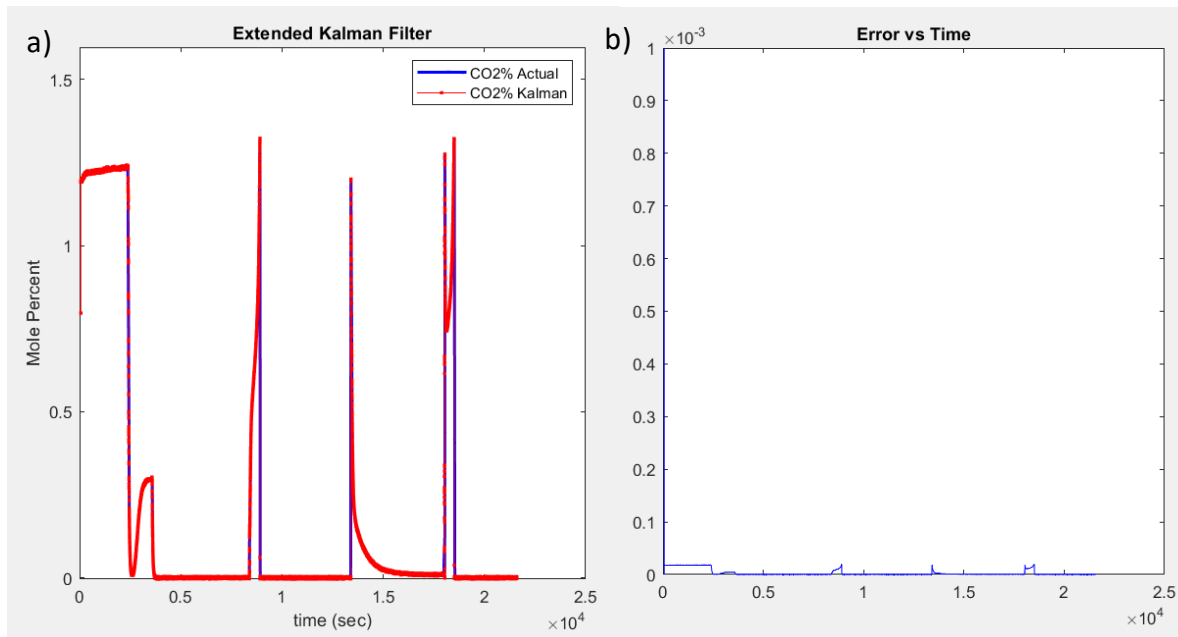


Figure 78. a) Outlet CO₂ Concentration and b) Estimation Error for Cyclic Operation

If the above parameters are set the same and C and F are set to 0.5 instead of 1, confidence in the sensor readings is tuned down and the results are generated as follows. The plots below indicate that the estimated value of the outlet concentration of carbon dioxide may be higher than the measured values. In addition, the error plot indicates that sensor measurements are not in agreement with theoretical estimates, facilitating analyses in off-nominal behavior

detection. Here, the error coincides with sensor measurements that read close to or at zero. These zero values are due to start-up and sensor saturation where the sensor writes a zero value to measurements above its upper limit. If sensor saturation during the desorption step was not present, it is expected that the error will not be seen in the plot on the right. Therefore, without sensor saturation effects, the error may facilitate the detection and identification of anomalous behavior among other steps and processes.

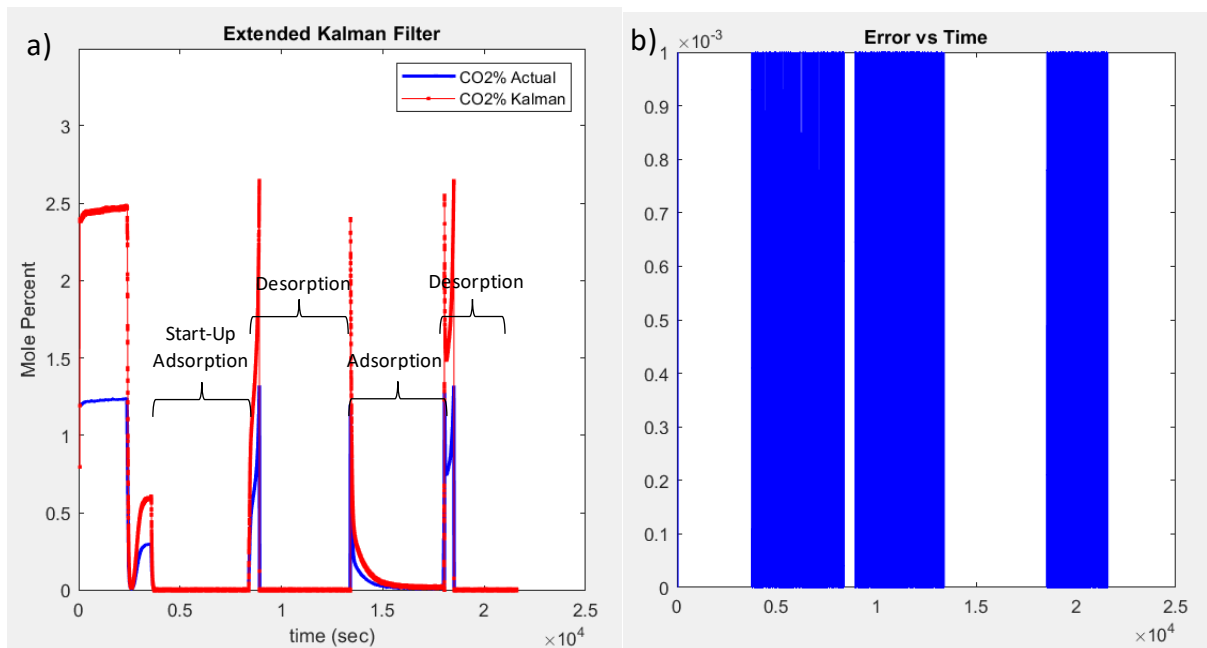


Figure 79. a) Outlet CO₂ Concentration and b) Estimation Error for Cyclic Operation

4.6 Discussion

Data management aboard an autonomous spacecraft requires capabilities that include, but are not limited to, data generation, validation, model-based estimation, storage, exchange, and transport. With the combination of physics-based modeling, system state estimation and integration with a Digital Twin data repository, the listed capabilities for a sorbent bed in a carbon dioxide removal system test bed were demonstrated [24]. This serves as a steppingstone to

validating a potential process for data management that boosts spacecraft self-awareness and autonomy.

In addition to future work to improve the model and estimation algorithm, work can be done to design the simulation experiments to consider and incorporate sensor criticality in different what-if scenarios like the injected faults in the previous chapter. For example, certain state estimates can be made based on the criticality and uncertainty of various sensors that take multiple factors into account. Such factors may be sensor life, historical discrepancies like drift and point anomalies, and severity of impact to crew safety. With a study on sensor criticality and uncertainty for life support systems, estimation algorithms can be tuned to flag faults more accurately and with greater confidence.

Chapter 5 Zeolite Degradation Testbed for Deep Space Habitat Research

The development of a testbed that compliments the modeling efforts in previous chapters is described here. Modeling carbon dioxide removal for spacecraft life support is challenging without the means to understand and test removal performance, and lack of it, for deep space applications.

5.1 ZeoDe Testbed

The Zeolite Degradation (ZeoDe) testbed built and located at UC Davis serves as a supplementary system to the STEVE testbed at CU Boulder. It also serves to generate additional data for the HOME community for carbon dioxide removal to specifically study component degradation. Deep space habitats will be built to withstand long mission durations and dormancy. Understanding and anticipating system degradation is of utmost importance when considering prognostics for life support systems aboard these future spacecrafts. The main considerations for the ECLSS onboard a deep space habitat, such as Gateway, are ramp-up testing in preparation for crew arrival, robotic maintenance for component repairs and reconfiguration operations, and improvement of the state of the art for ECLSS system health management. In alignment with these considerations, ZeoDe serves to generate data that will inform ramp-up testing after dormancy periods and highlight considerations for robotic maintenance.

The primary objective of the initial ZeoDe test plan was to generate degradation data for the HOME prognostics modeling team. It was designed in a way to address both crewed and uncrewed habitat conditions. The tests do not initially include auxiliary failure modes as done in the STEVE testbed, but it may include them in the future to enable data-rich repositories for the HOME community. Initially, the experiment plan is focused only on the degradation of the sorbent bed. The sorbent selected for this study is zeolite 13X due to its use in the STEVE

testbed and the ISS CDRA, and it is known to have recoverable performance after temporary degradation events. Sorbent degradation can occur in many ways such as through attrition, mechanical disruption, and contamination. The primary degradation mode with the highest probability of occurrence on station and highest impact is water vapor contamination which causes the sorbent bed performance to decrease and has lasting effects on efficiency if it is not addressed.

5.2 Sorbent Degradation

The two types of degradation modes that can take place are short-term and long-term degradation modes. Short-term degradation modes are recoverable faults that are temporary and can be mitigated. Long-term degradation modes are non-recoverable and cannot be mitigated. The result of long-term degradation is eventual removal and replacement of the unit. Historically, sorbent beds are subjected to thermal vacuum swing to regenerate or bakeout to recover from degradation caused by humidity. For situations where packed beds have too much pressure drop and cannot perform with the required metrics, those units are replaced by supply spares.

For the zeolite 13X sorbent bed, temporary degradation is most likely caused by humidity (presence of water vapor) at the inlet. Due to the structure of the material, water molecules attach to active sites on the zeolite crystal that would have been used for CO₂ adsorption. The material is known for its high affinity for water and co-adsorption of CO₂/H₂O gaseous mixtures. Carbon dioxide removal performance can recover after a long regeneration cycle using thermal vacuum swing. The key indicators of humidity-induced short-term degradation is increasing humidity sensor values at the inlet of the bed and lower outlet CO₂ concentration. The goal of testing humidity input in the ZeoDe testbed is to identify the rate of water loading, called creeping flow,

at varying humidity input levels and initial water loaded states. Outlet CO₂ concentration, humidity, breakthrough time, and temperature were tracked for these experiments. [50], [71]–[73]

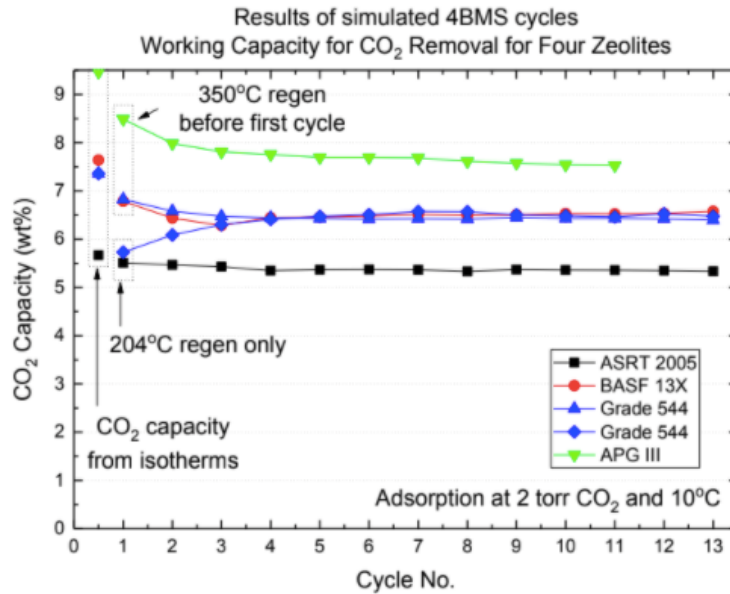


Figure 80. Results of working capacity for candidate materials for the development of the 4-BMS where Grade 544 (zeolite 13X) displayed short-term degradation (restoration) to nearly full capacity through normal operating cycles even after water loading [73]

Long-term degradation of the zeolite 13X sorbent bed is caused by breakdown of the clay binders of the pellets due to thermal cycling (causing contraction and expansion) in the presence of water. This leads to degradation of the clay binder, which causes the sorbent pellets to crumble and generate dust. Dust can enter the flow stream and cause blockages and accumulation downstream. The key indicator of long-term degradation due to the resulting dust is high pressure drop across the sorbent bed [74]. After an adsorption cycle, the pressure delta between the inlet and the outlet of the sorbent bed will increase due to the accumulation of dust at the outlet filter. The goal of this type of test would be to monitor pressure drop over time and determine an overall failure rate estimate and remaining useful life of the component. This

degradation mode takes a long time to test and simulate so it is not in scope of the current ZeoDe test plan. ZeoDe tests can inform prognostics modeling of the carbon dioxide removal system. The temporary degradation metrics will inform decision making such as suggestions for repair processes and timelines as well as identifying faults and root causes to prevent a future or a near-term anticipated failure.

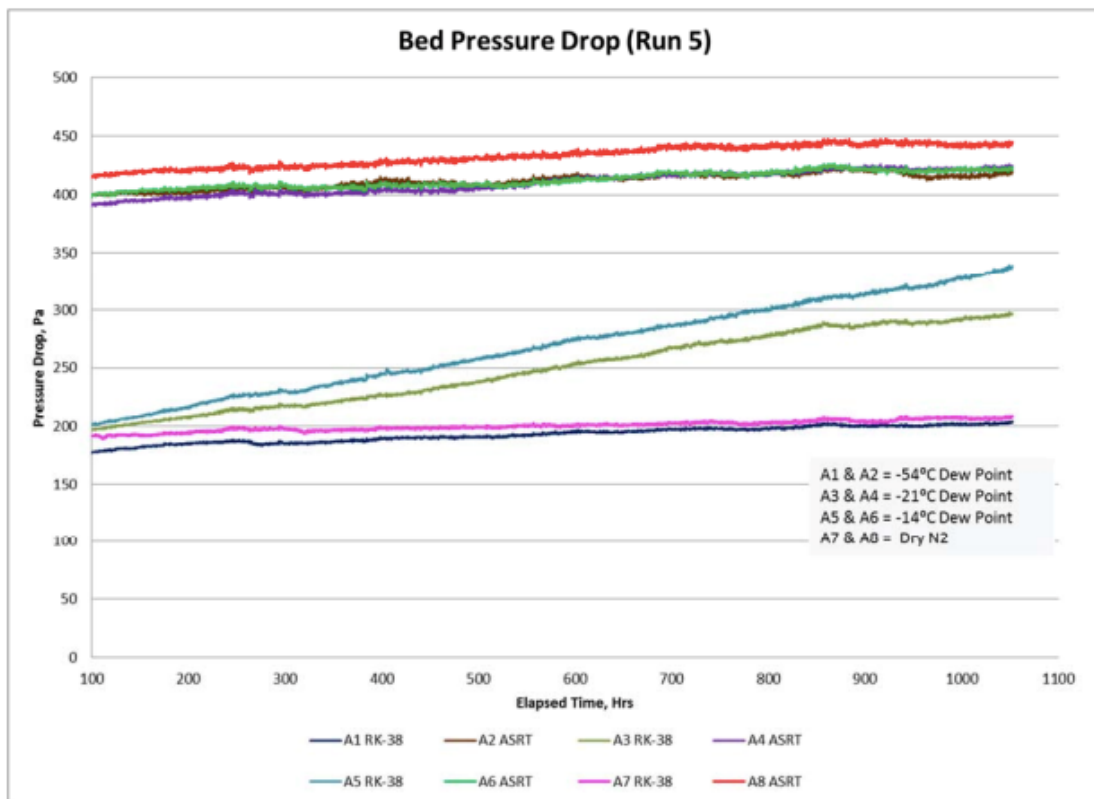


Figure 81. Differential Pressure across the testbed with different sorbent materials displaying pressure drop increase for materials that accumulated dust due to long term degradation. [74]

5.3 ZeoDe Testbed

The testbed was built by modifying an existing testbed that was used for catalyst experiments in the department of Viticulture and Enology at the UC Davis. Due to the nature of catalyst testing, additional sensors and modifications to hardware configurations were made. The testbed includes compressed gas cylinders for gas input, mass flow controllers, a gas mixing unit

with manual valves, a furnace and packed bed reactor, and finally a gas chromatography analyzer. The modifications were the addition of humidity and CO₂ sensors, a bubbler, tubing reconfigurations, and additional valves for counter current flow capability needed to desorption. There was no vacuum pump available for use to conduct pressure swing for desorption, so a nitrogen purge was used instead.

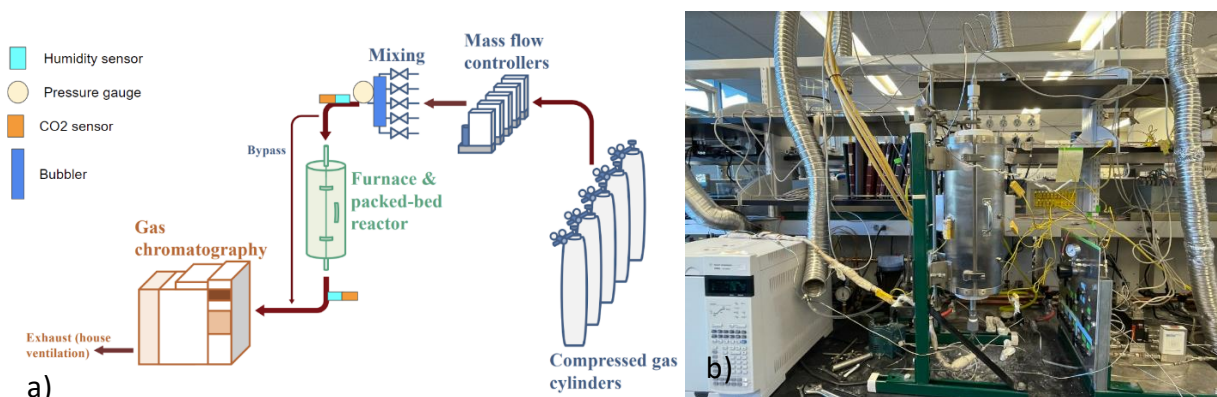


Figure 82. Zeolite Degradation Testbed a) Schematic and b) Image

During adsorption, the ZeoDe testbed supplies a specified flow of CO₂-laden air to the sorbent bed. Nominally, ZeoDe provides a gas mixture with 99% air and 1% carbon dioxide, and dew point of approximately -50°C. The 1% CO₂ composition was constrained by the testbed's mass flow control capabilities and could not be lowered to a value closer to STEVE operation which uses 0.25% CO₂. ZeoDe's objective is to conduct accelerated degradation testing; therefore, the higher 1% CO₂ could enable faster sorbent bed saturation and aligned with the testbed's objective. An automated LabVIEW system commanded the flow, compositions, and furnace heater from their setpoints for CO₂ adsorption to those needed for desorption. Flow rate was constrained to a maximum of 0.5 LPM while nominal STEVE operation uses 8 LPM. The much lower flow rate significantly affected the breakthrough time and overall correlation with STEVE operation since mass transfer is highly dependent on the flow rate.

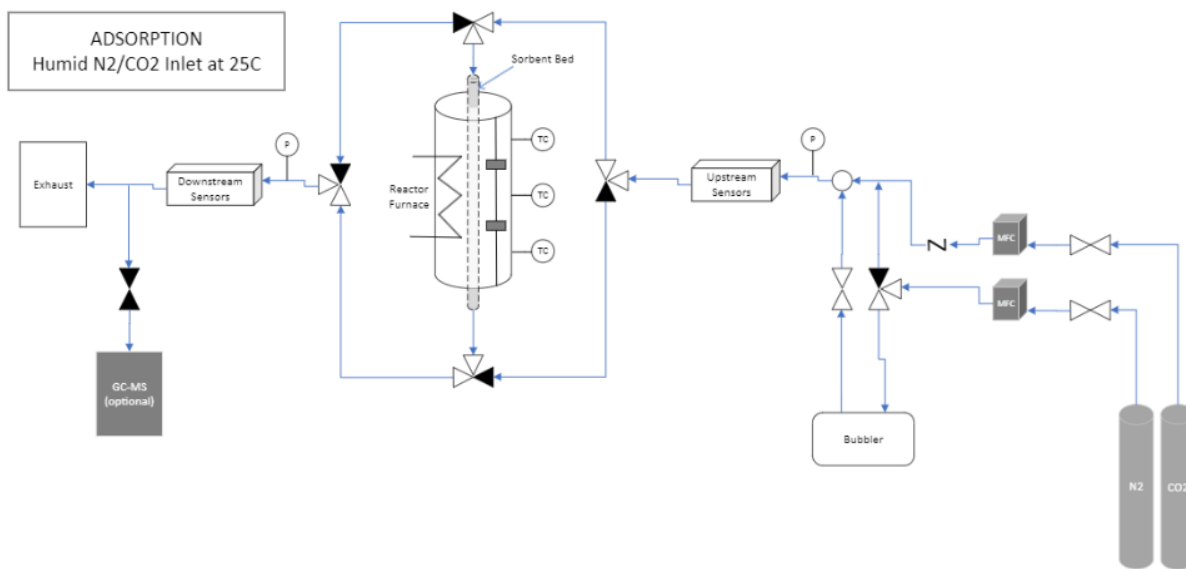


Figure 83. ZeoDe Schematic for Adsorption

A jacket furnace heater raised the insulated bed temperature to 250°C with a nitrogen purge to conduct CO₂ desorption and regeneration of the pellets via thermal swing. Degradation testing also utilizes a bubbler that will humidify an inlet nitrogen stream which will then mix with the rest of the gas stream before entering the sorbent bed. Although there are temperature, CO₂, and humidity sensors and one pressure gauge, the testbed can hookup to a gas chromatography mass spectrometer (GC-MS) for further gas stream characterization. The adsorption/desorption cycles can be repeated for a specified number of cycles. The schematics for adsorption and desorption are pictured below with black valve openings indicating a closed junction.

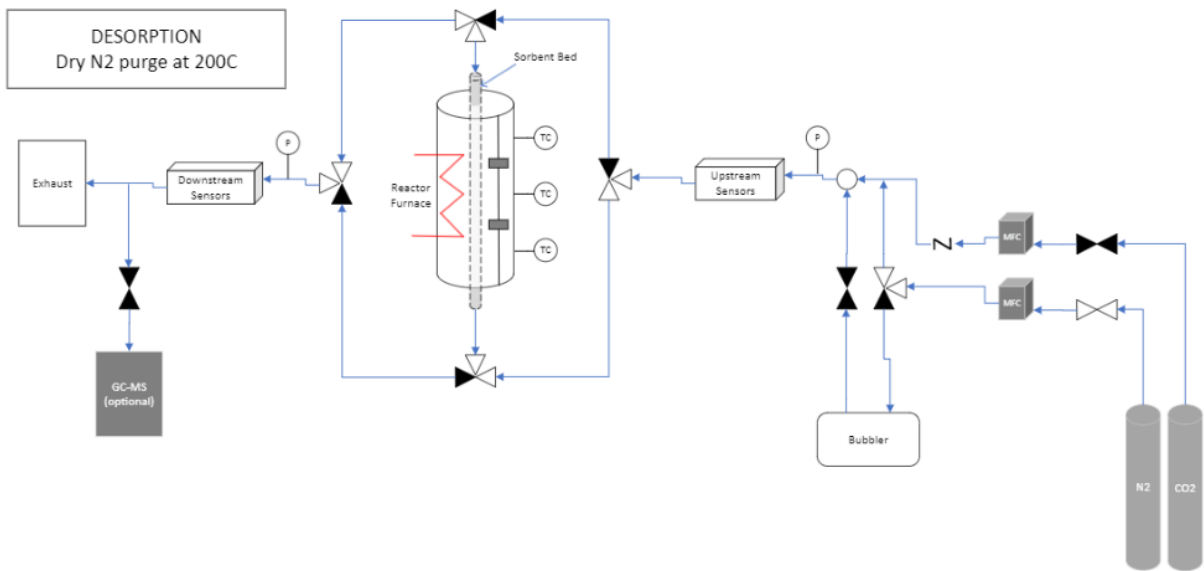


Figure 84. ZeoDe Schematic for Desorption

5.4 ZeoDe Results

ZeoDe testing was initiated in May of 2022 with set up and parts procurement completed in one month and baseline testing completed in the following month. The testing timeline was short and was only capable of providing proof of concept data. The preliminary results show agreement with expected breakthrough curves and cyclic operation.

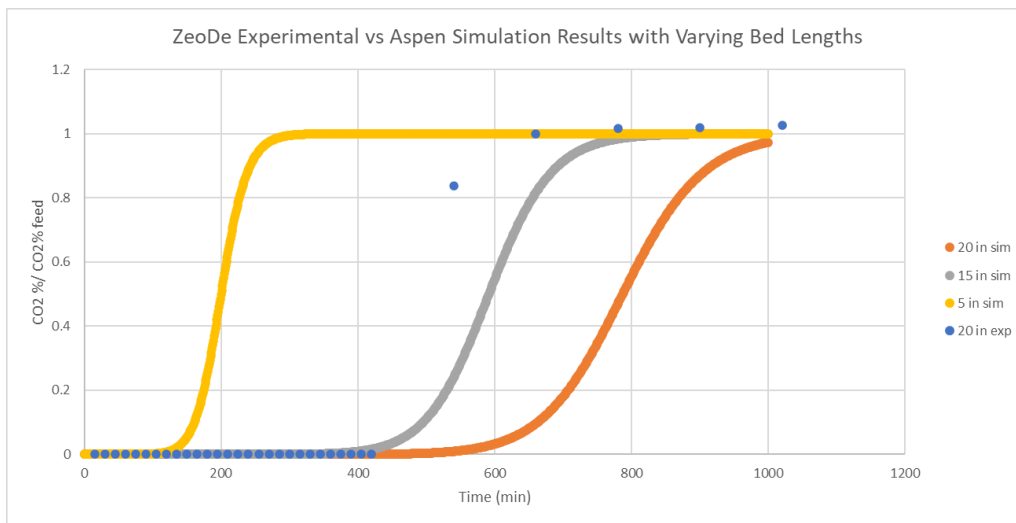


Figure 85. Breakthrough Curve Comparison for Varying Bed Lengths

Initial baseline tests were conducted to check if experimental values tracked well with simulated values using the MATLAB model. Above, the experimental breakthrough curve for a 20 inch sorbent bed with 1 inch diameter more closely tracked the simulated breakthrough curve of a 15 inch bed. The experimental results show that, as discussed in the previous chapter for model validation discrepancies, there may be many reasons behind the discrepancies between the theoretical and experimental results. The ZeoDe testbed results could be confirmed by testing the same conditions with the STEVE testbed but this could not be completed in the time of writing due to schedule conflicts. Regarding the simulated results, there may be discrepancy in the isotherm parameters used to describe the material. The isotherm parameters were meant for spherical zeolite 13X pellets while the ZeoDe testbed used cylindrical pellets with varying pellet lengths. In regard to the experiment itself, even if the sorbent bed was subjected to a long bakeout, there may still be some amount of water, undetected by the humidity sensors, that prevented the pellets from achieving full sorption efficiency.

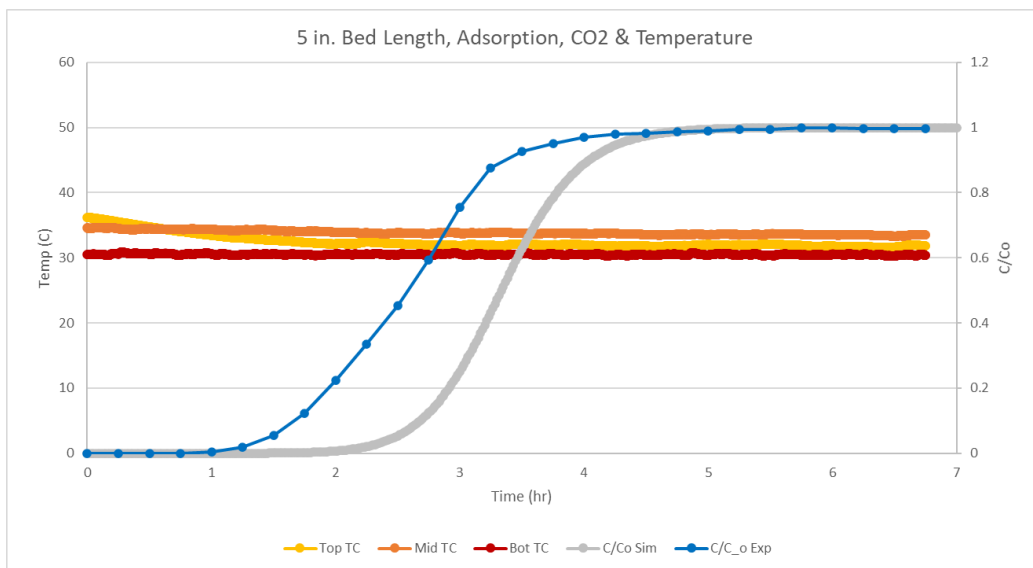


Figure 86. Breakthrough Curve Comparison for 5 inch Bed

Overall, the length of the bed and low flow rate caused the breakthrough time to be longer than desired for testing purposes. Therefore, given the breakthrough curve results and the maximum flow rate of 0.5 LPM that was allowable, the only tunable parameter that could be used was bed length and it was reduced to 5 inches to achieve faster breakthrough as seen in the plot above.

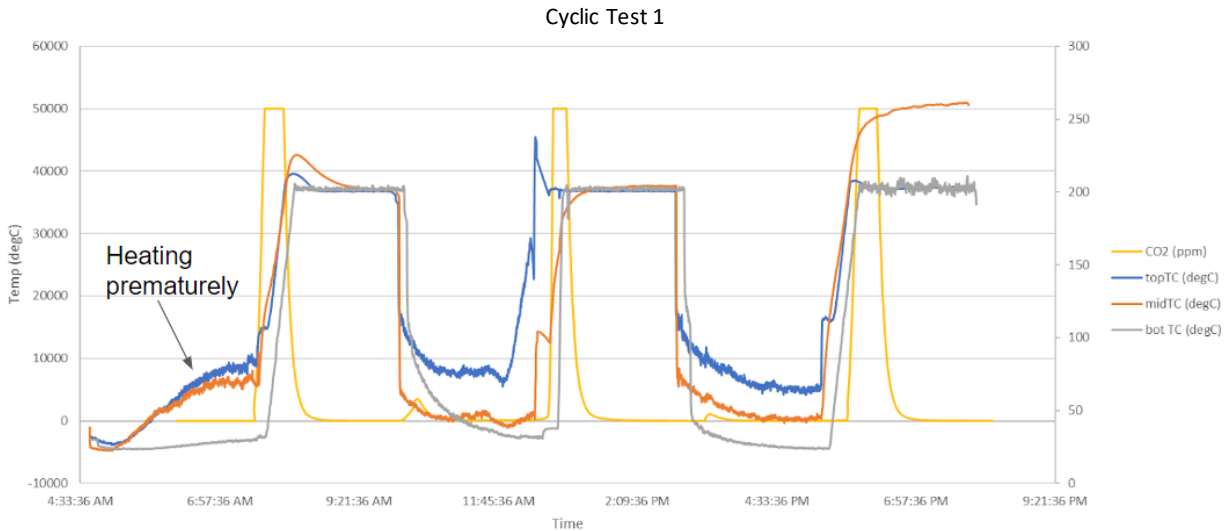


Figure 87. Outlet CO₂ Concentration and Temperature Profile for Baseline Cyclic Test 1

Considerable effort and time is needed to complete one experiment. Due to the low flow rate, three adsorption and desorption cycles could be completed in one test day with 8 to 10 hours allotted to preparation and bake-out the night prior. The temperature was controlled by the LabView software, but the flow rates and valves were controlled manually. The manual control dependence is not recommended for future testing as it was highly prone to error and schedule conflicts. Although the temperature profile control was automatic, there were still observed errors in the heater control as seen in the plot above. Therefore, the test was not accepted as baseline nominal data due to the undesired premature heating during all the adsorption phases. The cause of the error was due to a software bug that reset initial temperatures to a higher

temperature setting rather than remaining off, at room temperature, for the adsorption phases.

Test protocols were established to prevent future instances of premature heating.

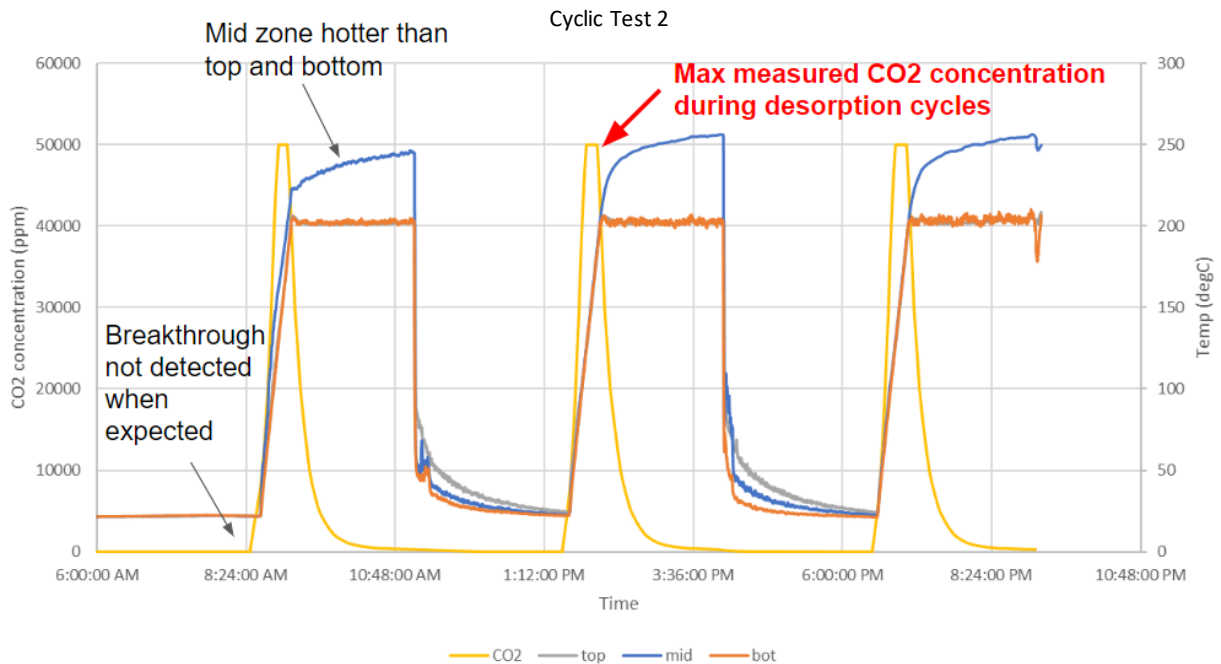


Figure 88. Outlet CO₂ Concentration and Temperature Profile for Baseline Cyclic Test 2

In the plot above, baseline data was still not achieved due to the undesired higher temperature at the middle zone compared to the inlet (bottom zone) and outlet (top zone). The temperature discrepancy is significant with 50°C difference. Because of the higher mid zone temperature, the desorption kinetics are affected, causing nonuniform desorption behavior along the length of the bed. This may be useful data for heater fault injection studies where heating is higher in the middle of the bed than the outlet and inlet, but the objective of Cycle Test 2 was to complete baseline control testing. In the plot above, one can also see that the CO₂ outlet sensors saturated at 50,000 ppm during the initial stage of the desorption phases. This is expected and is worth noting for future CO₂ sensor selection, where a higher sensor upper limit may be desired. Although the general behavior of the outlet CO₂ measurements is as expected, the onset of

breakthrough was not detected at the end of each adsorption phase. It is detected by a slight slope increase in the curve before the major release due to desorption. Because it was not detected, this means that the cycle time may need to be adjusted to be longer to be able to detect and confirm breakthrough, before switching to desorption.

5.5 Discussion

The ZeoDe testbed was successful at confirming proof of concept for zeolite degradation testing in the context of carbon dioxide removal for spacecraft life support. However, hardware and software reports as well as test protocols were documented for testbed improvement, not only for data generation purposes but also for operational ease. In addition, modifications and replacements can aid in making ZeoDe test conditions closer to STEVE and CDRA operation such as the addition of higher flow rate mass flow controllers, replacing manual valves with automated valves, adding a downstream filter, swapping with an electrical rope heater, and adding a vacuum pump. The lessons learned, test protocols, and hardware improvements were documented, reviewed, and is in transition to the next user for assembling a more permanent testbed setup. To facilitate prognostics modeling, data generation for humidity input will enable better estimates for remaining useful life, spares logistics, and repair processes for future deep space habitat life support systems.

Chapter 6 Conclusions and Future Work

The objective of this thesis was to generate data signatures for the HOME community and provide modeling instruction to the wider space community who are interested in modeling ECLSS and carbon dioxide removal (Chapter 1). Work included extensive literature review of the status of ECLSS roadmaps, lessons learned, maintenance and spares logistics as well as ECLSS data analysis processes relevant to diagnostics and prognostics applications for deep space habitats (Chapter 2). Then work was done to build a model of the one-bed carbon dioxide removal system using Aspen Adsorption, a ready-made platform with built-in mathematical computations and capabilities for fault injection, to generate a multitude of data signatures, nominal and off-nominal, and validate against experimental data (Chapter 3). Next, model development was done using MATLAB, a mathematical program with full customization and algorithm integration capabilities but challenging development of numerical computations and fault injections, to generate nominal data signatures with the off shoot of applying state estimation to increase the overall model's ability to combine measurement data with theoretical models to estimate sensor data, whether available or not (Chapter 4). Finally, work was done to assemble and test a supplementary carbon dioxide removal testbed focused on sorbent degradation which achieved proof of concept and generated test protocols and documentation for hardware and software improvements for the next generation ZeoDe testbed (Chapter 5).

The primary conclusions from each chapter are summarized in the list below followed by potential investigations and tasks for future work.

6.1 Conclusions

In Chapter 2, a thorough review of the literature was conducted to highlight the importance and role of modeling and simulations for future exploration-class ECLSS.

- The down-selection process to close the loop on future ECLSS design can be accelerated with modeling and simulation capabilities as time to estimate performance can be much shorter than procuring and assembling a working prototype of the system.
- ECLSS ground truths, assumptions, and functional allocations have been determined for Moon to Mars Habitation which will inform performance criteria for ECLSS modeling and simulation.
- Key indicators and faults have been recorded for ECLSS component service life which provide better estimates for future operation and design. Due to these findings, degradation-based modeling has become more important as mission durations get longer.
- Degradation rates must account for metrics on ordinary usage, temporary environmental disturbances or disruptions (expected and unforeseen), and sustained changes in the system (i.e. physical or control reconfigurations)
- For maintenance and spares logistics for deep space missions, some ECLSS units like the CO₂ Removal system may be powered down and others could be better replaced with storage and distribution of the consumable like oxygen for cabin air.
- The current ECLSS anomaly resolution process is ordered and hierarchical but can be slow and manual. Future ECLSS anomaly monitoring and resolution can benefit from automated processes for investigations like automated modeling and simulations to determine fault trees, root causes and corrective actions.

In Chapter 3, an Aspen Adsorption model for the carbon dioxide removal system was described and tested against various faults typically seen for the subsystem.

- Complete model development and rationale are given for each component in the model.

- Fault injections were successfully tested and analyzed for key indicators and overall deviation from nominal behavior.
- Model validation was conducted using experimental and simulated breakthrough and cyclic operation (nominal and off-nominal cases).

In Chapter 4, a MATLAB model for the carbon dioxide removal system was described and tested for correlation and augmented with state estimation to demonstrate virtual sensing and applications for diagnostics.

- Model development and mathematical foundations are given for the sorbent bed in the model for the adsorption phase. In addition, nonlinear Kalman state estimation was implemented and described.
- Estimation of outlet concentration for breakthrough and cyclic operation was successfully tested and analyzed for key indicators associated with anomaly detection.
- Model validation was conducted using experimental and simulated breakthrough data.

Chapter 5 describes the development and test of a supplementary carbon dioxide removal testbed that focuses on sorbent degradation to inform ECLSS diagnostics and prognostics.

- Testbed assembly and rationale were described, especially regarding sorbent degradation.
- Experimental results were provided for breakthrough and cyclic operation with descriptions of expected behaviors and potential discrepancies.
- Proof-of-concept was successfully completed and provided a plethora of information for testbed improvements and modifications.

6.2 Suggestions for Future Work

This thesis highlighted the paramount role of modeling and simulation for the HOME community as well as the wider space life support community and showed that further work can be done to

continuously move towards advanced SmartHab capabilities for upcoming deep space missions to the Moon, Mars, and beyond. The following list details suggestions for future work to continue this momentous effort:

Chapter 2

- For future ECLSS design, three trade studies should be addressed against Moon to Mars Habitation requirements: (1) sensor array versus mobile sensors, (2) self-actuation versus mobile (robotic) manipulation, and (3) in-place redundancy versus “repair and replace” spares philosophy.
- For future life support anomaly resolution, determining the optimal interface between system modeling, estimation, diagnosis, and prognosis with the current process of using subject matter expertise and disparate ECLSS databases is needed to create data-richness, increase organization and traceability, and further enable self-awareness and autonomy. Further work in degradation modeling can be utilized to determine nuanced effects of operational conditions, anomalies, and faults that can cause varying rates of degradation.

Chapter 3

- STEVE testbed experiments can benefit from more sensitivity analyses by varying bed lengths and flow rates to confirm effects on breakthrough curves as seen in the simulation results. In addition, the experiments should ensure that the sorbent and inlet gas stream is completely dry to prevent effects from humidity which decrease breakthrough time. The sorbent material should be confirmed to be the same as the material used in the references which provide the isotherm model. If the sorbent is the same as referenced material, in this case zeolite 13X, then isotherm experiments may be needed to confirm the current isotherm parameter values or establish new parameter values that better fit the STEVE testbed.

- Future work is needed to further analyze the generated data signatures from the Aspen Adsorption model and extract unique data features that can be used as labels or flags for diagnostics and prognostics modeling.

Chapter 4

- Future work is needed to improve the model and estimation algorithm as well as to design the simulation experiments in a way that considers and incorporates sensor criticality metrics for different what-if scenarios. For example, certain state estimates can be made based on the criticality and uncertainty of various sensors that take multiple factors into account. Such factors may be sensor life, historical discrepancies like drift and point anomalies, and severity of impact to crew safety. With a study on sensor criticality and uncertainty for life support systems, estimation algorithms can be tuned to flag faults more accurately and with greater confidence.

Chapter 5

- For future work with the ZeoDe testbed, hardware and software reports as well as test protocols were documented as guides for testbed improvement - not only for data generation purposes but also for operational ease. In addition, it is recommended that modifications and replacements be made to make ZeoDe test conditions closer to STEVE and CDRA operation. Some examples are the addition of higher flow rate mass flow controllers, replacing manual valves with automated valves, adding a downstream filter, replacing the furnace with an electrical rope heater, and adding a vacuum pump. In addition to hardware changes, it is recommended that special attention is allocated to software development to enable automated testbed controls and data acquisition through a program like LabView.

References

- [1] L. Hall, “Habitats Optimized for Missions of Exploration (HOME),” NASA, Oct. 03, 2019. http://www.nasa.gov/directorates/spacetech/strg/stri/stri_2018/Habitats_Optimized_for_Missions_of_Exploration_HOME (accessed).
- [2] C. Escobar, J. Nabity, and A. Escobar, “Quantifying ECLSS Robustness for Deep Space Exploration,” Jul. 2019, [Online]. Available: <https://ttu-ir.tdl.org/handle/2346/84455>
- [3] J. F. Russell and D. M. Klaus, “Maintenance, reliability and policies for orbital space station life support systems,” *Reliab. Eng. Syst. Saf.*, vol. 92, no. 6, pp. 808–820, Jun. 2007, doi: 10.1016/j.res.2006.04.020.
- [4] N. Li *et al.*, “Multi-Sensor Data-Driven Remaining Useful Life Prediction of Semi-Observable Systems,” *IEEE Trans. Ind. Electron.*, vol. 68, no. 11, pp. 11482–11491, Nov. 2021, doi: 10.1109/TIE.2020.3038069.
- [5] J. Broyan, M. McKinley, I. Stambaugh, G. Ruff, and A. Owens, “NASA Environmental Control and Life Support Technology Development for Exploration: 2021 to 2022 Overview,” Jul. 2022, [Online]. Available: <https://ttu-ir.tdl.org/handle/2346/89796>
- [6] R. M. Bagdigian, J. Dake, G. Gentry, and M. Gault, “International Space Station Environmental Control and Life Support System Mass and Crewtime Utilization In Comparison to a Long Duration Human Space Exploration Mission,” p. 16.
- [7] D. E. Sherif and J. C. Knox, “International Space Station Carbon Dioxide Removal Assembly (ISS CDRA) Concepts and Advancements,” Jul. 2005, pp. 2005-01–2892. doi: 10.4271/2005-01-2892.
- [8] R. M. Bagdigian, J. Dake, G. Gentry, and M. Gault, “International Space Station Environmental Control and Life Support System Mass and Crewtime Utilization In Comparison to a Long Duration Human Space Exploration Mission,” Jul. 2015, [Online]. Available: <https://ttu-ir.tdl.org/handle/2346/64374>
- [9] W. Bryan, “Space Station Regenerative ECLSS Flow Diagram,” NASA, Jun. 28, 2017. <http://www.nasa.gov/offices/oct/image-feature/space-station-regenerative-eclss-flow-diagram> (accessed).
- [10] M. S. Anderson, M. K. Ewert, J. F. Keener, and S. A. Wagner, “Life Support Baseline Values and Assumptions Document.” Mar. 01, 2015. [Online]. Available: <https://ntrs.nasa.gov/citations/20150002905>
- [11] P. D. Cronyn, S. Watkins, and D. J. Alexander, “Chronic Exposure to Moderately Elevated CO₂ During Long-Duration Space Flight.,” National Aeronautics and Space Administration, Houston, TX. Lyndon B. Johnson Space Center., N20120006045, 2012. [Online]. Available: <https://ntrl.ntis.gov/NTRL/dashboard/searchResults/titleDetail/N20120006045.xhtml>
- [12] S. P. Eshima and J. A. Nabity, “Failure Mode and Effects Analysis for Environmental Control and Life Support System Self-Awareness,” p. 13.
- [13] M. K. Ewert, T. T. Chen, C. D. Powell, T. T. Chen, and C. D. Powell, “life support baseline values and assumptions document,” Feb. 2022, [Online]. Available: <https://ntrs.nasa.gov/citations/20210024855>
- [14] D. Ivey, M. Torralba, and S. Robinson, “ECLSS Air Revitalization Technology Review 2022: Review of Current Published Units and their Fault Modes,” Jul. 2022, [Online]. Available: <https://ttu-ir.tdl.org/handle/2346/89720>
- [15] J. C. Knox and C. M. Stanley, “Optimization of the Carbon Dioxide Removal Assembly (CDRA-4EU) in Support of the International Space System and Advanced Exploration Systems,” Jul. 2015, [Online]. Available: <https://ttu-ir.tdl.org/handle/2346/64432>
- [16] W. Peters, G. Cmarik, and J. Knox, “4BCO₂ EDU Performance,” Jul. 2021, [Online]. Available: <https://ttu-ir.tdl.org/handle/2346/87252>

- [17] H. Ranz, S. Dionne, W. Papale, and J. Garr, “Thermal Amine Scrubber-- Operational Status, Optimization & Improvements,” Jul. 2022, [Online]. Available: <https://ttu-ir.tdl.org/handle/2346/89834>
- [18] A. Owens, W. Cirillo, N. Piontek, C. Stromgren, and J. Cho, “More Data Needed for Failure Rate Estimation, Validation, and Uncertainty Reduction,” Jul. 2021, [Online]. Available: <https://ttu-ir.tdl.org/handle/2346/87278>
- [19] R. J. Beil *et al.*, “International Space Station (ISS) Anomalies Trending Study,” *Int. Space Stn.*, p. 53, 2015.
- [20] D. Oberhettinger, “The PRACA system as an ‘incubator’ for lessons learned,” in *2015 IEEE Aerospace Conference*, Mar. 2015, pp. 1–8. doi: 10.1109/AERO.2015.7118880.
- [21] C. A. Jorgensen, “International Space Station Evolution Data Book,” p. 222, 2000.
- [22] H. Jones, “How Should Life Support Be Modeled and Simulated?,” Jul. 2017, [Online]. Available: <https://ttu-ir.tdl.org/handle/2346/72914>
- [23] S. Eshima, J. Nabity, M. Torralba, D. Ivey, and S. Robinson, “Generating Anomalous Regenerable CO2 Removal System Data for Environmental Control and Life Support System Self-Awareness,” Jul. 2022, [Online]. Available: <https://ttu-ir.tdl.org/handle/2346/89798>
- [24] M. Torralba, C. George, S. Robinson, S. Eshima, and J. Nabity, “Estimation of System States for Non-Measured Parameters and Integration with a Digital Twin framework to Boost Spacecraft Autonomy and Awareness,” Jul. 2022, [Online]. Available: <https://ttu-ir.tdl.org/handle/2346/89759>
- [25] M. Kayatin, “The Spacecraft Mass Balance as a Diagnostic Tool for Cabin Air Quality,” Jul. 2021, [Online]. Available: <https://ttu-ir.tdl.org/handle/2346/87237>
- [26] Y. Yang, M. Smits, D. Kas, J. Jauzion, and G. Gordon, “Optimizing Crop Selection Using Genetic Algorithms,” Jul. 2021, [Online]. Available: <https://ttu-ir.tdl.org/handle/2346/87228>
- [27] A. C. Owens, “Quantitative probabilistic modeling of environmental control and life support System resilience for long-duration human spaceflight,” Thesis, Massachusetts Institute of Technology, 2014. [Online]. Available: <https://dspace.mit.edu/handle/1721.1/93770>
- [28] J. Badger and J. D. Frank, “Spacecraft Dormancy Operational Design for a Crewed Martian Reference Mission,” in *2018 AIAA SPACE and Astronautics Forum and Exposition*, American Institute of Aeronautics and Astronautics, 2018. doi: 10.2514/6.2018-5117.
- [29] D. L. Carter, D. Tabb, and M. Anderson, “Water Recovery System Architecture and Operational Concepts to Accommodate Dormancy,” p. 15.
- [30] D. Kaschubek and J. Nabity, “Modeling and Simulation of Component Degradation and Faults in the Carbon Dioxide Removal Assembly,” Jul. 2022, [Online]. Available: <https://ttu-ir.tdl.org/handle/2346/89758>
- [31] J. C. Knox, A. D. Ebner, M. D. LeVan, R. F. Coker, and J. A. Ritter, “Limitations of Breakthrough Curve Analysis in Fixed-Bed Adsorption,” *Ind. Eng. Chem. Res.*, vol. 55, no. 16, pp. 4734–4748, Apr. 2016, doi: 10.1021/acs.iecr.6b00516.
- [32] J. L. Broyan *et al.*, “NASA Environmental Control and Life Support Technology Development for Exploration: 2020 to 2021 Overview,” p. 12.
- [33] L. Shaw *et al.*, “International Space Station as a Testbed for Exploration Environmental Control and Life Support Systems ♦ 2021 Status,” Jul. 2021, [Online]. Available: <https://ttu-ir.tdl.org/handle/2346/87044>
- [34] M. Abney *et al.*, “Evaluation of Heritage Hardware for Use in Cabin Environments with Reduced Pressure and Increased Oxygen Concentration,” Jul. 2022, [Online]. Available: <https://ttu-ir.tdl.org/handle/2346/89596>
- [35] D. W. Harris *et al.*, “Moon to Mars (M2M) Habitation Considerations: A Snap Shot As of January 2022,” M–1538, Jan. 2022. [Online]. Available: <https://ntrs.nasa.gov/citations/20220000524>
- [36] “ISS Transition Report.” [Online]. Available: https://www.nasa.gov/sites/default/files/atoms/files/2022_iss_transition_report-final_tagged.pdf
- [37] H. Jones, “The System Complexity Metric (SCM) Predicts System Costs and Failure Rates,” Jul. 2020, [Online]. Available: <https://ttu-ir.tdl.org/handle/2346/86398>

- [38] K. Yang, C. Yang, H. Yang, and C. Zhou, “Complexity Evaluation of an Environmental Control and Life-Support System Based on Directed and Undirected Structural Entropy Methods,” *Entropy*, vol. 23, no. 9, Art. no. 9, Sep. 2021, doi: 10.3390/e23091173.
- [39] G. Detrell, E. Messerschmid, and E. G. Ponsati, “ECLSS Reliability Analysis Tool for Long Duration Spaceflight,” Jul. 2016, [Online]. Available: <https://ttu-ir.tdl.org/handle/2346/67649>
- [40] H. Jones, “Improving Reliability and Maintainability (R&M) in Space Life Support,” Jul. 2018, [Online]. Available: <https://ttu-ir.tdl.org/handle/2346/74069>
- [41] J. Rohrig, J. O’Neill, and T. Stapleton, “In-Flight Maintenance Design Philosophy for Gateway and Deep-Space Life Support Systems,” Jul. 2019, [Online]. Available: <https://ttu-ir.tdl.org/handle/2346/84417>
- [42] J. Badger, “Spacecraft Dormancy Autonomy Analysis for a Crewed Martian Mission,” p. 156, 2018.
- [43] A. Owens and O. de Weck, “International Space Station Operational Experience and its Impacts on Future Mission Supportability,” Jul. 2018, [Online]. Available: <https://ttu-ir.tdl.org/handle/2346/74165>
- [44] M. J. Sargusingh and J. R. Nelson, “ECLSS Reliability for Long Duration Missions Beyond Lower Earth Orbit,” p. 6.
- [45] M. J. Sargusingh and J. R. Nelson, *Environmental Control and Life Support System Reliability for Long-Duration Missions Beyond Lower Earth Orbit*. 44th International Conference on Environmental Systems, 2014. [Online]. Available: <https://ttu-ir.tdl.org/handle/2346/59710>
- [46] J. A. Matelli and K. Goebel, “Resilience evaluation of the environmental control and life support system of a spacecraft for deep space travel,” *Acta Astronaut.*, vol. 152, pp. 360–369, Nov. 2018, doi: 10.1016/j.actaastro.2018.08.045.
- [47] H. W. Jones, “Going Beyond Reliability to Robustness and Resilience in Space Life Support Systems,” p. 9.
- [48] A. Ridley *et al.*, “International Space Station as a Testbed for Exploration Environmental Control and Life Support Systems -- 2022 Status,” Jul. 2022, [Online]. Available: <https://ttu-ir.tdl.org/handle/2346/89816>
- [49] D. L. Cloud, M. C. Keilich, P. T. Polis, and S. J. Yanczura, “Assessment of Service Life for Regenerative ECLSS Resin Beds,” p. 10.
- [50] J. C. Knox, “Development of Carbon Dioxide Removal Systems for NASA’s Deep Space Human Exploration Missions 2016-2017,” p. 17.
- [51] K. Takada, A. Ridley, L. Velasquez, S. Van Keuren, S. Mcdougale, and P. Baker, “Status of the Advanced Oxygen Generation Assembly Design,” Jul. 2020, [Online]. Available: <https://ttu-ir.tdl.org/handle/2346/86443>
- [52] H. Jones, “Dormancy Should Be Avoided for Mars and Deep Space Recycling Life Support,” Jul. 2019, [Online]. Available: <https://ttu-ir.tdl.org/handle/2346/84486>
- [53] “Environmental Control and Life Support System ECLSS 21002.” [Online]. Available: https://www.nasa.gov/centers/johnson/pdf/383445main_eclss_21002.pdf
- [54] “Final Report of the International Space Station Independent Safety Task Force.” [Online]. Available: https://www.nasa.gov/pdf/170368main_IIST_%20Final%20Report.pdf
- [55] D. Klaus, S. Zaccarine, P. Pischulti, and A. Rollock, “Establishing Assessment Criteria for Intelligent Infusion of ‘Smart Systems’ into a Space Habitat,” Jul. 2020, [Online]. Available: <https://ttu-ir.tdl.org/handle/2346/86403>
- [56] D. Klaus, S. Zaccarine, P. Pischulti, and A. Rollock, “Functionally Aligning Emergent Technologies for Self-Sufficient Deep Space Smart Habitats,” Jul. 2022, [Online]. Available: <https://ttu-ir.tdl.org/handle/2346/89689>
- [57] M. Y. Hwang, B. Akinci, and M. Berges, “An Overview of Root Cause Analysis of Faults in Heating, Ventilation, and Air Conditioning (HVAC) Systems,” pp. 1441–1448, May 2022, doi: 10.1061/9780784483893.176.
- [58] K. N. Son, “Improved Prediction of Adsorption-Based Life Support for Deep Space Exploration,” thesis, Purdue University Graduate School, 2019. doi: 10.25394/PGS.7423451.v1.

- [59] G. Cmarik, K. Son, and J. Knox, “Standard Isotherm Fit Information for Dry CO₂ on Sorbents for 4-Bed Molecular Sieve,” Dec. 01, 2017. <https://ntrs.nasa.gov/citations/20180002395> (accessed).
- [60] “A review of mathematical modeling of fixed-bed columns for carbon dioxide adsorption - ScienceDirect.” <https://www.sciencedirect.com/science/article/abs/pii/S026387621300347X> (accessed).
- [61] K. R. Wood, Y. A. Liu, and Y. Yu, *Design, Simulation and Optimization of Adsorptive and Chromatographic Separations: A Hands-On Approach*. Weinheim, Germany: Wiley-VCH Verlag GmbH & Co. KGaA, 2018. doi: 10.1002/9783527815029.
- [62] “Introduction to Aspen Adsorption.” [Online]. Available: https://www.researchgate.net/profile/M_Quader2/post/I_want_to_simulate_PSA_process_with_Aspen_adsorption_primmitive_Aspen_ADSIM_I_need_some_tutorial_files_for_this_software_is_there_anyone_helps_me/attachment/59d64c3779197b80779a6125/AS%3A483636639211520%401492319368809/download/Intoduction+Aspen+Adsorption_ES288.071.07.pdf
- [63] “Simulation of Adsorption Processes.” [Online]. Available: https://application.wiley-vch.de/books/sample/3527344691_c01.pdf
- [64] K. N. Son, G. E. Cmarik, J. C. Knox, J. A. Weibel, and S. V. Garimella, “Measurement and Prediction of the Heat of Adsorption and Equilibrium Concentration of CO₂ on Zeolite 13X,” *J. Chem. Eng. Data*, Apr. 2018, doi: 10.1021/acs.jced.8b00019.
- [65] K. N. Son, J. A. Weibel, J. C. Knox, and S. V. Garimella, “Calibration and uncertainty analysis of a fixed-bed adsorption model for CO₂ separation,” *Adsorption*, vol. 24, no. 8, pp. 781–802, Nov. 2018, doi: 10.1007/s10450-018-9982-x.
- [66] S. Eshima, J. Nabity, A. Mohany, H. Rozas, and N. Gebrael, “A Diagnostics Model for Detecting Leak Severity in a Regenerable CO₂ Removal System,” Jul. 2022, [Online]. Available: <https://ttu-ir.tdl.org/handle/2346/89813>
- [67] T. L. P. Dantas *et al.*, “Modeling of the fixed - bed adsorption of carbon dioxide and a carbon dioxide - nitrogen mixture on zeolite 13X,” *Braz. J. Chem. Eng.*, vol. 28, pp. 533–544, Sep. 2011, doi: 10.1590/S0104-66322011000300018.
- [68] “Formulas for Numerical Differentiation.” [Online]. Available: https://lcn.people.uic.edu/classes/che205s17/docs/che205s17_reading_01e.pdf
- [69] R. E. Kalman, “A New Approach to Linear Filtering and Prediction Problems,” *J. Basic Eng.*, vol. 82, no. 1, pp. 35–45, Mar. 1960, doi: 10.1115/1.3662552.
- [70] D. Simon, “Optimal State Estimation: Kalman, H_∞, and Nonlinear Approaches,” 2006. doi: 10.1002/0470045345.
- [71] R. Huang, T.-M. J. Richardson, G. Belancik, D. Jan, J. Hogan, and J. Knox, “Zeolite Degradation: An Investigation of CO₂ Capacity Loss of 13x Sorbent,” Jul. 2017, [Online]. Available: <https://ttu-ir.tdl.org/handle/2346/72938>
- [72] D. Howard, J. Knox, D. Long, L. Miller, J. Thomas, and G. Cmarik, “Long Duration Sorbent Testbed,” Jul. 2016, [Online]. Available: <https://ttu-ir.tdl.org/handle/2346/67491>
- [73] J. C. Knox, D. W. Watson, T. J. Giesy, G. E. Cmarik, and L. A. Miller, “Investigation of Desiccants and CO₂ Sorbents for Exploration Systems 2016-2017,” presented at the International Conference on Environmental Systems, Charleston, SC, Jul. 2017. [Online]. Available: <https://ntrs.nasa.gov/citations/20170008962>
- [74] J. C. Knox, H. Gauto, and L. A. Miller, “Development of a Test for Evaluation of the Hydrothermal Stability of Sorbents Used in Closed-Loop CO₂ Removal Systems,” presented at the International Conference on Environmental Systems, Bellevue, WA, Jul. 2015. [Online]. Available: <https://ntrs.nasa.gov/citations/20150016501>